A study on the impact of surface and bulk oxidation on the recyclability of NdFeB magnets

Name: Matthew Farr

MRes Thesis

Supervisors: Dr Allan Walton & Dr Andrew Williams

Magnetic Materials Group

Department of Metallurgy and Materials

University of Birmingham

May 2013

UNIVERSITYOF
BIRMINGHAM

University of Birmingham Research Archive

e-theses repository

Abstract

Rare earth metals have come under considerable supply constraints in recent years due to export quotas imposed by the largest producer, China. This has led to considerable interest in the possibility of recycling rare earth magnets based upon neodymium-iron-boron (NdFeB). It has previously been shown by researchers at The University of Birmingham that hydrogen gas can be used to remove NdFeB magnets from electrical scrap in the form of a demagnetised powder, which can subsequently be re-processed to form new magnets directly from the alloy powder by re-sintering [Zakotnik, 2009; Walton, 2012]. One of the problems associated with the recycling of scrap magnets is the fact that they are likely to contain a higher level of oxygen, both at the surface and in the bulk of the material, compared to primary sources of NdFeB alloys. Oxidation of NdFeB can cause problems with the initiation of hydrogen at the surface of the material as well as having a detrimental effect on the mechanical and magnetic properties of the final recycled magnet [Jacobson, 1987; Meakin, 2013].

The aims of this project were to investigate and characterise the surface and near surface oxidation behaviour of bulk NdFeB magnets, in air, at room temperature as well as attempting to track the oxygen content throughout the novel multi-stage re-sintering process developed in the lab at the University of Birmingham. 3-D confocal scanning laser microscopy, raman spectroscopy and secondary ion mass spectrometry (SIMS) were employed in order to characterise the surface/near surface oxidation behaviour of sintered NdFeB magnets. A Leco oxygen analyser was used to track oxygen contamination throughout all of the steps in the recycling process.

Surface oxidation appeared to be exclusive to the Nd-rich triple junctions on the surface of the material, which is unlike higher temperature oxidation observed on sintered NdFeB magnets [Li, 2002]. Alloying additions of Dy and Co were also shown to increase the resistance to oxidation of NdFeB magnets. SIMS analysis showed that oxygen was concentrated in the grain boundary phase in the near surface. The oxygen content was shown to increase almost linearly throughout the recycling process outlined in this report with an overall increase of ~1100-1200 ppm, which is much smaller than that observed for commercial primary production of sintered NdFeB magnets.

Dedication

I would like to dedicate this work to the late Dr Andy Williams, who sadly passed away during the course of this project. Without his encouragement I would not have pursued postgraduate study, and for that I am thankful.

Table of Contents

List of Figures

List of Tables

1.0 Introduction

Rare earth (RE) based permanent magnets are widely used in many applications, such as computer hard disk drives (HDD's), hybrid vehicles and wind turbine generators. Neodymium-iron-boron (NdFEB) magnets, which will be the main focus of this project, possess the highest energy product of all the permanent magnets available today with reported energy densities of up to 50 MGOe [Kaneko, 2000]. Two forms of NdFeB magnet exist; bonded magnets, using a polymer or resin bonding agent, and fully dense sintered magnets. Sintered NdFeB magnets contain a Nd-rich phase at the grain boundaries and $Nd_2Fe_{14}B$ matrix grains. Bonded NdFeB magnets contain nanocrystalline NdFeB powders, produced either by HDDR processing or melt spinning and a polymer or resin bonding agent. Although the energy product of NdFeB magnets is very high, they do suffer from low corrosion resistance [Coey, 1995] and a relatively low Curie temperature (312°C) compared with other permanent magnet materials [Sagawa, 1984].

China currently produces over 95% of the world's rare earth metals including Nd and Dy. However, in recent years China has introduced export quotas and in 2010 this quota was cut by 40% [Hatch, 2012]. Rare earth prices have subsequently increased dramatically with the cost of Nd rising from $30/kg in January 2010 to $210/kg in February 2012 (Nd peaked at $450/kg)[www.metal-pages.com]. Figure 1 shows the global share of rare earth production between 1986 and 2009. It can be observed that, in the 1990's and the early part of the 2000's, many other producers began closing down their mining operations. This was due to the falling price of rare earths, caused by the huge supply coming from China. In recent years, companies such as Molycorp have been re-opening mining operations that were not previously economically viable.
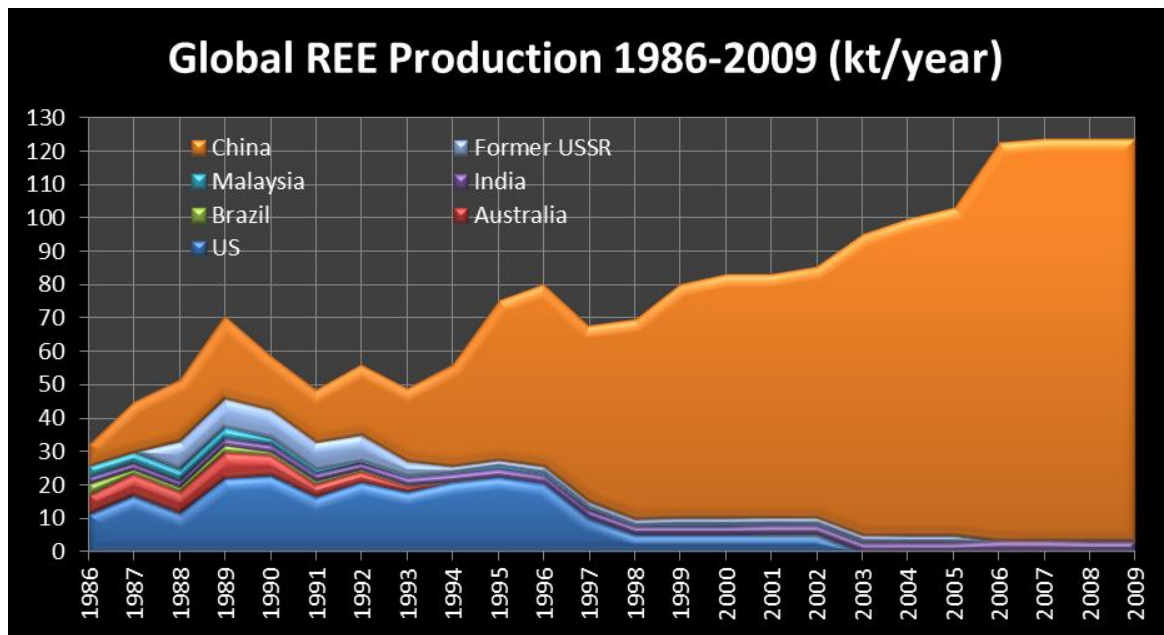
Figure 1 – Global rare earth production from 1986-2009 [Keane, 2010]
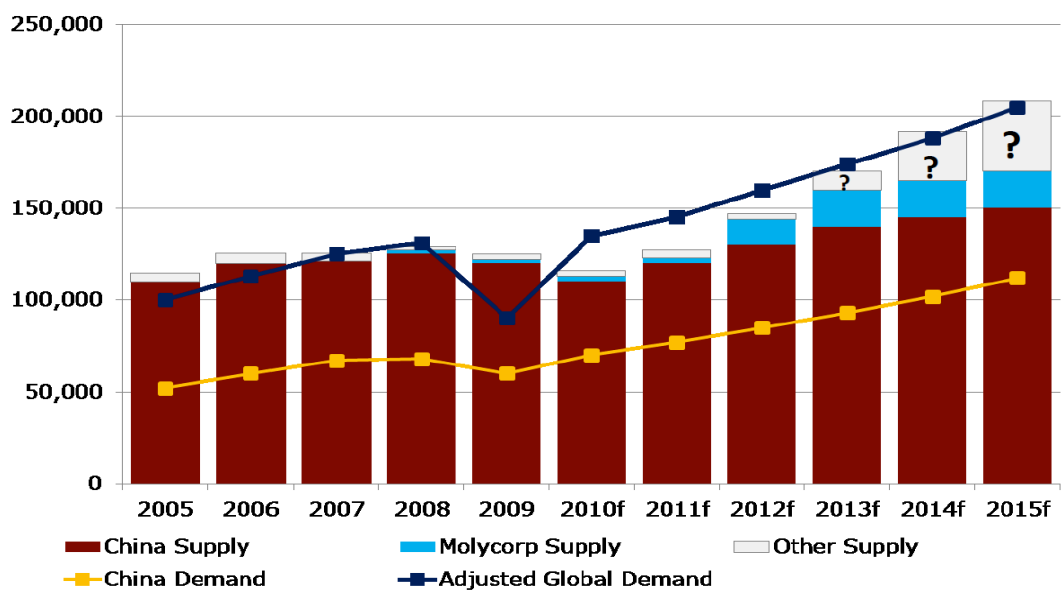
Figure 2 – Global supply and demand for rare earth materials since 2005 and projected until 2015 [Trout, S., Molycorp, UK Magnets Society meeting]

It can be observed from Figure 2, that over the next few years, global supply may not meet the growing demand for rare earth materials. This is especially true if NdFeB magnets continue to

be used in wind turbines and electric vehicles. Although a number of companies are re-opening rare earth mines, the demand may still not be fulfilled.

There are several possible solutions to the rare earth 'crisis'. Other than re-opening old mines, one option would be to switch to other technologies, where rare earth magnets are not required or to reduce the quantity of rare earths used in magnet production. Another potential solution would be to recycle permanent magnets contained within scrap electrical devices. The Magnetic Materials Group (MMG) at the University of Birmingham have been investigating recycling solutions and have shown that hydrogen can be used to break down NdFeB magnets contained within hard disk drives into a hydrided powder, which is soft magnetic. This soft magnetic powder can then be easily separated from electronic equipment [Walton, 2012]. After separation, this powder can be re-processed into either sintered or bonded magnets.

When producing sintered NdFeB magnets it is important to the limit oxygen concentration as oxygen has a detrimental effect on the magnetic properties of the final sintered magnet [Brown, 2002]. Therefore when directly re-processing recycled NdFeB material into new sintered magnets it is important to determine the oxygen concentration of the starting material and to monitor further oxygen pickup during processing. This is one of the main aims of this project. Secondly, scrap magnets are likely to have a considerable surface oxide layer, which could impede the reaction of hydrogen. Once hydrogen decrepitation has taken place then this surface oxide will be entrained in the hydrogenated powder and will be incorporated into the final recycled magnet. Therefore, the second aim of this project is to assess the growth mechanism and characteristics of surface oxides on air exposed sintered NdFeB magnets.

2.0 Literature Review

2.1 Magnets in the 20th Century
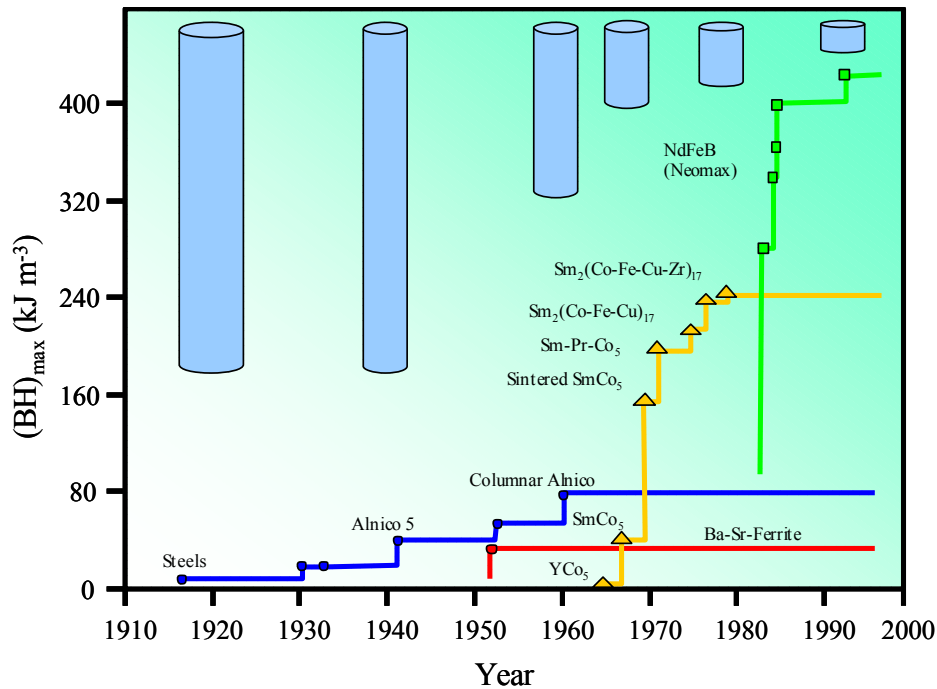
Figure 3 - Permanent magnet development between 1910 and 2000.

Figure 3 shows the development of magnetic materials between 1910 and 2000. Currently, the most commonly used magnets are Ferrites, Alnico (Al, Ni, Co), $SmCo_5$, Sm_2(Co, Fe, Cu, Zr)$_{17}$ and NdFeB. Each material is suited to different applications depending on their requirements. Figure 3 shows the maximum energy product (BH_{max}) of the most commonly used magnets and the blue cylinders illustrate the comparative size of each material required to produce the same energy product. Maximum energy product is a figure of merit that indicates the useful amount of work that is performed by a magnet.

Ferrites have a low energy product and coercivity when compared with other modern magnets, however, they have a very low relative cost. This means that they are well suited for

applications where cost has priority over performance. $SmCo_5$ and $Sm_2(Co, Fe, Cu, Zr)_{17}$ type magnets have a high coercivity and very good temperature stability and corrosion resistance; therefore they are suitable for applications where the magnets are subject to

 harsh operating environments. However, SmCo type magnets have traditionally been more expensive than NdFeB magnets. NdFeB magnets suffer from extremely low corrosion resistance and relatively high cost, which means that they are primarily used in high performance applications where a high field is required for a small volume of material.

2.2 The Study of Magnetic Materials

In the study of magnetic materials, there are two main unit systems. These are the metres-kilograms-seconds (mks) system and the centimetres-grams-seconds (cgs) system. The most commonly used system is mks and this was later revised to form the rationalised metres-kilograms-seconds system (rmks). It is the rmks system that has been adopted as the S.I. unit in the study of magnetic materials.

Quantity	Gaussian (cgs units)	S.I. Units	Conversion factor (cgs to S.I.)
Magnetic Induction (B)	G	T	10^{-4}
Applied Field (H)	Oe	A m^{-1}	$10^3 / 4\pi$
Magnetisation (M)	emu cm^{-3}	A m^{-1}	10^3
Magnetisation ($4\pi M$)	G	-	-
Magnetic Polarisation (J)	-	T	-
Specific Magnetisation (σ)	emu g^{-1}	J T^{-1} kg^{-1}	1
Permeability (μ)	Dimensionless	H m^{-1}	$4\pi . 10^{-7}$
Relative Permeability (μ_r)	-	Dimensionless	-
Susceptibility (χ)	emu cm^{-3} Oe^{-1}	Dimensionless	4π
Product of $B . H$	M G Oe	k J m^{-3}	$10^2 / 4\pi$

Table 1 - A comparison of the cgs and rmks (S.I.) unit systems. Also shown is the conversion factor from cgs to rmks. [Williams, A.J.]

An important parameter for characterising magnetic materials is magnetic susceptibility (x). The susceptibility of a material describes the way in which it responds to an applied field. The equation for calculating the magnetic susceptibility of a material is shown below:

$$x = \frac{M}{H}$$
Equation 1

Where:

M = magnetisation of the material with the units: $JT^{-1}m^{-3}$
H = applied field with the units: Am^{-1}

A second important parameter in the study of magnetic materials is magnetic induction (B). This describes the total magnetic flux through a unit of cross sectional area. Magnetic induction can be calculated using the following equation:

$$B = \mu_0(H + M)$$
Equation 2

Where:

μ_0 = permeability of free space
M = magnetisation of the material with the units: $JT^{-1}m^{-3}$
H = applied field with the units: Am^{-1}

A third parameter, which is commonly used in the study of magnetic materials, is magnetic polarisation (J). This gives the value for the magnetisation of a material, measured in Tesla. Magnetic polarisation can be calculated as follows:

$$J = \mu_0 M \qquad \text{Equation 3}$$

Where:

μ_0 = permeability of free space
M = magnetisation of the material with the units: $JT^{-1}m^{-3}$

2.3 The Source of Magnetism

The field produced by a magnetic material originates from the orbital angular motion of the electrons around the nucleus of the atom (Figure 4) and the electron's intrinsic magnetic moment. In non-magnetic materials, the electrons are arranged in such a way that their magnetic moments cancel out, thus no field is produced.
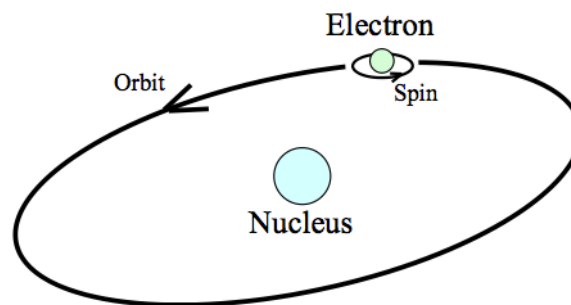
Figure 4 – The orbit of a spinning electron around the nucleus of an atom [Williams, A. J.]

2.4 Types of Magnetism

There are 5 types of magnetic material: diamagnetic, paramagnetic, ferromagnetic, anti-ferromagnetic and ferrimagnetic.

Diamagnetism

Diamagnetic materials have a small negative magnetic susceptibility, which means that they are weakly repelled by externally applied magnetic fields. They have filled electron shells and therefore do not have magnetic dipoles (shown in Table 2). The diamagnetic effect can be observed in all materials, however other forms of magnetism such as paramagnetism and ferromagnetism can easily overpower it. Examples are copper, gold and silver.

Paramagnetism

Paramagnetic materials have a small positive magnetic susceptibility. As such they are weakly attracted to an externally applied magnetic fields. They have unfilled electron shells and therefore they contain magnetic dipoles. However, with zero applied field a paramagnetic material has randomly orientated magnetic moments, which cancel each other out (shown in Table 2). When a field is applied, there is a magnetisation in the direction of the applied field; however, the material does not retain any magnetic properties when the field is removed. Some examples of paramagnetic materials are magnesium and lithium.

Ferromagnetism

Ferromagnetic materials have a large positive magnetic susceptibility meaning that they are strongly attracted to externally applied magnetic fields. They have unfilled electron shells and therefore they contain magnetic dipoles. Ferromagnets have parallel aligned magnetic moments (shown in Table 2), which can be aligned in the direction of an applied magnetic field. Ferromagnetism is the strongest form of magnetism and is also responsible for permanent magnetism, where a material retains its magnetic properties after an applied field has been removed. Iron, nickel and cobalt are examples of the only room temperature ferromagnetic materials.

The Curie-Weiss Law states that the magnetic susceptibility of a ferromagnetic material is inversely proportional to the difference in temperature compared to the Curie temperature [Arrot, 1985]. At temperatures above the Curie point, thermal disordering overcomes the dipoles' tendency to align and permanent magnetic properties are lost. Although these materials cannot maintain spontaneous magnetisation above their Curie temperature, they still behave paramagnetically when an external field is applied. The equation for calculating a materials' Curie point is as follows:

$$\chi = \mu - 1 = \frac{C}{T - T_c} \qquad \text{Equation 4}$$

Where:

χ = magnetic susceptibility
μ = relative magnetic permeability of the material
C = a constant characteristic for a given substance and
T_c = Curie temperature
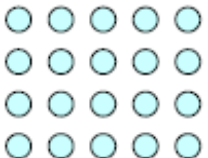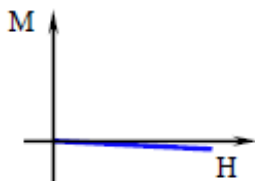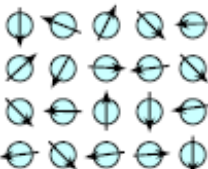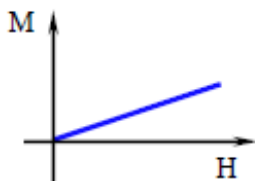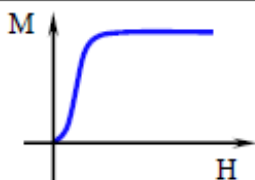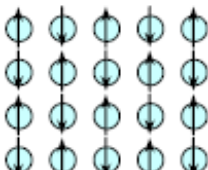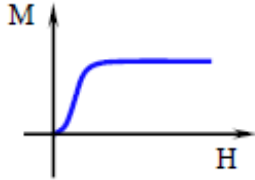
Equation 4 is only valid above the Curie temperature.

Anti-ferromagnetism

Anti-ferromagnetic materials, like paramagnetic materials, have a small positive magnetic susceptibility, which means that they are weakly attracted to applied fields. They have unfilled electron shells, thus they contain magnetic dipoles. Anti-ferromagnetic materials have an equal number of anti-parallel aligned magnetic moments meaning that they cancel each other out (shown in Table 2). The threshold where this ordering disappears is known as the Néel temperature. Above this temperature these materials behave like a paramagnet [Néel, 1948]. Chromium is an example of an anti-ferromagnetic material.

Ferrimagnetism

Ferrimagnetic materials have a large positive magnetic susceptibility. As such they are strongly attracted to externally applied magnetic fields. They have unfilled electron shells and therefore they contain magnetic dipoles. The atoms in a ferrimagnetic material have mixed parallel and anti-parallel aligned magnetic moments (shown in Table 2). The moments of atoms on different sub lattices are opposed, like in anti-ferromagnetism, however, the opposing forces are unequal so they do not cancel each other out. This means that there is spontaneous magnetisation [Smart, 1955]. Ferrite magnets (eg. $SrO \cdot 6Fe_2O_3$) are ferrimagnetic.

Type	Atomic / Magnetic Behaviour	
Dia-magnetism	Atoms have no magnetic moment	M vs H curve (negative slope)
Para-magnetism	Atoms have randomly oriented magnetic moments	M vs H curve (positive linear slope)
Ferro-magnetism	Atoms have parallel aligned magnetic moments	M vs H curve (saturating)
Antiferro-magnetism	Atoms have anti-parallel aligned magnetic moments	M vs H curve (positive linear slope)
Ferri-magnetism	Atoms have mixed parallel and anti-parallel aligned magnetic moments	M vs H curve (saturating)

Table 2 – A summary of the types of magnetism with illustrated magnetic moments and magnetisation curves where M is magnetisation and H is applied field.

2.5 Magnetocrystalline Anisotropy

Crystalline magnetic materials often have a preferred direction of magnetisation. This is

known as the easy direction and in NdFeB this is along the c-axis of the tetragonal crystal.

Magnetic anisotropy is brought about by a coupling of the electron orbitals to the lattice and

in the easy direction of magnetisation the electron orbitals are in the lowest energy state. Magnetic materials also have hard directions of magnetisation. In the hard directions, the magnetic moments have a much greater resistance to rotation and therefore higher fields are required to magnetise the material. A materials' anisotropy field, H_a (shown in Figure 5) is a measure of the magnetocrystalline anisotropy in the easy direction and it is the field required to rotate all of the magnetic moments by 90°. The anisotropy field is the magnitude of the externally applied field required to achieve saturation polarisation. Figure 5 shows that a much higher field is required to rotate all of the magnetic moments into the hard direction than is needed to do the same for the easy direction.
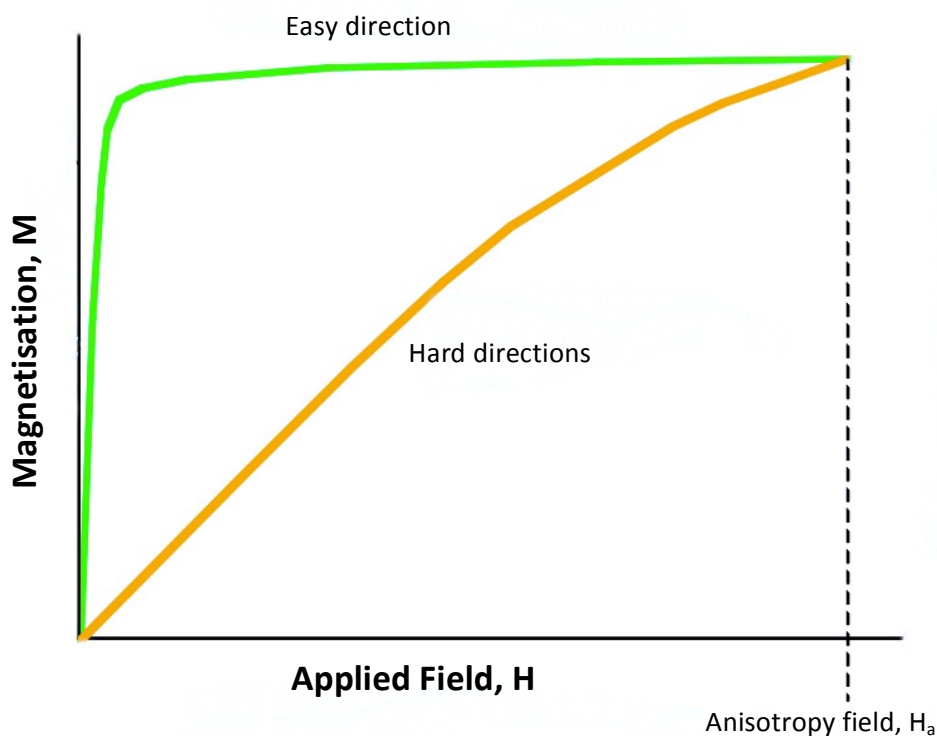
Figure 5 – Typical magnetisation curves for the easy and hard directions in a magnetic material.

2.6 Magnetic Domains

Both ferromagnetic and ferrimagnetic materials demonstrate spontaneous magnetisation. However, both of these types of material can exist in a demagnetised state. This is possible because of regions in these materials called magnetic domains. Within any one of these domains the magnetic dipoles are aligned, causing that domain to have spontaneous magnetisation in a particular direction. The direction of magnetisation can vary between domains, and if totally random this results in zero net magnetisation. Magnetic domains exist in order to reduce the materials free energy. As a magnetic material is broken down into more domains, the demagnetising field (shown in Figure 6) and the magnetostatic energy are reduced. The demagnetising field, H_d, is produced as a result of the presence of free poles at the surface of the material. This demagnetising field is in opposition to the magnetisation of the material and its magnitude is dependent on material geometry and magnetisation. If a specimen has a large length to diameter ratio and is magnetised in the long axis, the demagnetising field and magnetostatic energy will be reduced. If a material breaks down into X number of domains, then the magnetostatic energy is reduced by a factor of 1/X. This means that, in Figure 6, (c) has a quarter of the magnetostatic energy of (a).
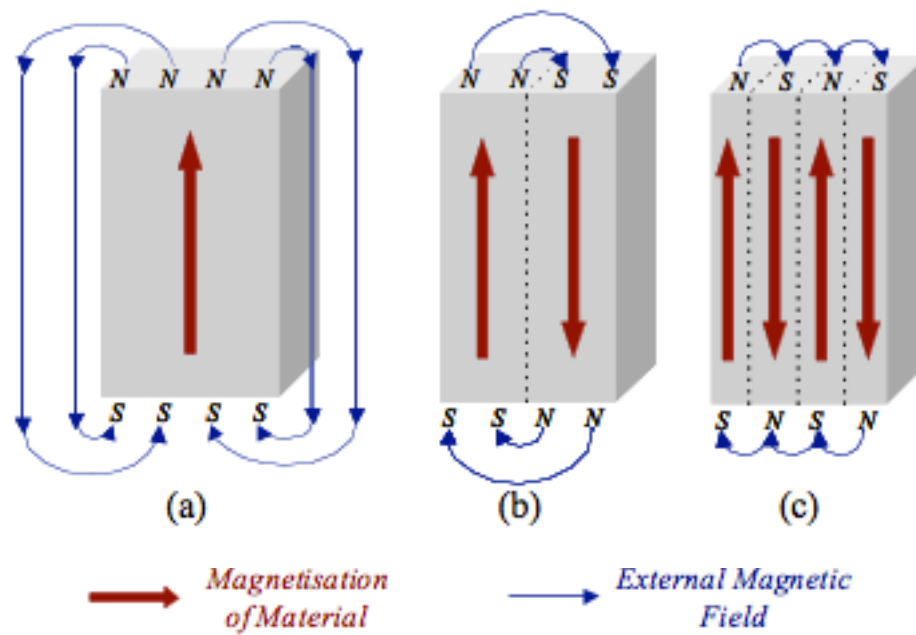
Figure 6 – Schematic of the break up of magnetisation into domains. (a) single domain, (b) two domains, (c) four domains [Williams, A.J., Harris, I.R.]

A magnetic material will not continue to divide into smaller and smaller domains indefinitely because the introduction of domain walls will increase the overall energy of the system. A domain wall has its own energy associated with it and this is proportional to the domain's area. This higher energy state is caused because the magnetic dipole moments within the domain wall are not oriented in the easy direction of magnetism. Domain wall energy varies dependent on the degree of magnetocrystalline anisotropy and the magnitude of the exchange interactions between adjacent atoms.

2.7 Magnetic Hysteresis

A hysteresis loop is a method for plotting bulk magnetic properties and can either be shown as Applied field vs. Polarisation (J) or Applied field vs. Induction (B). Figure 7 shows a typical hysteresis loop for a permanent magnetic material. The red and blue dotted lines show the initial magnetisation curves for the material, which increase quickly at first. The red line represents the relationship between the polarisation of the material and the magnetising field. The blue line shows the relationship between the induced magnetic flux density and the magnetising force. As an external field is applied to the material, domains that are favourably aligned grow at the expense of misaligned domains. As the applied field increases, the magnetic moments in the unfavourably aligned domains overcome the anisotropy energy and rotate into the direction of the easy axis that is nearest to the field direction. As the applied field continues to increase in magnitude, the magnetic moments begin to gradually rotate from the easy axis into the direction of the external field. The magnetisation of the material increases until magnetic saturation, or saturation polarisation, is reached. When the external field is removed, some of the magnetism is retained, this is known as the magnetic remanence (B_r or J_r), which is labelled in Figure 7.

To demagnetise a permanent magnetic material, a magnetic field is applied in the opposite direction to the magnetisation of the sample. The demagnetisation curve for a ferromagnetic material appears in the second quadrant of the hysteresis loop shown in Figure 7. When the demagnetising field is strong enough, the curve passes through the x-axis into the third quadrant. The point at which the demagnetisation curve crosses the x-axis is known as the coercivity. Coercivity is a measure of the reverse magnetic field required to fully demagnetise a material, i.e., the resistance of a material to demagnetisation.
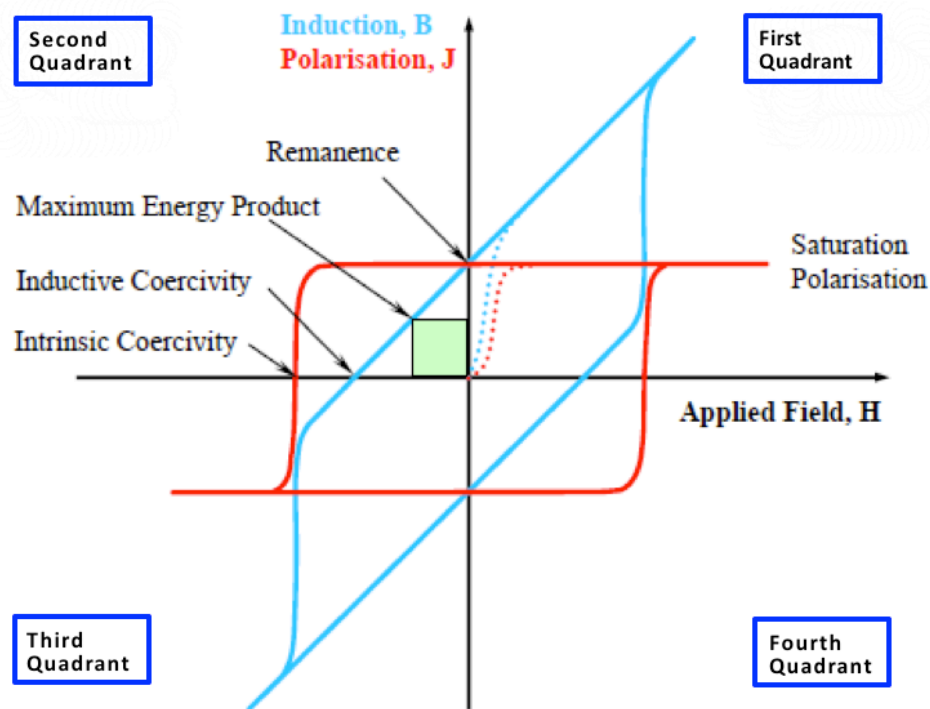
Figure 7 – A typical hysteresis loop for a ferromagnetic material.

The maximum energy product, or BH_{max}, of a material indicates the maximum amount of useful work a magnet can perform. BH_{max} is the maximum product of B and H that can be obtained on the demagnetisation curve for the material (shown as a green square in Figure 7). Materials with a large BH_{max} require a smaller volume of material to perform the same amount of work as a material with a lower BH_{max}. Most magnet manufacturers use this value to market their products as it provides a good overview of the properties of a material.

As the reverse field is increased, the curve continues down into the third quadrant until saturation is reached in the negative direction. When the field is removed, the curve moves back towards the y-axis where it crosses, giving the remanent magnetisation in the negative direction. At this point the applied field is switched back to the positive direction and the curve moves up through the fourth quadrant to complete the hysteresis loop.

2.8 Coercivity Mechanisms

The coercivity of a magnetic material is affected by both intrinsic and extrinsic factors. Magnetocrystalline anisotropy is an intrinsic factor that affects the properties of a magnetic material. Extrinsic factors include the microstructure of the material. The microstructure of a magnetic material has an effect on coercivity because domains can interact with microstructural features. There are several different coercivity mechanisms related to the microstructure of a material, including: Nucleation control, domain wall pinning and single domain grains/particles

In nucleation controlled magnets the nucleation of reverse domains is very difficult. These materials will have smooth grain boundaries surrounding the magnetic phase, which removes most reverse domain nucleation sites. This effect occurs because of liquid phase sintering and any potential domain nucleation sites are removed as a result. Nucleation control is the coercivity mechanism that can be observed in sintered NdFeB and $SmCo_5$ type magnets.

A second coercivity mechanism for permanent magnetic materials is domain wall pinning. This mechanism is demonstrated in $Sm_2(Co,Fe,Cu,Zr)_{17}$ type magnets where the magnetic domain walls in the Sm_2Co_{17} based phase have a significantly higher energy than those in the $SmCo_5$ phase. This means that the domain walls are pinned at the $SmCo_5$ grain walls. The coercivity of these materials can be very high, however, it also makes the material difficult to magnetise in the first place.

Another coercivity mechanism is the existence of single domain grains/particles. If a grain is below a critical size then the decrease in magnetostatic energy achieved by splitting into two domains is less than the increase in energy due to the introduction of a new domain wall. Therefore, only one domain will exist per grain/particle. If these grains have strong enough

magnetocrystalline anisotropy to prevent the easy rotation of the magnetic domains then the grains will have a high resistance to demagnetisation. Melt spun NdFeB is an example of a material with single domain grains.

2.9 NdFeB

Neodymium-iron-boron permanent magnets have the highest energy product (max of around 55 MGOe) of all magnetic materials. NdFeB magnets have two main processing routes; powder processing, developed by Sagawa (1984) and melt quenching, developed by Croat (1984). The high energy product of this type of magnet means that a significantly smaller volume of material is required to perform the same work as a larger magnet produced using an alternative material such as Alnico or ferrite. NdFeB magnets have two major disadvantages. They have a relatively low Curie temperature and very poor corrosion resistance. This low Curie temperature (312°C) means that it is not possible to use NdFeB magnets in high temperature applications.

Sintered NdFeB

Sintered $Nd_2Fe_{14}B$ magnets have 3 major phases (shown in Figure 8). These are the; $Nd_2Fe_{14}B$ matrix phase, boron rich $Nd_{1+\varepsilon}Fe_4B_4$ phase and a Nd-rich grain boundary phase.
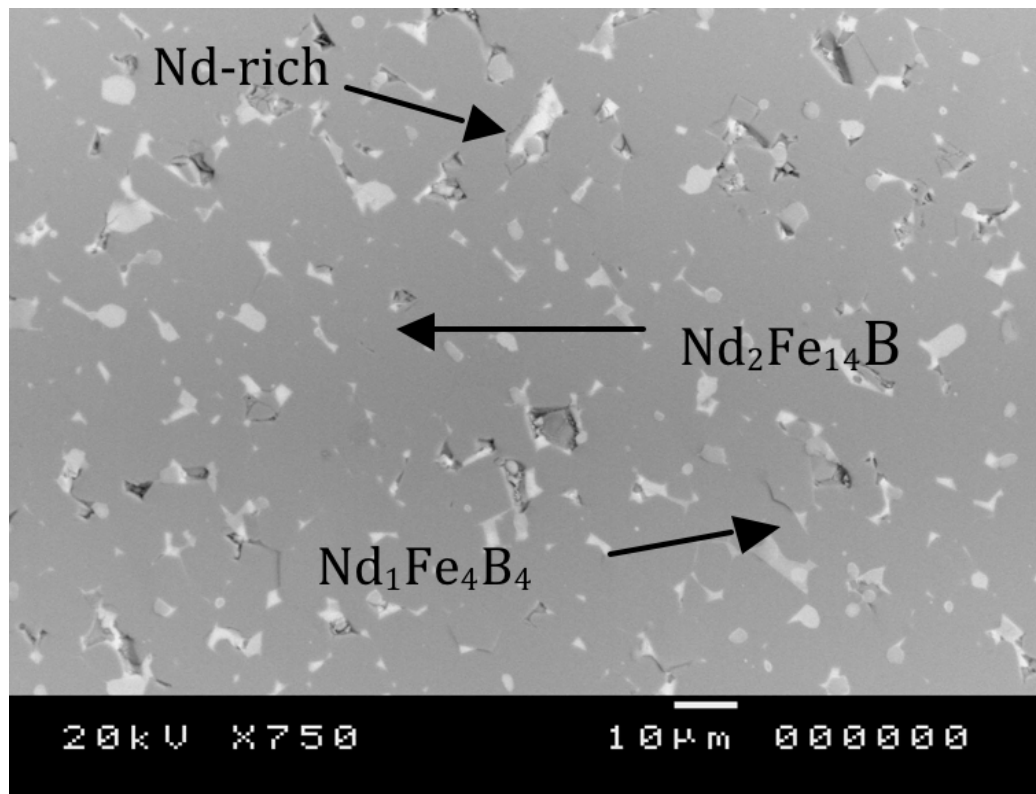
Figure 8 – SEM backscattered image showing the microstructure of a NdFeB type magnet [Zakotnik, 2008]
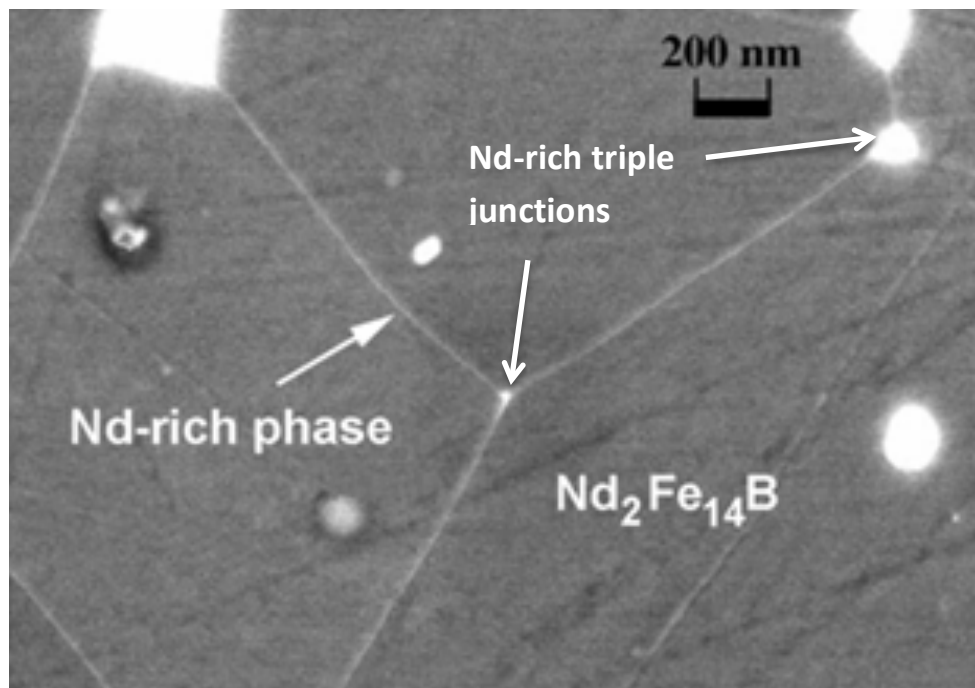
Figure 9 – High resolution backscattered electron micrograph showing Nd-rich grain boundary phase and triple junctions [Walton, A].

$Nd_2Fe_{14}B$

The $Nd_2Fe_{14}B$ matrix phase makes up approximately 85% of the NdFeB system with the other 15% consisting of boron rich $Nd_{1+\epsilon}Fe_4B_4$ and the Nd-rich grain boundary phase. Neutron diffraction [Herbst, 1985] and x-ray diffraction [Givord, 1984] have been used to characterise the crystal structure of the $Nd_2Fe_{14}B$ phase. A schematic of the crystal structure of the $Nd_2Fe_{14}B$ matrix phase is shown in Figure 10. $Nd_2Fe_{14}B$ has a tetragonal structure containing 68 atoms per unit cell and with the lattice parameters a=0.88nm and c=1.22nm [Herbst, 1984]. The Nd atoms form alternating large and small, nearly regular, rhombus in z=1 and z=1/2. The Fe atoms form a planar net of slightly deformed hexagons and triangles [Givord, 1984]. The high anisotropy and spontaneous magnetisation of the $Nd_2Fe_{14}B$ matrix phase mean that it is the sole contributor to the magnetic properties of the material.
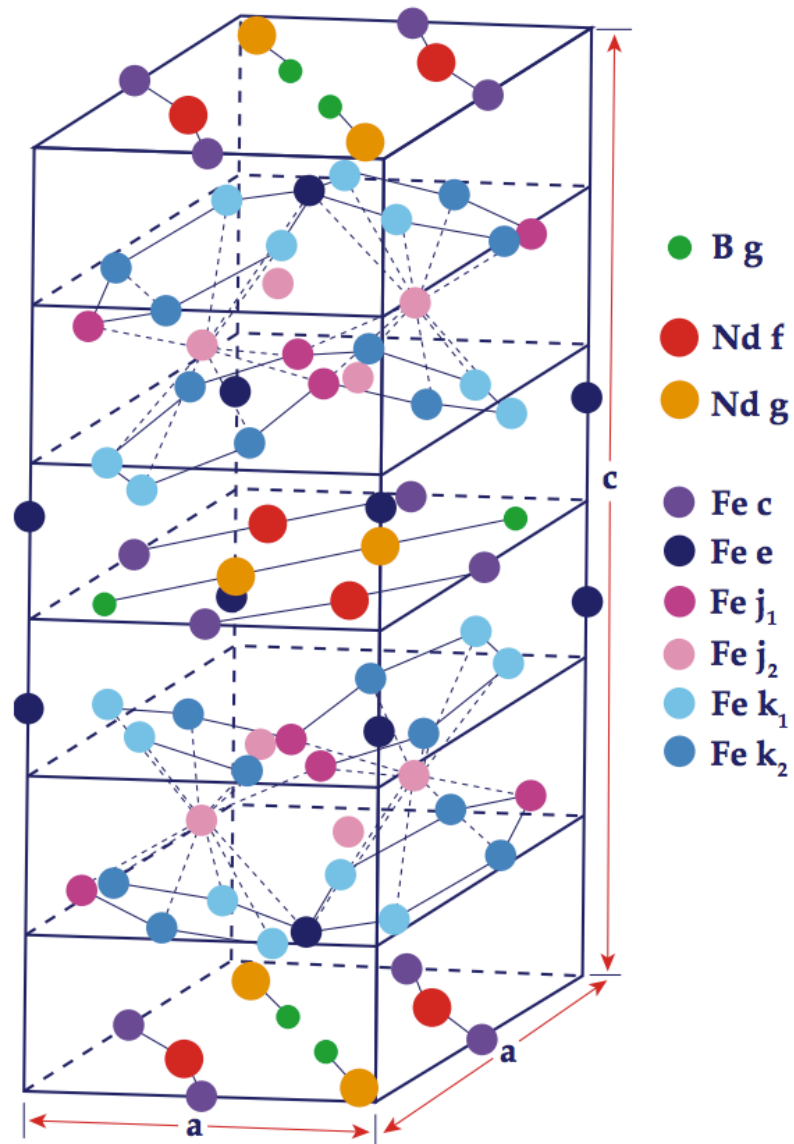
Figure 10 – Crystal structure of Nd$_2$Fe$_{14}$B [Herbst, 1984]

Nd$_{1+\varepsilon}$Fe$_4$B$_4$

A second phase in the NdFeB system is the boron rich Nd$_{1+\varepsilon}$Fe$_4$B$_4$ phase. This phase forms in irregularly distributed grains that are approximately the same size of those in the Nd$_2$Fe$_{14}$B phase. The Nd$_{1+\varepsilon}$Fe$_4$B$_4$ phase has a Curie temperature of 13K; therefore it is not ferromagnetic at room temperature. This means that this phase has detrimental effects on the magnetic properties of the material [Wang, 2005].

Nd-rich Phase

The grain boundaries in NdFeB type sintered magnets contain around 85 at% Nd and 15 at% Fe, with small amounts of B [Fidler, 1987]. The boundary phase has a face-centred cubic (fcc) crystal structure [Makita, 1999; Shinba, 2005]. However, Shinba (2005) reported that in regions where the boundary phase is thinner than about 2 nm, the material was found to be amorphous. It has been reported that the Nd-rich phase contains considerable amounts of oxygen [Makita, 1999; Wang, 2004; Shinba, 2005], however it is thought that this is as a result of the post sintering heat treatment. As well as these thin layers at the grain boundaries, larger grains of this Nd-rich phase exist at the junctions where the $Nd_2Fe_{14}B$ matrix grains meet. These areas are referred to as triple junctions (shown in Figure 9). It has been reported by Woodcock (2012) that these triple junctions contain multiple phases. These include crystalline oxides such as NdO, Nd_2O_3 and NdO_2. If other additions are present in the material, Pr or Dy for example, then phases such as $(Nd,Pr,Dy)_2O_3$ are formed. The Nd-rich phase in the NdFeB system is considered to have a strong positive influence on the magnetic properties of the material [Wang, 2004]. It is considered that the Nd-rich phase has 2 effects on the $Nd_2Fe_{14}B$ matrix grains. The first is that it reduces any exchange interactions between the matrix grains and the second is that it is thought to heal defects on the matrix grain surfaces [Gutfleisch, 2000]. This smoothing of the matrix grains reduces the number of potential nucleation points for reverse magnetic domains and therefore increases coercivity.

2.10 NdFeB Processing

There are multiple processing routes for NdFeB type magnets, including; conventional sintering, melt spinning and HDDR processing. As this project focuses of sintered magnets, this section will be limited to describing only the conventional sintering route.

Conventional Processing Route for Sintered NdFeB Magnets

The starting cast NdFeB ingot is produced either by a conventional book mould process or by strip casting. Strip casting is a process where molten alloy is poured onto a spinning, water-cooled wheel. The fast cooling rate (10^4 K/sec) during this process suppresses the formation of α-Fe dendrites and encourages the growth of fine lamellae, making the microstructure more favourable in terms of magnetic properties. If Fe precipitates are present then they must be removed because of the negative effects they have on the properties of the material. Their presence, together with segregation of the Nd-rich grain boundary phase, causes problems during the ingot crushing and powder milling stages in the processing of sintered magnets as well as reducing the magnetic properties of the material. Therefore, reduction and removal of these precipitates has the effect of improving the magnetic properties of NdFeB type magnets.

Cast NdFeB alloys are typically hydrogen decrepitated to produce a brittle and friable powder, which is then jet-milled to reduce the particle size. Jet-milling is discussed later in this report. The powder is then aligned and pressed to form partially dense (50-60%) green compacts ready for sintering. The green compacts are then vacuum sintered at a temperature of ~1060°C for 1 hour to form the finished magnet. Figure 11 shows the commercial processing route for NdFeB sintered magnets.
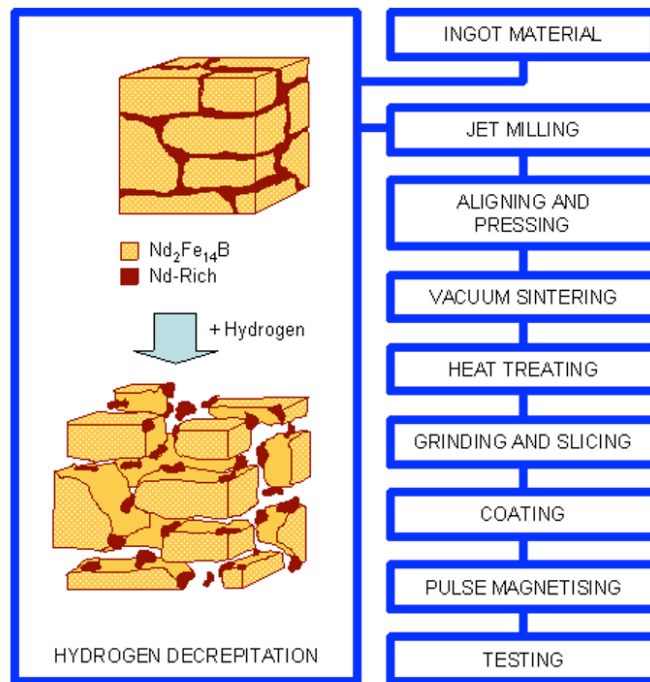
Figure 11- Schematic showing the commercial processing route for sintered NdFeB magnets.

Hydrogen Decrepitation

During the hydrogen decrepitation process (as illustrated in Figure 11) the NdFeB type alloys or magnets are exposed to ~1 bar of hydrogen at room temperature [Harris, 1985]. The hydrogen reacts initially with the Nd-rich grain boundary phase in an exothermic reaction to form Nd $H_{2.7}$ (Nd-trihydride) with an associated volume expansion [McGuiness, 1989]. This expansion results in inter-granular stress, which causes the brittle material to fracture along the grain boundaries. The heat produced from the initial exothermic reaction allows the hydrogen to be interstitially absorbed by the $Nd_2Fe_{14}B$ matrix phase, causing trans-granular cracking [Harris, 1987]. The HD process produces friable granules/powder, which can easily be milled to a finer particle size. Hydrogen decrepitation of strip cast alloy produces a much

finer powder when compared with hydrogen processed book moulded ingots. This is due to the finer microstructure that is produced by strip casting.

Most of the entrained oxygen in a sintered magnet originates from the milling stage (Figure 12). NdFeB powders can be milled mechanically via ball milling or jet milling. Ball milling is a process where a cylinder is partially filled with NdFeB powder and a grinding medium, usually hardened steel balls. This cylinder is then rotated around a horizontal axis and an internal cascading effect reduces the material to a fine powder. Ball milling has been shown to cause an increase in oxygen content of up to 500 ppm [Lian, 1995]. Jet milling is a technique used to reduce the particle size of the hydrogen-processed material and is achieved using a nitrogen cyclone, at high velocities, to cause particle-on-particle impact. These impacts cause the particles to break down into a much finer powder. Breaking the material down into a finer powder exposes a larger surface area, thus allowing more oxidation to occur. Oxygen content has been reported to increase by up to 4400 ppm as a result of jet milling [Namkung, 2011].
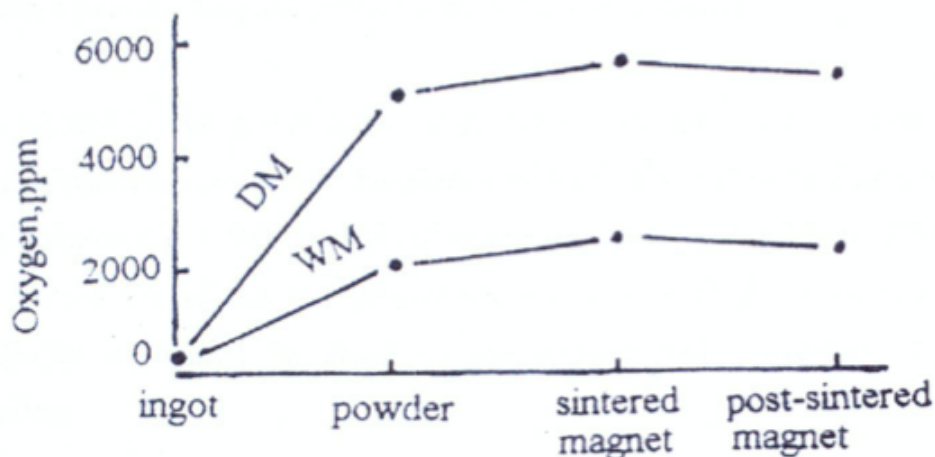
Figure 12 - Oxygen content during various stages in the processing of a Nd-Fe-B magnet. (DM) =Dry milling under argon, (WM) =Wet milling with toluene [Lian, 1995]

2.11 Additions to NdFeB

Additions of various elements have been reported to influence the magnetic properties and environmental stability of NdFeB type permanent magnets.

Cobalt (Co)

It has been reported that the addition of Co to NdFeB magnets has the effect of increasing the Curie temperature [Kim, 1995a]. In addition, Kim (1996) reported that at additions above 15 at% there is a reduction in the coercivity of the material. This could be due to the substitution of some of the Nd-rich phase. The added cobalt replaces Fe atoms to form a $Nd_2(Fe_{1-x}Co_x)_{14}B$ phase, which has smaller grains than the normal $Nd_2Fe_{14}B$ matrix phase.

Dysprosium (Dy)

Dy is added to NdFeB magnets in order to increase the coercivity of the material [Yu, 2004; Bai, 2007]. This improved coercivity is caused by the substitution of Dy atoms for Nd atoms in the $Nd_2Fe_{14}B$ phase. This forms a new $Dy_2Fe_{14}B$ phase, which has a larger anisotropy field than the $Nd_2Fe_{14}B$ phase (15.8T compared to 7.6T for $Nd_2Fe_{14}B$) thus increasing coercivity [Bai, 2007]. Although the coercivity of NdFeB is increased by the addition of Dy, the remanence decreases (Figure 13). This is because Dy couples with Fe in the opposite direction compared to Nd.

The addition of Dy also affects the manner in which the alloy solidifies; When Dy is present in the melt the grains within the material form in a more uniform manner and are finer. This is because Dy can suppress the separation of α-Fe branch crystals during solidification leading

to a reduced number of surface defects on the grains and hence reducing the likelihood of nucleation of reversal walls [Bai, 2007].
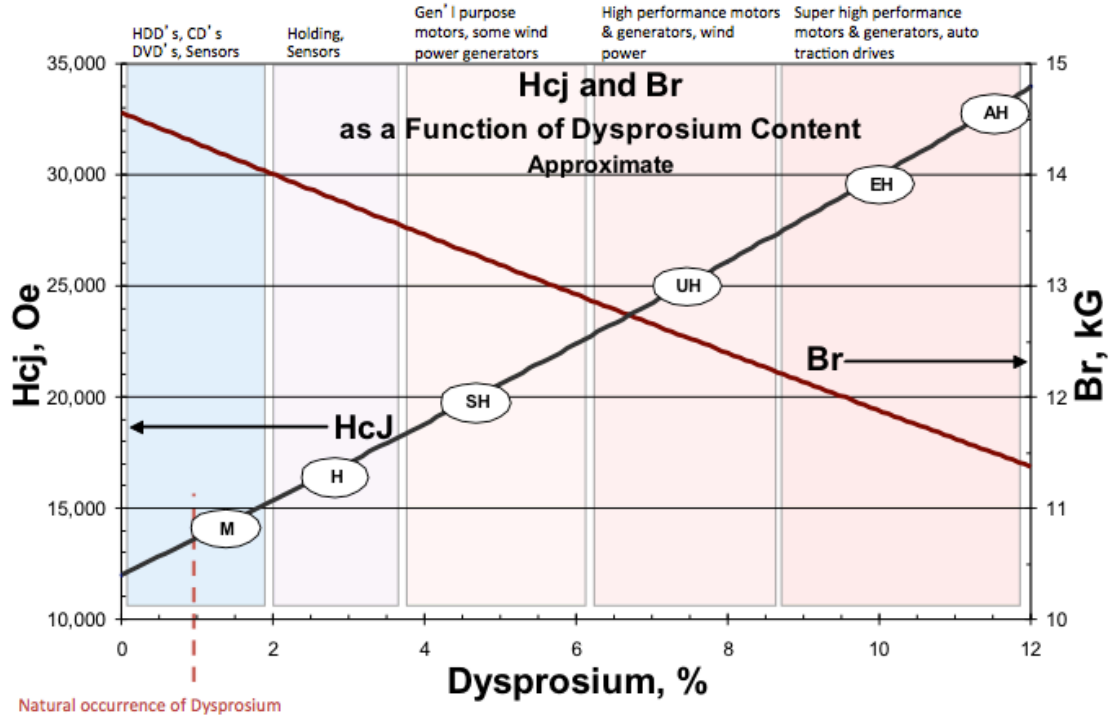
Figure 13 – Effects of Dy content on the coercivity and remanence of NdFeB. Also shown are the typical applications of magnets containing varying concentrations of Dy. [Arnold Magnetic Technologies]

Praseodymium (Pr)

Additions of Pr to the NdFeB system have been shown to increase the coercivity of the material by the substitution of Pr for Nd atoms. This coercivity increase is due to the higher anisotropy field of $Pr_2Fe_{14}B$ compared to that of $Nd_2Fe_{14}B$. It has also been established that the addition of Pr reduces the spin reorientation temperature of the material [Liu, 2007]; Spin reorientation refers to a change in the preferred direction of magnetisation. In $Nd_2Fe_{14}B$, this spin reorientation transition occurs at around 140 K, below this temperature, the easy direction of magnetisation switches from the c-axis to a cone around the c-axis. In $Pr_2Fe_{14}B$

this change does not occur, and cannot be observed down to 4.2 K [Huang, 1987], meaning that NdFeB materials with small additions of Pr can be used for lower temperature applications compared to $Nd_2Fe_{14}B$.

Copper (Cu)

Pandian (2002) reported that small additions of Cu to the NdFeB system increase the material's coercivity dramatically. Cu addition reduces the grain size in the material, thus increasing coercivity as the grains become more similar to the size of a single magnetic domain. Cu additions also help to smooth the grain boundaries, thus reducing potential sites for reverse domain nucleation [Yu, 2012].
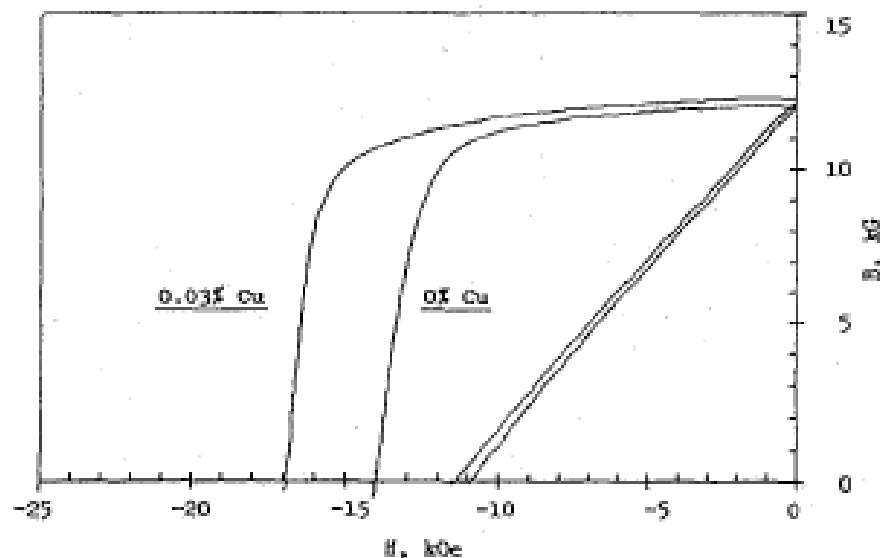
Figure 14 – Demagnetisation curves for NdFeB magnets with and without Cu addition [Kim, 1996]

Although the addition of Cu alone increases the coercivity of NdFeB materials, Cu together with Co has a more dramatic effect. It has been shown that very small additions of Cu do not have a negative effect on the remanence or Curie temperature of the material. Therefore, it

can overcome any negative effects of Co addition and further increase coercivity [Kim, 1995a]. Kim (1995a) theorised that this increase in coercivity with both Co and Cu addition may be caused by a change from the Nd-rich grain boundary phase to a NdFeCoCu intermetallic phase.

Aluminium (Al)

Pandian (2002) stated that Al additions of up to 10 at% bring about significant improvements in the coercivity of NdFeB magnets. The increase in coercivity is due to improved densification and reduced grain size. Improved densification means that there are fewer pores present in the material. These pores act as reverse domain nucleation sites, thus their removal improves the properties of the material. This densification improvement is a result of the Al being liquid at sintering temperatures, increasing the wettability of the Nd-rich phase. This means that the resulting microstructure is closer to ideal, where all grains are embedded in the Nd-rich phase [Knoch, 1989]. With increasing Al content the wetting angle decreases; this effect can be observed in Figure 15. At 5 at% Al addition, there is a small reduction in wetting angle and above 5 at%, larger reductions can be observed.
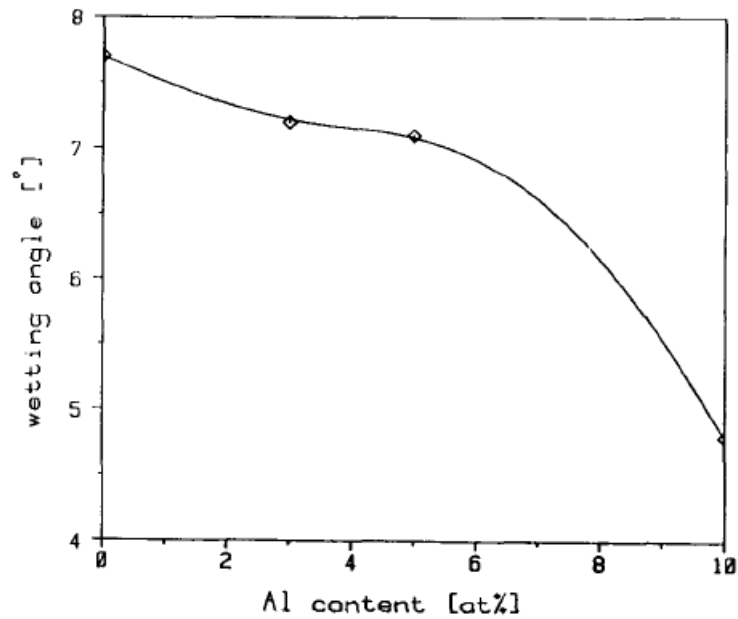
Figure 15 - Wetting angle vs Al content [Knoch, 1989]

It should also be noted that Al, in combination with Co gives further improvements in coercivity than either additions can independently. However, Al addition has the effect of reducing the Curie temperature of the material [Kim, 1995a]. This is a major problem, as NdFeB already has a relatively low Curie temperature and poor temperature stability would limit its possible applications further.

Niobium (Nb)

Nb additions in small amounts are known to improve the magnetic properties in NdFeB type materials, especially intrinsic coercivity [Pandian, 2002]. This improvement is brought about by the substitution of Nb atoms for Fe atoms in the NdFeB phase. The effect of Nb on the magnetic properties of NdFeB can be observed in Figure 16. Coercivity, remanence and BH_{max}

can all be observed to increase up to 1 wt% Nb. Coercivity experiences a further, more rapid, increase up to 1.5 wt%, however, B_r and BH_{max} begin to deteriorate beyond 1 wt%.
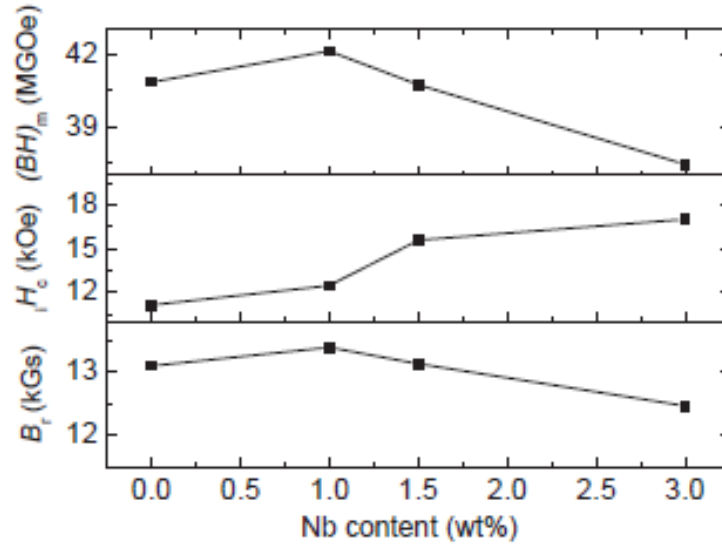
Figure 16 - Effects of Nb content on the magnetic properties of NdFeB magnets [Yu, 2004]

Liu (1992) also investigated the impact of Nb on the precipitation of Fe during casting and found that its presence can reduce the number of precipitates forming. Nb was found to suppress the amount of precipitated Fe by around 50%, as a result the annealing time required to remove these precipitates is greatly reduced.

Commercial NdFeB magnets often contain a mixture of alloying additions in order to bring about the best magnetic properties rather than just having single elements added.

2.12 Recycling Route for Sintered NdFeB Magnets

Use of hydrogen to separate magnetic scrap

Walton *et al.* (2012) demonstrated that hydrogen can be used to separate sintered NdFeB magnets from electrical scrap. This separation process is especially useful for products such as hard disk drives (HDD), where the manual removal of the voice coil magnet would normally be very time consuming. To disassemble a typical HDD, up to 12 security screws must be removed and then the magnet is coated and glued down, adding to the time required to recover it. Currently, scrap hard drives are shredded in order to destroy the data on the disk. HDD's contain 2 types of magnets; The voice coil magnets (VCM), which form part of the voice coil actuator responsible for positioning the read head and the magnet inside the electric motor that is responsible for turning the disk. Typically, HDD's are shredded to destroy the data on the disk. However, the voice coil magnets are very brittle and they break up during this process. This means that the resultant powder, which has retained its permanent magnetisation, sticks to the shredder and to the ferrous components in the scrap. The powder is then lost as a slag during steel production. It is possible to avoid the waste of valuable NdFeB powder by using hydrogen to separate the scrap materials prior to shredding. The HDD's are initially sectioned (as shown in Figure 17) to concentrate the NdFeB fraction and allow a route out for the powdered NdFeB. Then HDD section is then distorted to break the magnets into a few pieces. When hydrogen is introduced the magnetic material decrepitates and becomes demagnetised and the nickel coating peels away from the surface. The demagnetised powder can be removed from the scrap using a porous rotating drum and a series of sieves. This separation method can achieve separation efficiencies of >95%, which would make this technique viable for commercial recycling of NdFeB voice coil magnets [Walton, 2012].

Figure 17 – Sectioned HDD [Walton, 2012]

The HD process can be implemented relatively easily on clean uncoated scrap magnets, as the hydrogen will readily react with this material. In some cases, where the scrap material has been left exposed to air for extended periods of time, an oxide layer can form. This oxide layer can act as a barrier to the HD process, thus preventing or dramatically slowing the initiation of hydrogen decrepitation. There are two possible methods to overcome this problem. The first is to fracture the magnet, thus exposing fresh material, shortly before hydrogen processing. It has been shown that voice coil magnets will react in hydrogen 30 days after they have been fractured [Yi, 2012]. The second method is to score the surface of the magnets, creating an initiation point for decrepitation. Research by Meakin (2013) showed that initiation could be achieved in magnets that had been exposed for months after scoring to a depth of around 3µm. These magnets would close off to hydrogen very rapidly after scoring (~30 mins) [Meakin, 2013].

Processing of hydrogen decrepitated powders

There are a number of options for re-processing the decrepitated powder that has been separated from scrap electrical devices. The different processing routes are as follow:

- Chemical processing to extract Nd from recovered NdFeB alloy

- Re-melt the powder to a master alloy

- Directly re-sinter the separated NdFeB alloy powder

- HDDR processing or melt spinning routes to produce nanocrystalline powder for resin bonded magnets

If the rare earth elements are stripped from the resultant alloy powder then a lot of cost and energy will be associated with re-processing that material back into a new form of magnet.

A very promising route for re-processing of the extracted NdFeB alloy is to directly reuse it to produce new sintered magnets. This method has few processing stages and requires minimal energy input and cost. When the HD process is used to separate sintered magnets from electrical equipment the material retains its original fine microstructure from the starting material, which means the powder requires less milling when compared to cast hydrided NdFeB. It has previously been shown by researchers at the University of Birmingham that sintered NdFeB magnets can be recycled using the HD process, followed by ball milling, pressing and then re-sintering (shown in Figure 18). These recycled magnets retain approximately 80-90% of their original magnetic properties [Zakotnik et al, 2009].
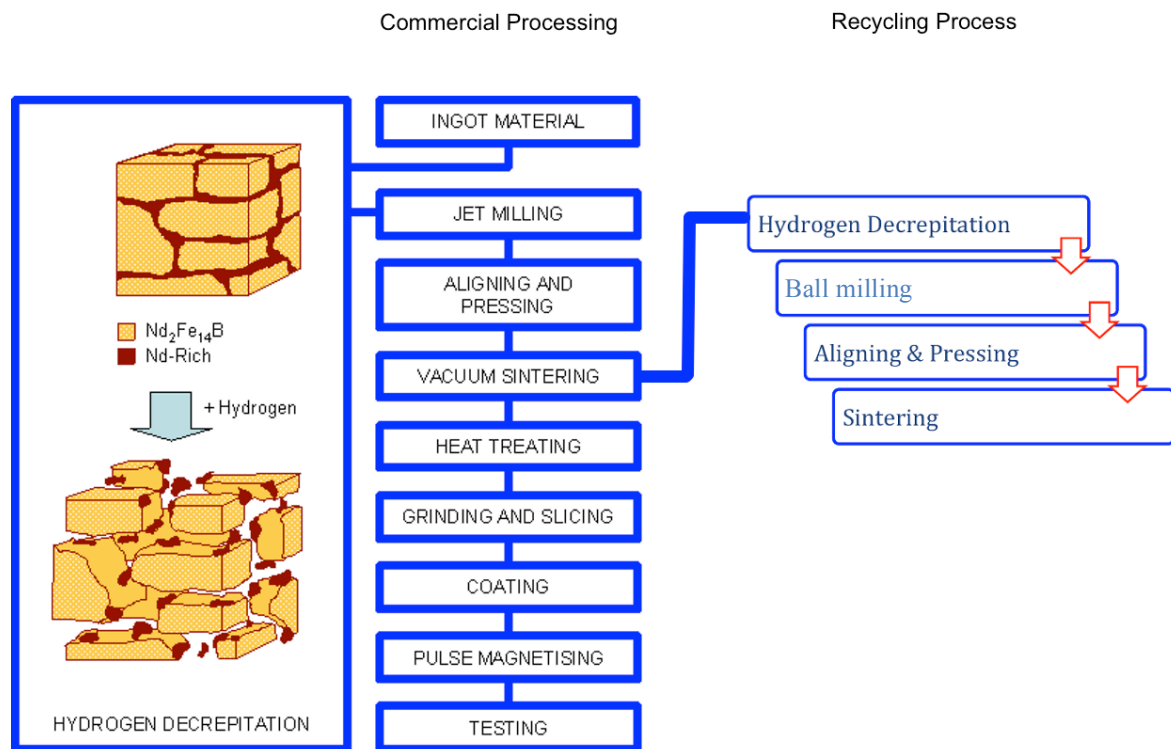
Figure 18 - A schematic showing the conventional processing method for NdFeB permanent magnets compared with the re-sintering recycling route, developed at the University of Birmingham.

2.13 Corrosion of NdFeB

The use NdFeB magnets is often limited because of their poor corrosion resistance. It is generally accepted that NdFeB magnets require some form of corrosion protection to make them suitable for use in a wider range of applications [Cygan, 1995; Drak, 2007; Takada, 1990]. The mode of corrosion is determined by the composition of the surrounding environment and the attack on the magnet may be via an aqueous electrolyte or by direct oxidation.

Corrosion via Aqueous Electrolyte

In environments where water is present, corrosion is much more rapid than when it is dry, especially at high temperatures. It is possible for hydroxides ($NdOH_3$) and hydrogen containing compounds to form in these conditions. Cygan (1994) found that in these, hot and humid, conditions the corrosive attack occurs initially at the Nd-rich grain boundaries and the triple junctions in the material causing the ferromagnetic $Nd_2Fe_{14}B$ phase to loosen and ultimately resulting in the loss of structural integrity. The intergranular attack causes small pits to form in the surface of the magnet. These pits then expose more of the material to the corrosive environment, therefore increasing the rate of corrosion. Yan (2009) studied pit corrosion in NdFeB alloys and identified the chemical reactions taking place. It was shown that H_2O dissociates into H^+ and OH^- ions. The hydrogen ions are then reduced cathodically at the boron rich $Nd_{1+\varepsilon}Fe_4B_4$ phase and the $Nd_2Fe_{14}B$ matrix phase. Some of the hydrogen atoms are absorbed by the $Nd_2Fe_{14}B$ phase and cause lattice expansion and decrepitation. The hydrogen also reacts with the Nd-rich grain boundary phase to form neodymium hydride, resulting in the expansion of the grain boundary phase, leading to mechanical stresses and thus the breakage of the material's microstructure. The corrosion products form in a ring

around the edge of the pit, which can be observed in Figure 19.
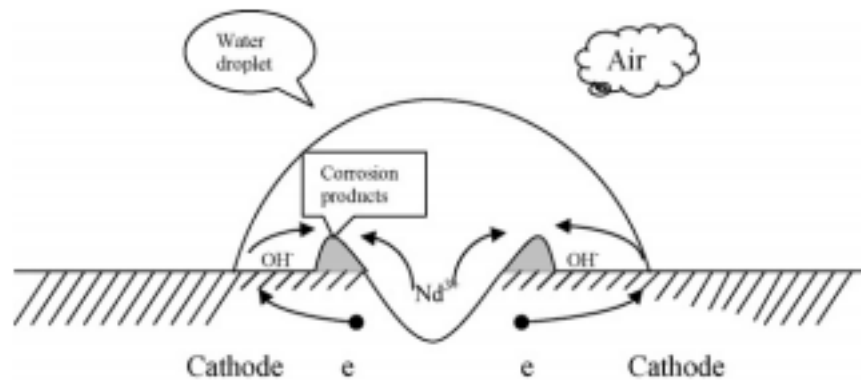
Figure 19 – Schematic diagram of a vertical section of the mechanism for pitting in NdFeB magnets [Yan, 2008]

Jacobson (1987) compared the corrosion behaviour of magnetised and non-magnetised NdFeB alloys. Figure 20 shows Jacobson's findings; it was observed that aerated salt water caused more severe corrosion, and thus weight loss, than distilled water. It is also interesting to note that the magnetised samples corroded less rapidly than those that were non-magnetised. The material loses weight linearly in the distilled water for both magnetised and non-magnetised samples. The non-magnetised material in the aerated salt water lost weight rapidly over time and followed an inverse parabolic rate law due to the localised corrosion attack. The magnetised sample lost weight linearly, but at a faster rate than those in the distilled water. The magnetisation of this sample reduced the corrosion rate, when compared with the non-magnetised sample, by limiting the localised attack and promoting more uniform corrosion [Jacobson, 1987]. It is possible that the reason for the reduced mass loss in the magnetised sample is that the oxidised powder remains stuck to the magnet rather than falling away like it would in the non-magnetised sample. It is not clear from the literature whether the oxidised material was removed from the magnets, therefore these results may not be conclusive.
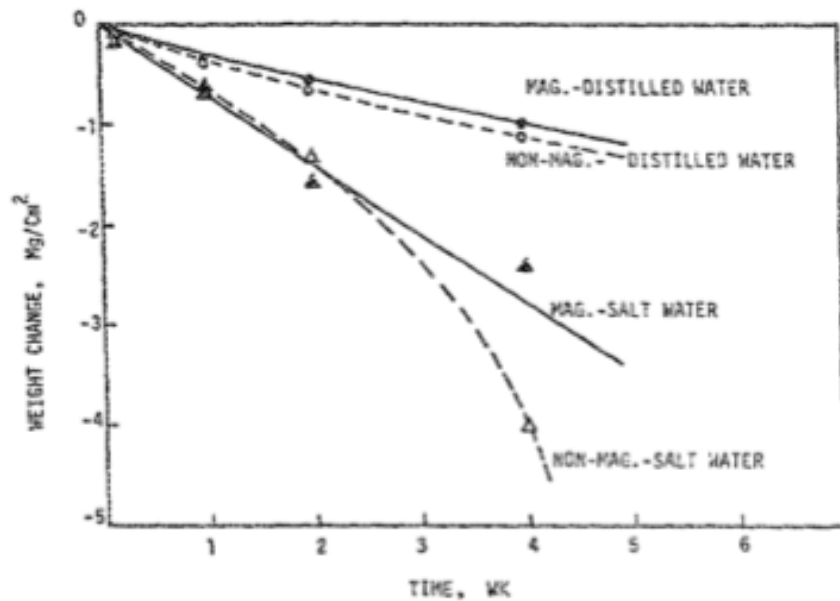
Figure 20 – Weight loss of magnetised and non-magnetised NdFeB alloy in aerated salt and distilled water [Jacobson, 1987]

Direct Oxidation

Oxidation of NdFeB can have a significant effect on the magnetic properties of the material, as well as being problematic when attempting to perform the recycling process using hydrogen decrepitation.. The oxidation behaviour of NdFeB is determined by a number of factors, including; material form (bulk or powdered), temperature, alloying additions and surface finish.

Bulk Samples

Edgley (1997) studied oxidation in NdFeB bulk samples at temperatures between 350ºC and 600ºC. It was found that the $Nd_2Fe_{14}B$ phase dissociates to form a mosaic of α-Fe nanocrystals with small precipitates of Nd oxides and undetermined B compounds. The final

oxidation products from the matrix phase were shown to be Fe_2O_3, NdO and Nd_2O_3. Edgley also showed that the Nd-rich grain boundary phase oxidises to form Nd_2O_3 and that there is no observable change in the composition of the boron rich $Nd_{1+\varepsilon}Fe_4B_4$ phase. These products form a passive oxide layer on the surface of the material, as shown in Figure 21.

Li (2002), who investigated oxidation of NdFeB between 350ºC and 500ºC also found similar transgranular oxide growth. Figure 21 shows where the oxide layer has travelled evenly through the material. However, it was also reported that external scales of Fe_2O_3 and Fe_3O_4 were formed. The main process, however, is internal oxidation where the $Nd_2Fe_{14}B$ matrix phase is dissociated.
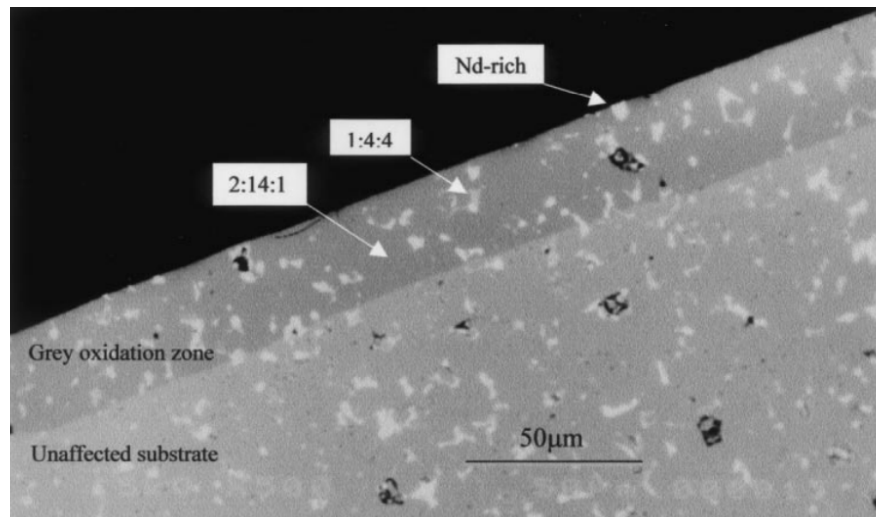
Figure 21 - Back-scattered electron image of a NdFeB magnet after oxidation at 500ºC for 1 day [Li, 2002]

Li (2002) showed that the kinetics of penetration of the zone of internal oxidation are significantly higher than would be expected if oxygen was travelling through the $Nd_2Fe_{14}B$ matrix grains by lattice diffusion. It is clear that another mechanism is taking place and it is possible that the oxygen is following a faster path through the Nd-rich grain boundaries [Li, 2002].

Cygan (1995) stated that up to 150°C, oxidation rates of solid NdFeB in air are relatively low and difficult to characterise. It was shown that when oxidation occurs under atmospheric conditions, an oxide film comprising of an α-Fe matrix containing Nd-oxide particles is produced on the surface of the magnet. This passive oxide layer acts as a barrier to corrosion, thus protecting the magnet from further damage or significantly slowing absorption of hydrogen [Meakin, 2013].

The majority of studies on the oxidation of magnetic materials have been performed at temperatures that are significantly higher than room temperature. This means that more drastic changes are observed in the materials, making the oxidation kinetics easier to characterise. Blank (1987) reported that oxidation between 400 and 600°C produced a grey layer of oxidized material on the surface of bulk materials and that the thickness of this layer increased parabolically with oxidation time. This parabolic relationship was also observed at lower relative temperatures (~150°C). Edgley (1997), who studied the microstructure and composition of the oxide layer, found that the main reaction was the dissociation of the $Nd_2Fe_{14}B$ phase into α-Fe nanocrystals and Nd-oxide particles. However, oxide products have been shown to vary dependent on temperature. Figure 22 shows the difference in oxide products that are formed depending on the temperature at which the material has oxidised.
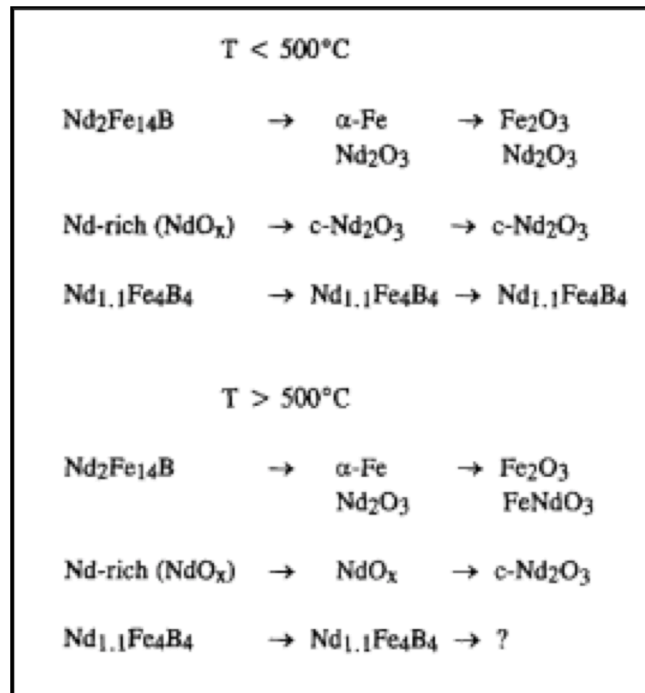
Figure 22 – Chemical reactions observed in the oxidation of NdFeB above and below 500ºC [Edgley, 1997]

Edgley (1993) also showed that, at higher temperatures, there is accelerated oxidation coupled with more extensive oxygen penetration into the material. From Figure 23 it can be observed that the material oxidised at a higher temperature has a much higher oxygen content as well as more extensive oxygen penetration.
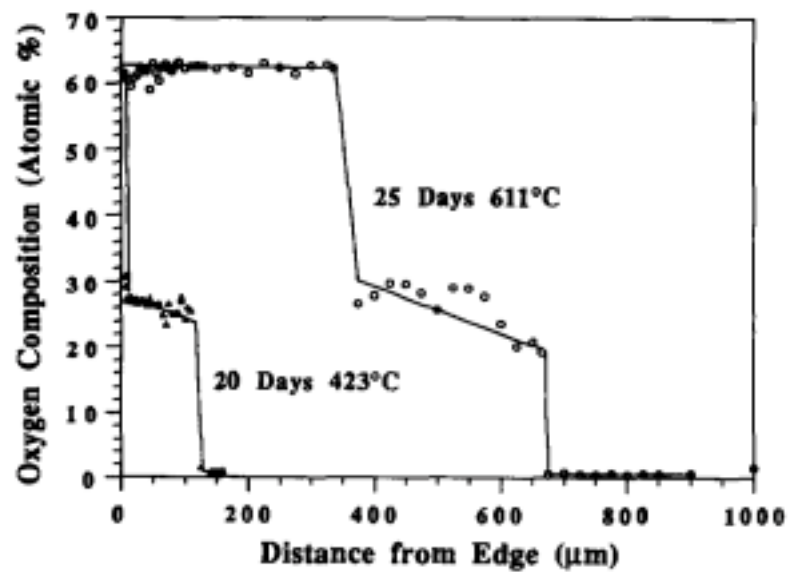
Figure 23 – WDX analysed oxygen profile of oxidised NdFeB magnets [Edgley, 1993]

Meakin *et al.* (2013) investigated the growth mechanism of oxide products on the surface of bulk NdFeB samples at room temperature using 3-D confocal scanning laser microscopy to measure the height of surface triple junctions. It was reported that the oxidation appeared to be exclusive to the Nd-rich triple junctions on the surface of the material. Meakin *et al.* (2013) showed that these surface triple junctions could grow up to a height of around 0.9 μm over a 3 hour period when exposed to air.

Powdered Samples

When NdFeB alloys are in powdered form, oxidation is observed at an accelerated rate compared to bulk materials. This increased oxidation is due to the larger surface area of the powder that is exposed to allow the NdFeB to react with the oxygen in the atmosphere [Higgins, 1987; Lemarchand, 1992; Osawa, 1992]. This does not occur to the same extent in bulk samples because they are more compact and have a smaller exposed surface area [Skulj, 2006]. For these powdered samples, the oxidation reaction exhibits parabolic behaviour

[Higgins, 1987]. Lian (1995) showed that the milling stage of magnet production, where the material is broken down into a fine powder, causes a dramatic increase in the oxygen content of the material (Figure 12). As with bulk samples, the majority of oxidation studies carried out on powdered samples have been conducted at very high temperatures. More work is required in order to characterise the oxidation behaviour of NdFeB powders at room temperature. It is assumed that, other than the increased rate, the mode of oxidation and the oxidation products will be similar to those for bulk samples.

Alloying Additions

It has been shown that additions of Co, Dy, Al, Cu and Nb all have the effect of increasing the corrosion resistance of the material. These improvements can be brought about either by the reduction of grain size in the material or by reducing the reactivity of the material. However, it should be noted that the improvement of corrosion resistance using alloying additions can be accompanied by a sacrifice of magnetic properties [Man, 1996].

Cobalt

When cobalt is added to NdFeB magnets the added cobalt replaces Fe atoms in the matrix phase to form a $Nd_2(Fe_{1-x}Co_x)_{14}B$ phase, which has smaller grains than the normal $Nd_2Fe_{14}B$ matrix phase. These smaller grains mean that NdFeB alloys with added cobalt have a better corrosion resistance [Chandrasekhar, 1999]. The cobalt also alloys with the grain boundaries and triple junctions, leading to the formation of a Nd_3Co or $Nd(Fe,Co)_2$ grain boundary phases, which are less reactive than the Nd-rich phase, thus further increasing the corrosion resistance of the material [Kim, 1996].

Dysprosium

Dy additions to NdFeB magnets have been shown to improve the material's resistance to oxidation when added along with Co [Skulj, 2008]. It is expected that the substitution of Dy atoms for Nd atoms in the $Nd_2Fe_{14}B$ phase is the reason for this improvement as Dy is less reactive than Nd [Hamric, 2007]. Additionally, Yu *et al.* (2004) reported that the corrosion resistance of NdFeB magnets improves with increasing Dy and Nb content. When Dy is added to NdFeB alloys, it distributes through the whole material, including the very reactive Nd-rich grain boundary phase [Dr Allan Walton, personal communication, May. 8]. This will have the effect of increasing the corrosion resistance of the material, as Dy is more environmentally stable than Nd [Hamric, 2007].

Copper

Additions of Cu to NdFeB magnets have the effect of reducing the grain size in the material, thus improving it's corrosion resistance. Scott (1996) suggested that the improvement in corrosion resistance might also be brought about by the more even distribution of the Nd-rich phase. Cu additions also influence the composition of the grain boundary phase, forming NdCu [Ohmori, 1992], which is less reactive than the non-altered Nd-rich grain boundary phase in NdFeB magnetic materials.

The addition of Cu and Co together also improves the material's temperature stability and corrosion resistance, as can be observed in Figure 24. Kim (1995a) showed that the optimum quantities of Cu and Co additions to achieve the best magnetic and corrosion resistance properties are 0.2 at% Cu and 1.2 at% Co.
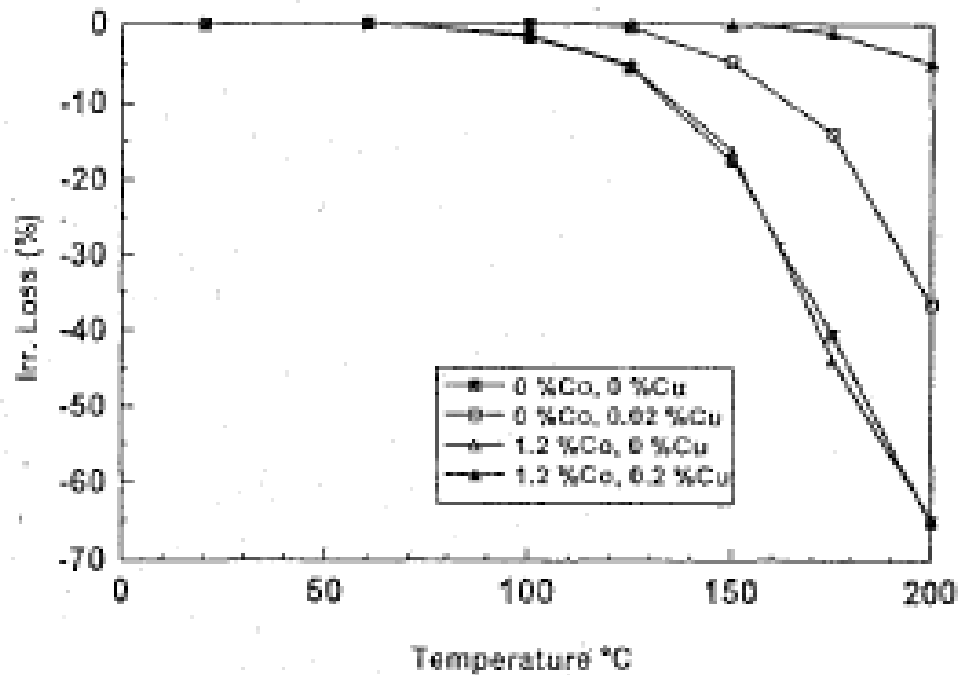
Figure 24 – Irreversible mass loss of NdFeB magnets as a function of Cu and Co content [Kim, 1995a]

Aluminium

Pandian (2002) reported that additions of Al to NdFeB type materials causes a reduction in grain size and improved densification. This reduction in grain size has the effect of increasing the material's corrosion resistance and the improved densification will reduce the number of sites where corrosion can initiate.

Niobium

As well as coercivity improvements, Nb addition improves the corrosion resistance and the temperature coefficient of induction of NdFeB magnets [Liu, 1992]. Nb has been found to suppress the amount of precipitated Fe by around 50%, and as a result the annealing time required to remove these precipitates is greatly reduced. Precipitates must be removed

because of their negative effects on the properties of the material. Their presence causes a reduction in the corrosion resistance of the material, therefore, reduction and removal of these precipitates has the effect of improving the corrosion resistance of NdFeB magnets.

Surface Finish and Coatings

The surface characteristics of NdFeB type alloys have a significant effect on the oxidation behaviour of the material. Samples with a smooth surface finish have a reduced oxidation rate compared to those with a rough surface [Skulj, 2006]. The increase in oxidation rate is due to the larger surface area that is exposed to the atmosphere for rough samples. This effect is similar to the oxidation behaviour in bulk samples compared to powdered samples. Smooth surfaces reduce the likelihood of localised attack and lead to even distribution of oxidation products. Whereas rough surfaces have a much more varied oxide distribution caused by localised attack, which initiates in particularly rough areas.

It is generally accepted that, due to their poor corrosion resistance, NdFeB magnets require some form of protective coating to make them suitable for many applications. Magnets can be coated with a variety of metals such as gold, nickel, zinc and tin plating or with resins and polymers. These treatments form a protective barrier to corrosive environments, allowing the material to be used in a much wider range of applications. While many magnets are coated with a single layer of protective material, its effectiveness is not always assured.
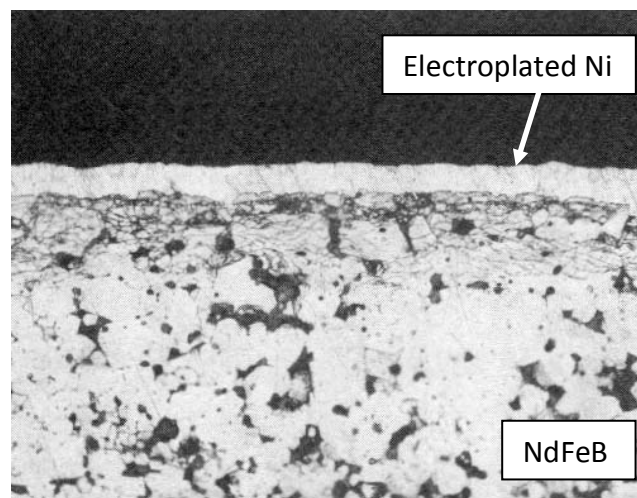
Figure 25 – SEM image of electroplated Ni protective coating on a NdFeB magnet [Ribitch, 1990].

3.0 Aims and Objectives

3.1 Project Aims

Magnetic scrap can come in many different forms including coated voice coil magnets from hard disk drives and large, uncoated magnets that have been removed from large commercial assemblies such as rotors from electric vehicles. In many cases, the scrap material will have been stored for extended periods of time, which could result in significant oxidation on their surface. This oxide layer can cause problems for initiation of hydrogen during the HD recycling route, which means that magnets must be fractured or scored in order to break up the surface oxide and make the HD process more effective. When this fracturing or scoring is carried out, newly exposed, fresh material can oxidise quickly. Therefore the first aim of this project was to investigate the oxidation behaviour and kinetics of sintered NdFeB magnets in order to refine the recycling process for rare earth based permanent magnets. This was achieved by studying the kinetics and characteristics of surface oxidation using confocal laser microscopy and raman spectroscopy and investigating the depth of penetration of oxygen with time using secondary ion mass spectrometry (SIMS). The characterisation of the oxidation behaviour was performed at room temperature, rather than high temperatures, in an attempt to fill a gap in the current literature on the subject. During re-processing of sintered NdFeB magnets it is not clear how much oxygen the magnets are picking up. Therefore, the second aim of this work was to investigate oxygen pick up at each stage of the re-sintering route., including a new burr milling technique.

3.2 Objectives

- To study the surface oxidation/corrosion behaviour of NdFeB commercial sintered magnets of varying compositions at room temperature, in air.

- To determine the composition of the triple junction reaction products on NdFeB magnets on exposure to air.

- To study the depth of oxygen penetration in bulk NdFeB samples.

- To identify the stages in the recycling process at which oxygen levels are increased.

- To determine whether surface oxidation constitutes a significant fraction of the overall oxygen content of the recycled magnet.

4.0 Methodology

4.1 Materials

Two sources of scrap sintered NdFeB magnets were used in this project in order to study two different commercial magnet compositions. The two magnets were used for different applications. The voice coil magnets, supplied by Phillips, were used in a relatively low end application (hard disk drive) compared to that of the square material, supplied by Ugimag, which is likely to have been used in a motor application.

Square material (SQ)

NdFeB sintered magnets from Ugimag. These magnets did not have a protective coating and had been stored in air for over 10 years. ICP data is shown in Table 3. Oxygen content – 4510 ppm

Voice coil material (VC)

Recovered hard disk drive (HDD) magnets were supplied by Phillips. These magnets had a nickel protective coating, which was removed using a scalpel before testing. ICP data for this material is shown in Table 3. Oxygen content – 5080 ppm

At%	Al %	B %	Co %	Cu %	Dy %	Fe %	Nd %	Pr %	Nb %
SQ	0.88	6.44	4.98	0.04	1.80	72.50	12.52	0.17	0.62
VC	0.75	6.01	1.44	0.09	0.53	77.89	11.61	1.59	0.00

Table 3 – ICP data for the square material (SQ) and voice coil material (VC) used in this project (there are other minor additions not being included). All values are shown in At%

4.2 ICP Analysis

Inductively Coupled Plasma Spectroscopy (ICP- Optima 5300V) was performed at Less Common Metals Ltd in order to ascertain the composition of the materials.

4.3 Oxidation Studies

Once the samples from each material composition had been cut to size, they were mounted in Bakelite and transferred to an argon filled glove box. All sample preparation after this point was performed inertly in order to minimise exposure to oxygen. The samples were ground using P400, P800 and P1200 silicon carbide grinding paper in cyclohexane. This grinding was performed in order to remove the oxide layer from the sample surface. The samples were then polished using 6μm, 1μm and 0.25μm diamond polishing paste and polishing cloths. The samples were then transferred to the microscope under an argon atmosphere in sealed sample bags, which were also inside a sealed argon filled kilner jar. This was to minimise the samples' exposure to oxygen prior to being observed under the microscope.

4.4 Confocal Microscopy

The samples were imaged using a confocal scanning laser microscope (LEXT OLS3100) at 100x magnification in air. Samples were transferred under argon from the glove box to the confocal microscope after they had been polished. Each sample was scanned at set intervals over a 3 hour period. Scans were taken every 5 minutes for the first hour and then every 10 minutes for the remaining 2 hours. The resulting images were analysed using step measurement readings to measure the height of the cumulating oxide at its highest point for a series of NdFeB triple junctions. The height measurement values were then averaged to give a mean value for the height of oxidation growth at the different time intervals.
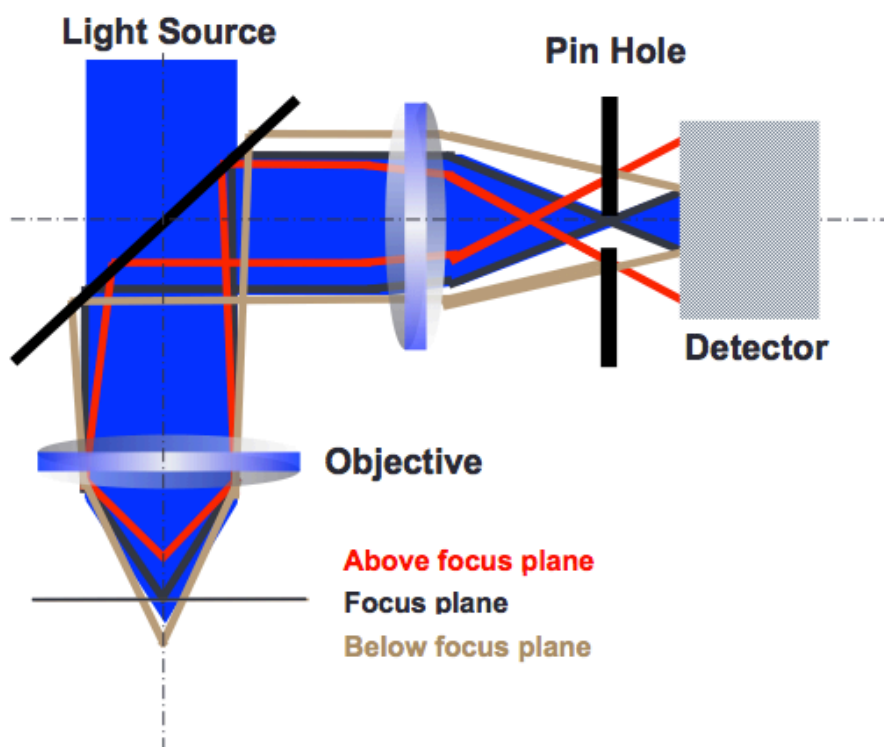
Figure 26 – Schematic of a confocal scanning laser microscope.

4.5 Raman Spectroscopy

Raman spectroscopy was used to investigate the composition of the oxide/corrosion product that was found on the Nd-rich triple junctions. Samples were ground and polished in argon before being left to oxidise for 3 hours in air. The spectra were taken using a Renishaw inVia Raman Microscope equipped with a confocal microscope. The wavelength used was 633nm. Pure Nd_2O_3 was supplied by Sigma Chemical Co. (N-1751. Lot 129F0287). Pure Dy_2O_3 was supplied by Sigma Chemical Co. (D-0381. Lot 123H3508).

4.6 SIMS Testing (Secondary Ion Mass Spectrometry)

Voice coil magnets had their Ni coatings removed using a scalpel and tweezers before being cut to size (using a diamond cutting wheel) according to the dimensions required for the SIMS instrument used (ION-TOF GmbH). Samples of SQ material were also cut to the required size using a diamond cutting wheel. Once they had been cut to size, they were transferred into an argon filled glove box. All samples were ground and polished inertly in the same manner as described for the oxidation studies. Each sample was then exposed to air for set time periods for comparison. There were 5 samples in total exposed for 30 minutes, 1 hour, 3 hours, 6 hours and 24 hours. Samples were transported from Birmingham to Nottingham for testing inside samples tubes under argon, which were then sealed in argon filled kilner jars. Transferring samples into the SIMS instrument could not be performed inertly, however, no sample was exposed to air for more than 3 minutes. Once all of the samples had been loaded into the SIMS instrument, the chamber was evacuated as quickly as possible ready for testing.

ToF-SIMS measurements were performed using an ION-TOF GmbH system using a 5 kV Cs^+ ion sputter source. The sputter crater was 250×250 μm with an analysis area of 100×100 μm (rasterring 256×256 pixels). A 25 kV Bismuth ion analysis source was used to obtain data. In this system, the secondary ions are accelerated up to 10 kV energy before being analysed.
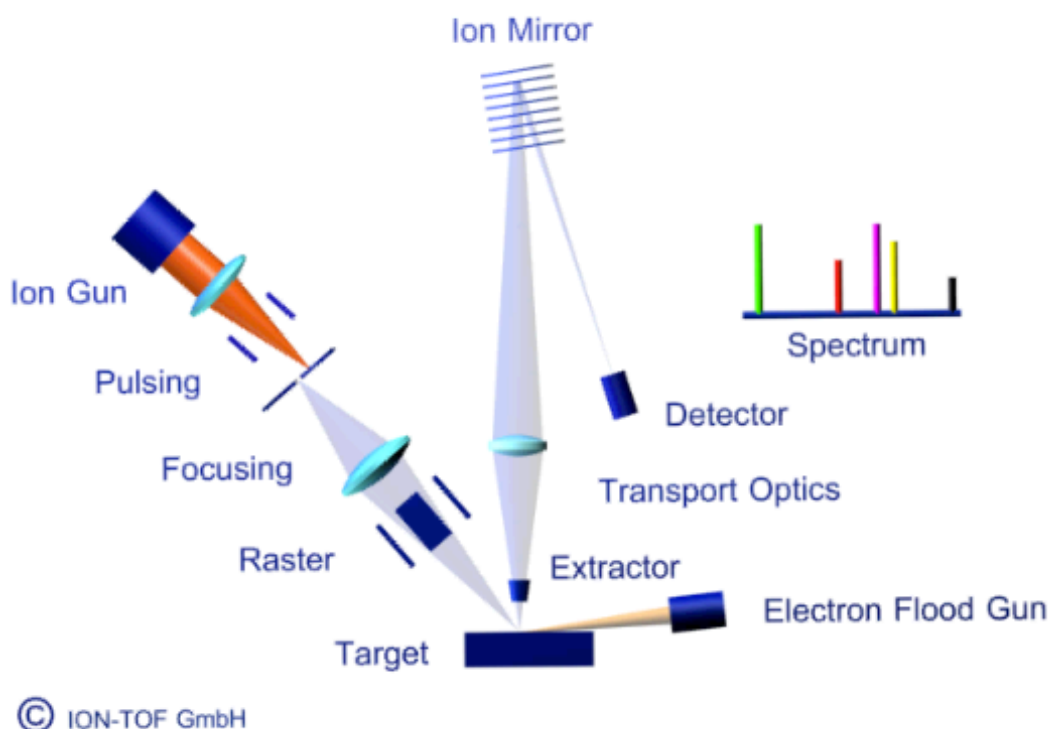
Figure 27 – A schematic of the ToF-SIMS apparatus used for this study
[http://serc.carleton.edu/18395]

4.7 Recycling and Oxygen Analysis

The stages of the recycling process are both explained below and also shown in Figure 31.

Breaking Magnets/Removing Nickel Coatings

Sintered Ugimag Magnets (SQ material) were fractured using a uniaxial press to produce a clean surface. The material was then placed in a HD vessel ready for hydrogen processing. The voice coil magnets were stripped of their Ni coatings, using a scalpel and tweezers, to expose the NdFeB material inside. These stripped voice coil magnets were then placed into a HD vessel. All processing after this point was performed inertly to minimise exposure to

oxygen. A schematic diagram is shown in Figure 31 of the processing steps that were undertaken.

HD Processing

The HD vessel was evacuated and then backfilled with hydrogen at 2 bar and at room temperature. During hydrogen absorption, the gas pressure was maintained at 2 bar by manually opening and closing a valve. Once the material had fully decrepitated, the vessel was evacuated and sealed before transferring into an argon filled glove box. The powder was then removed from the HD vessel and stored in a sealed sample bag inside a kilner jar.

Figure 28 – Image showing the HD Processing equipment used for this project.

Burr Milling

The HD powder was ground using an electric coffee grinder, which uses a form of burr milling. A burr mill uses two revolving abrasive surfaces to break up the material. The HD powder is very friable and hence breaks up very easily; the resulting, finer, powder was

passed through a 45µm sieve. 15g of sieved powder was collected for the next stage of the recycling process. The 15g of powder required for each recycled magnet was milled when required in order to limit any potential for oxidation in the glove box (reduced particle size increases the risk of oxidation). The sieving procedure used for this project has previously been used by researchers at the University of Birmingham.
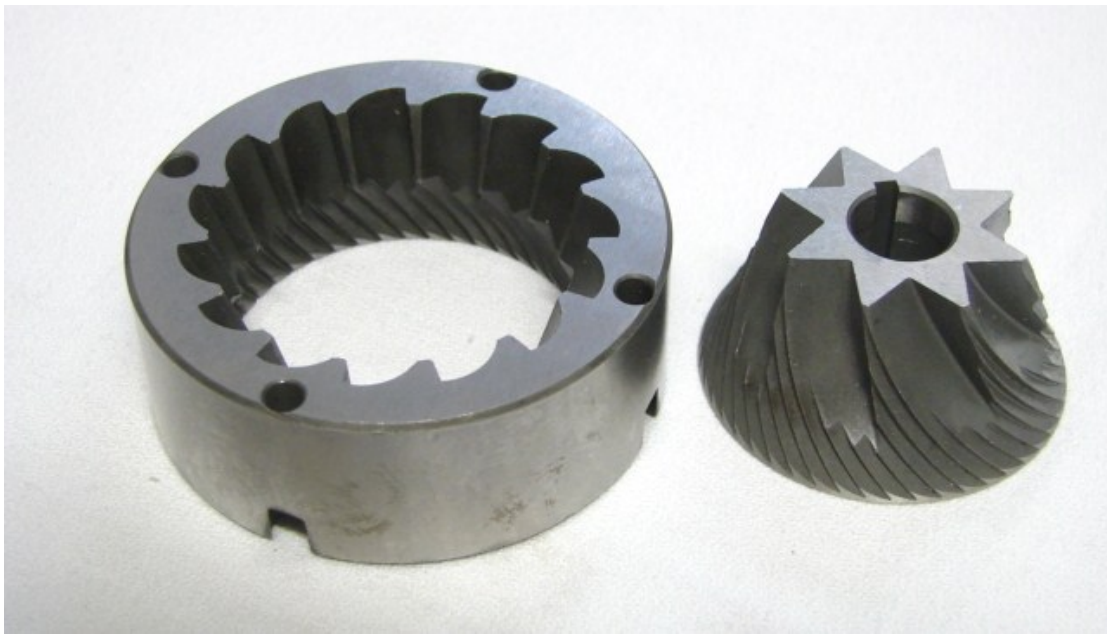
Figure 29 – Image showing the two revolving abrasive surfaces in a burr mill.

Aligning and Pressing

The 15g of <45µm sieved powder was placed into an isostatic bag and sealed using a bung and electrical tape. The powder was aligned using a pulse magnetiser and each sample was pulsed 4 times to ensure proper alignment. The powder was then isostatically pressed to 10 tons before being transferred back into a glove box.

Sintering

The green compact was then transferred from the isostatic bag into a 321 stainless steel foil tube. This was then placed in a vacuum furnace tube (shown in Figure 30) with a valve on the end. The furnace tube was sealed and transferred into a vacuum sintering rig. Next, the system was evacuated to 8.3 x 10^{-2} mBar and the furnace was ramped at 400°C per hour up to a temperature of 1070°C. The temperature was then held at 1070°C for 1 hour before the furnace was cooled. After the furnace was fully cooled, the valve on the furnace tube was closed again and it was transferred back into the glove box. The sintered magnet was removed from the furnace tube and stored inside a sealed sample holder in a kilner jar.
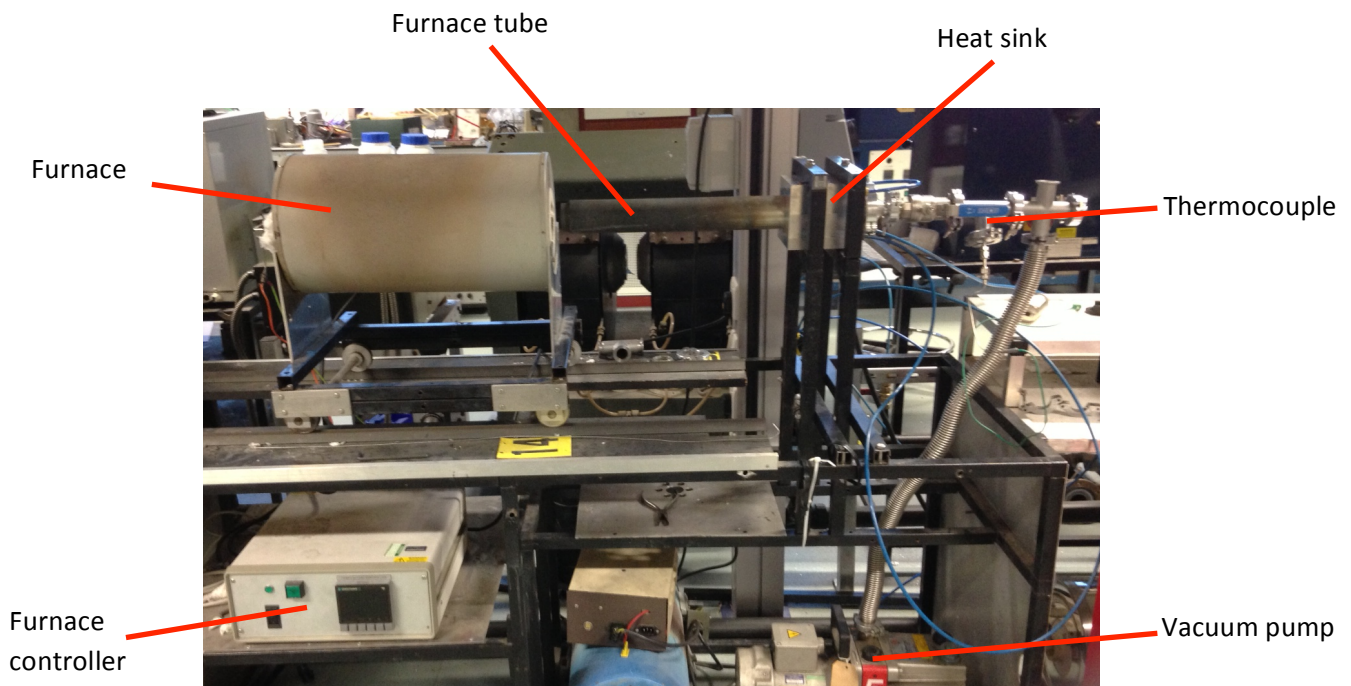
Figure 30 – Image showing the sintering furnace used for this project.
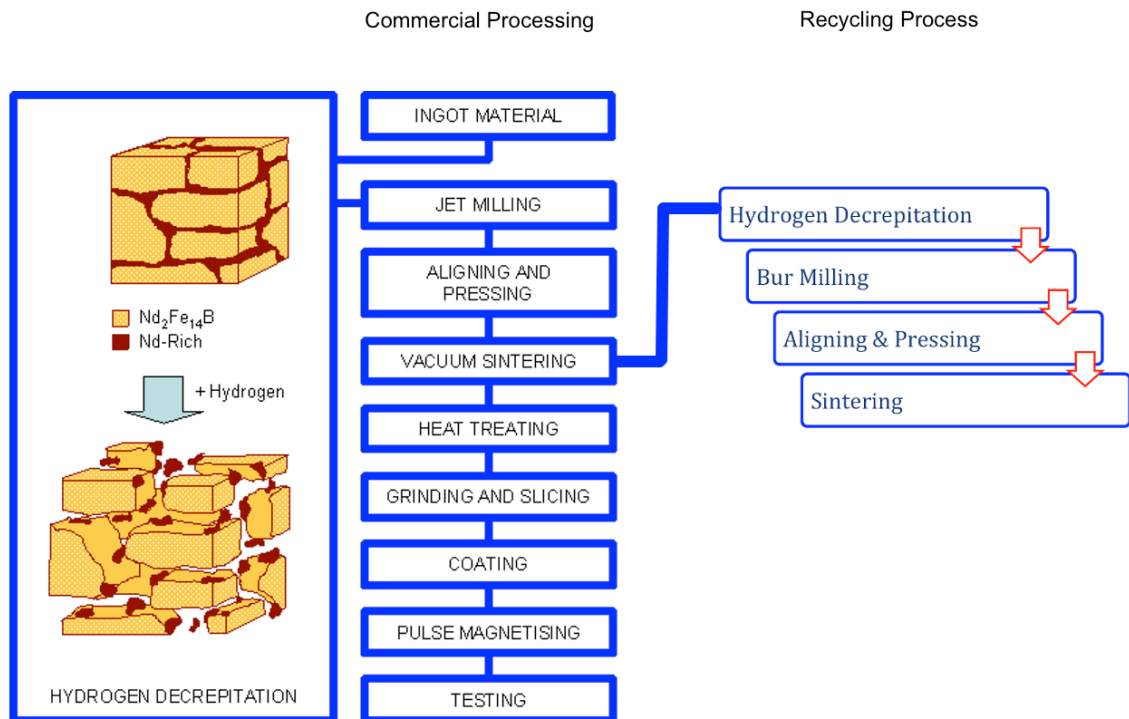
Figure 31 – A schematic showing the conventional processing method for NdFeB permanent magnets compared with the recycling process, developed at the University of Birmingham.

Optical Microscopy

The <45µm sieved powder was placed on to a mirror and spread out using a magnet on the under side. The powder was spread out in this way because it is prone to clumping together, thus making it difficult to image the individual particles. An optical microscope was then used to image the powder. A mirror was used in order to increase the amount of light that is reflected back into the microscope. A small amount of powder was placed on to the mirror and then a magnet was used underneath to spread the powder out as evenly as possible. This allows a better image of the individual particles to be produced. Particle size was measured using the image analysis software, JMicrovision.

Oxygen Analysis

To study the oxygen content of the material throughout the recycling process, 8 samples from each stage of the process were prepared (4 square material and 4 voice coil material for comparison). The 5 stages of the recycling process are as follows:

1. Starting material

2. HD powder

3. Burr milled powder passed through 45μm sieve

4. Green compacts

5. Sintered magnets

All powder samples were weighed out to 15g inside the argon filled glove box and then placed in a sample holder, which was sealed with electrical tape. The samples holders were then stored inside sealed sample bags, each of which were then sealed inside kilner jars. The sintered samples were prepared as explained in the Sintering section on page 58 and then stored in the same way as the powder samples. The samples were then analysed using a LECO TC 136 oxygen analyser at Less Common Metals.

5.0 Results and Discussion

5.1 ICP Analysis

ICP analysis (Optima 5300V) was carried out on both starting sintered magnets (SQ and VC) so that predictions could be made about their comparative oxidation/corrosion behaviour. The data is shown below in

At%	Al %	B %	Co %	Cu %	Dy %	Fe %	Nd %	Pr %	Nb %
SQ	0.88	6.44	4.98	0.04	1.80	72.50	12.52	0.17	0.62
VC	0.75	6.01	1.44	0.09	0.53	77.89	11.61	1.59	0.00

Table 4 – ICP data for the square material (SQ) and voice coil material (VC) used in this project (there are other minor additions not being included). All values are shown in at%

From Table 4 it can be observed that there are a number of compositional differences between the square material and the voice coil material. The ICP data shows that the square material is richer in Nd compared to the voice coil material. This is due to the fact that this material was being used in applications where higher coercivities were required. The data also shows that the high rare earth square material has significantly larger quantities of Co and Dy, which again give higher coercivity values.

The oxygen content of the two materials also differs. The square material (4510 ppm) contains a smaller amount of oxygen when compared with the voice coil material (5080 ppm), which could be for a number of reasons. It is possible that this material was contaminated as a result of poor manufacture. It has also previously been shown that oxygen can be introduced to the material during the coating process [Walton, 2001].

5.2 Confocal Microscope Oxidation/Corrosion Studies

In order to characterise the surface oxidation/corrosion behaviour of sintered NdFeB magnets, 3-D confocal microscopy was used to image the Nd-rich triple junctions on the polished surfaces of both SQ and VC magnets. This technique was previously used by Meakin *et al.* (2013), who showed that the triple junctions on VC NdFeB magnets can preferentially oxidise/corrode compared to the matrix phase. These images were then used to measure the growth rate of these triple junctions through time as they oxidise/corrode for different compositions. The results for the oxidation/corrosion studies conducted in this project are presented below.
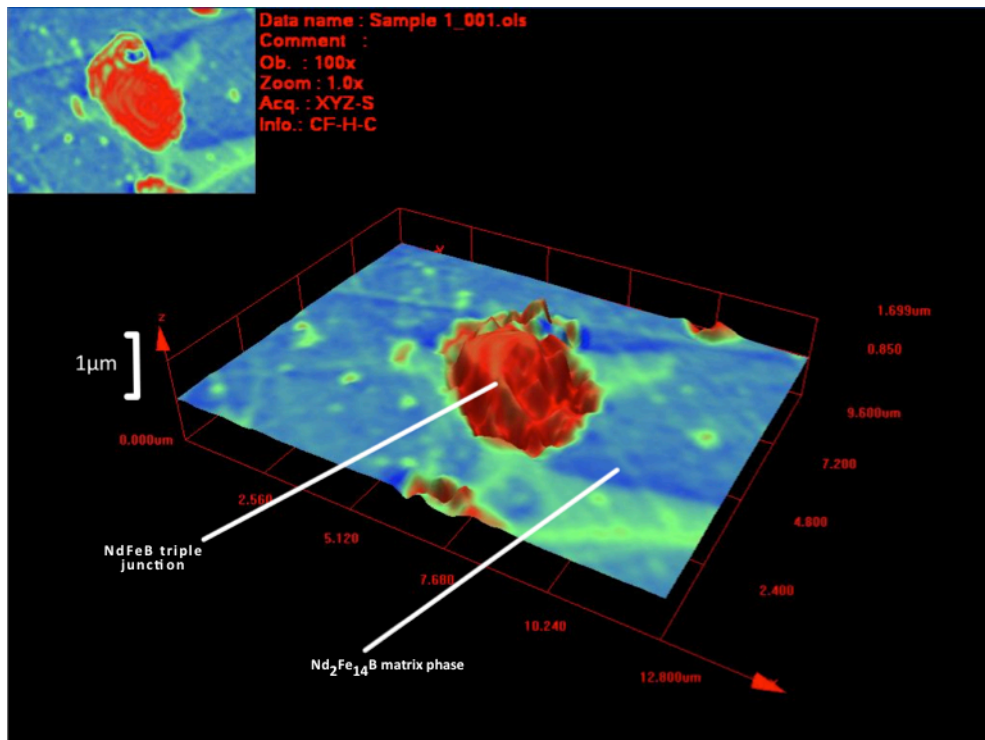
Figure 32 – 3-D confocal microscope image of a NdFeB triple junction imaged at 100x magnification (SQ material). The colours represent the height of the different regions; red shows higher regions, while blue shoes the lowest regions.

Figure 32 shows a 3D image of a NdFeB triple junction on the surface of the SQ material produced using a 3-D confocal scanning laser microscope. It was shown that the Nd-rich triple junctions on the surface of the sintered magnets expanded preferentially compared to the matrix grains. This finding lends support to the theory put forward by Li (2003), who suggested that it is possible that the oxygen follows a faster path into the material via the Nd-rich grain boundaries. It was observed that, as time progressed, the triple junctions were measured to increased in height. This observation is representative of the majority of the NdFeB triple junctions present on the surface of the bulk samples that were tested. Some of the larger triple junctions do not show such a dramatic increase in height. This is because the oxide/corrosion product layer spreads out over the larger surface area. As the material oxidises/corrodes, it grows upwards. However, with the larger triple junctions this column of material appears to collapse, and spread out over the whole triple junction. Oxidation/corrosion appears to be selective for different regions within each triple junction. This uneven growth could be caused by the presence of different compositions and crystal structures within the triple junction, resulting in a number of different oxidation/corrosion products [Shinba, 2005; Woodcock, 2012], This could also lead to different oxidation/corrosion rates. It could also be that a combination of oxidation and corrosion has taken place leading to the uneven growth of the reaction products. This pattern of uneven growth within individual triple junctions is also mirrored in the VC material, as can be observed in **Figure 33**. Raman spectroscopy was used in an attempt to identify the oxidation/corrosion products and these results are presented in section 5.3.
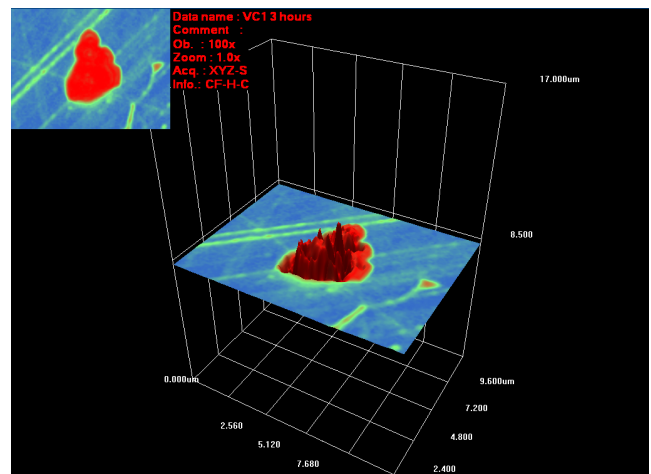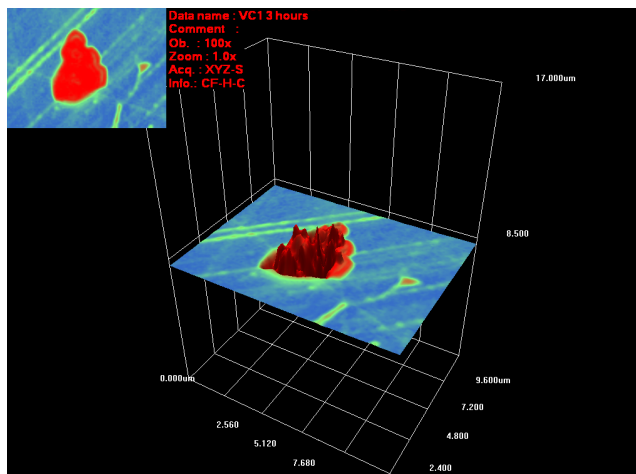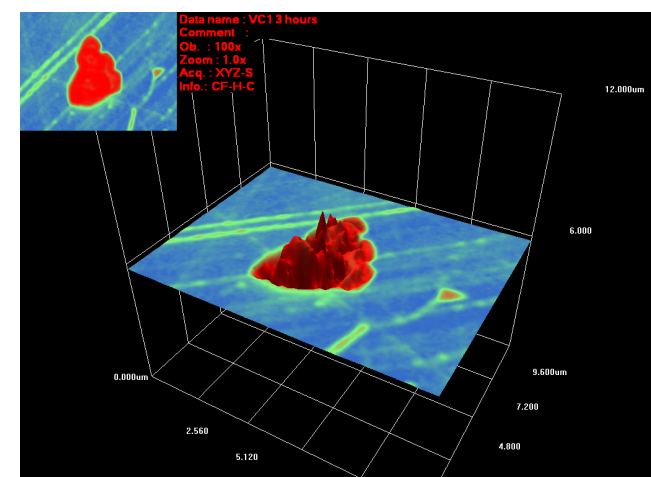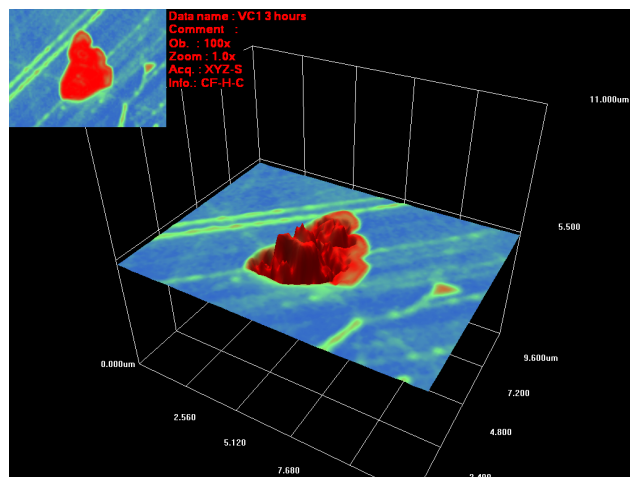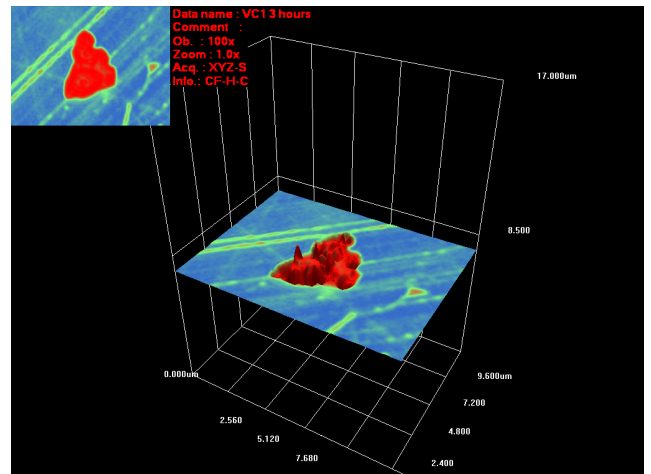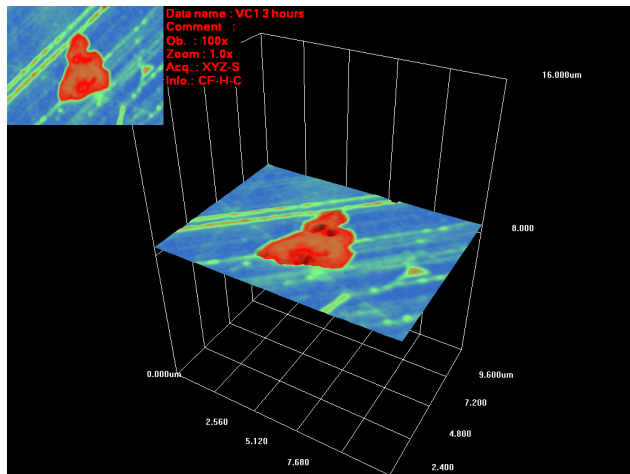
Figure 33 – 3-D Confocal microscope images showing the growth of a NdFeB triple junction throughout the 3 hour experiment imaged at 100x magnification (VC material).

Figure 33, above, shows a series of 3-D confocal microscope images of a single triple junction on the surface of the VC material at different stages throughout 3 hours of exposure to air.
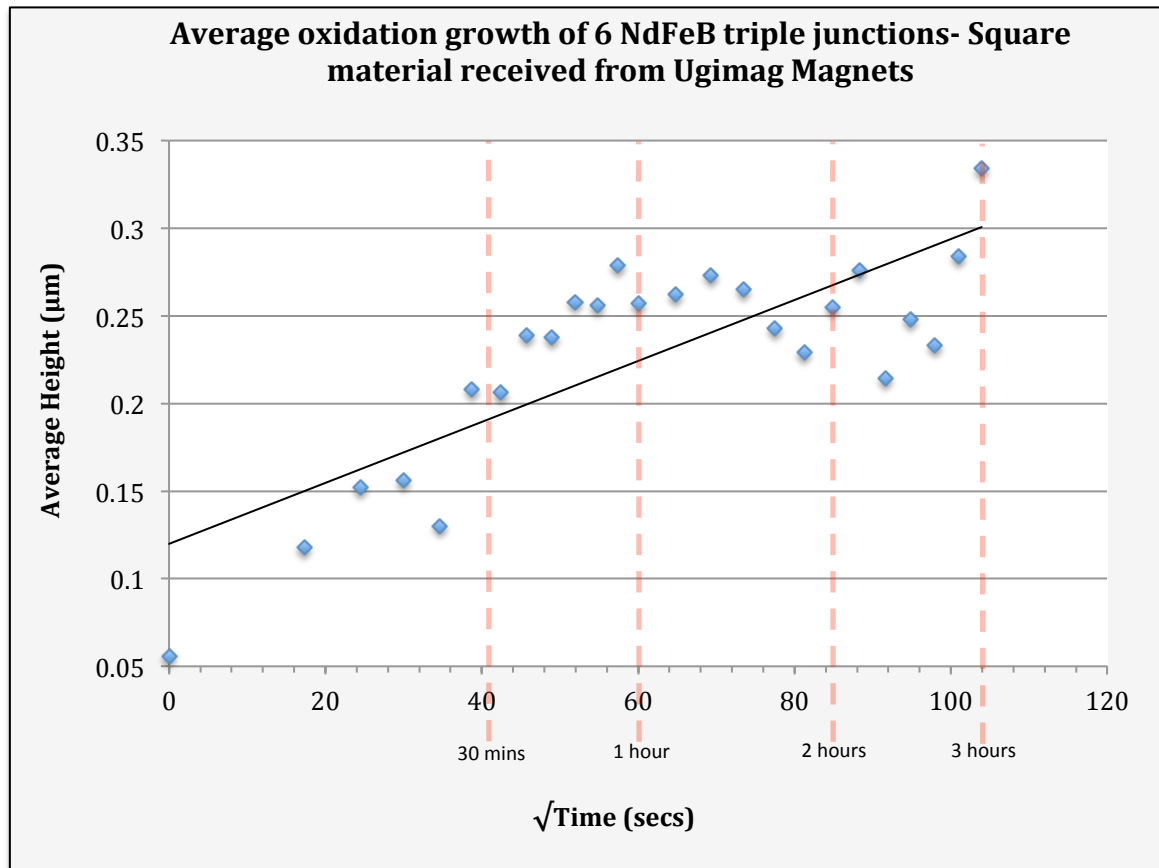
Figure 34 –Average oxidation/corrosion growth of 6 NdFeB triple junctions- Square material received from Ugimag Magnets.

Figure 34 shows the average oxidation/corrosion growth of 6 NdFeB triple junctions in the SQ material, which were exposed to air over a 3 hour period. Line scans were taken of the highest point on each triple junction in relation to the matrix phase and then averaged. An example of one of these line scans is shown in Figure 35.
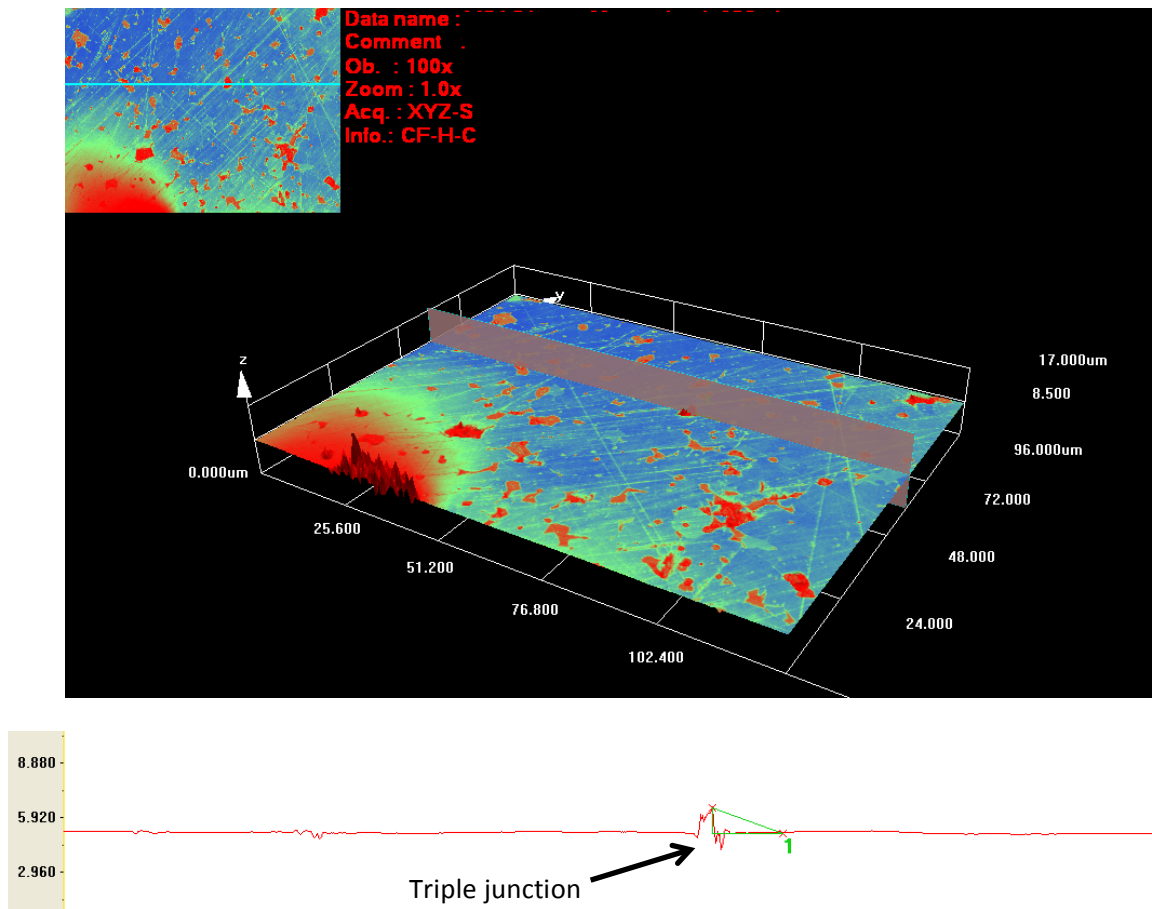
Figure 35 – Line scan of a surface triple junction. VC material.

The reference point for the measurement shown in Figure 35 is the matrix phase (shown in blue). It is possible, however, that the matrix phase moves during the course of the experiment. The LEXT OLS3100 confocal microscope is accurate to 20 nm and it is also possible that this error could influence the triple junction height measurements.

The data in Figure 34 can be observed to form a wave like shape, where growth is constant up to about 0.25 µm. The triple junctions then appear to shrink as time elapses, before growing past the height that was previously achieved. This wave like trace is possibly caused by the structural collapse of the growing triple junctions. The oxide/corrosion product then builds up again and grows beyond the height of the previous peak. It should be noted that the oxidation

rate observed here is likely to be slower than would be seen for un-polished scrap material, as the grinding and polishing of the sample reduces the surface area that is exposed to air.
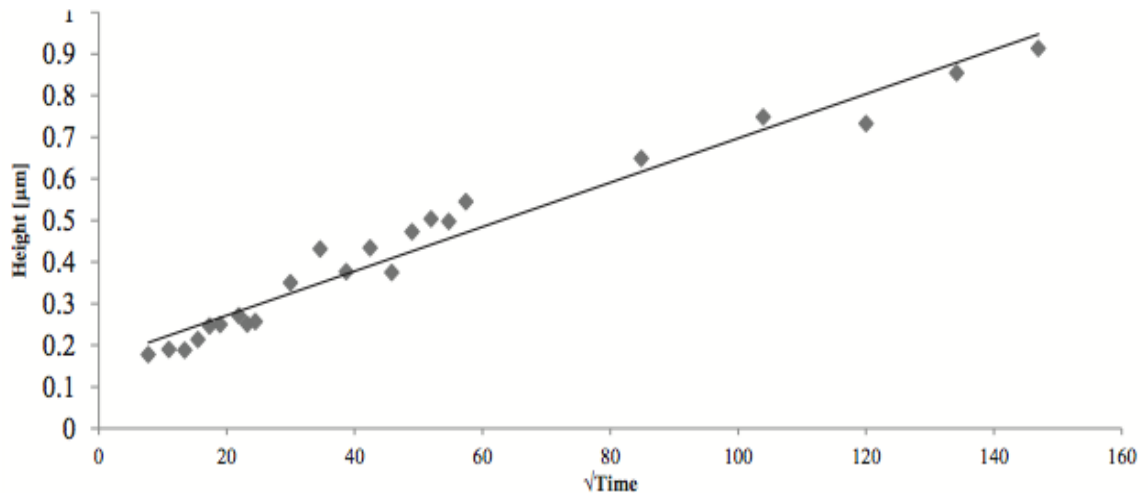
Figure 36 – Change in grain boundary triple junction height measured by confocal microscopy against the root of time for a sample exposed to air at room temperature. VC material [Meakin, 2013].

Figure 36 shows the change in height of surface triple junctions on the surface of the VC material. It can be observed that the oxide/corrosion growth is linear over the 3 hour experiment. By comparing Figure 34 and Figure 36 it can be observed that, over a 3 hour period, the triple junctions on the VC material grew to a greater extent. It can be observed that the VC triple junctions grew to approximately twice the height of the triple junctions on the surface of the SQ material.

Voice Coil Material Pit measurements

An interesting observation that can be made from these confocal microscopy studies of surface oxidation/corrosion is the existence of pits within the surface of the material. Pits tend to form due to the pull out of the NdFeB matrix grains and triple junctions during polishing. The formation of these pits via matrix grain pull out is illustrated in

Matrix grain pulled out as a result of grinding and polishing

$Nd_2Fe_{14}B$ matrix grain

Nd-rich grain boundary phase

Grinding and polishing
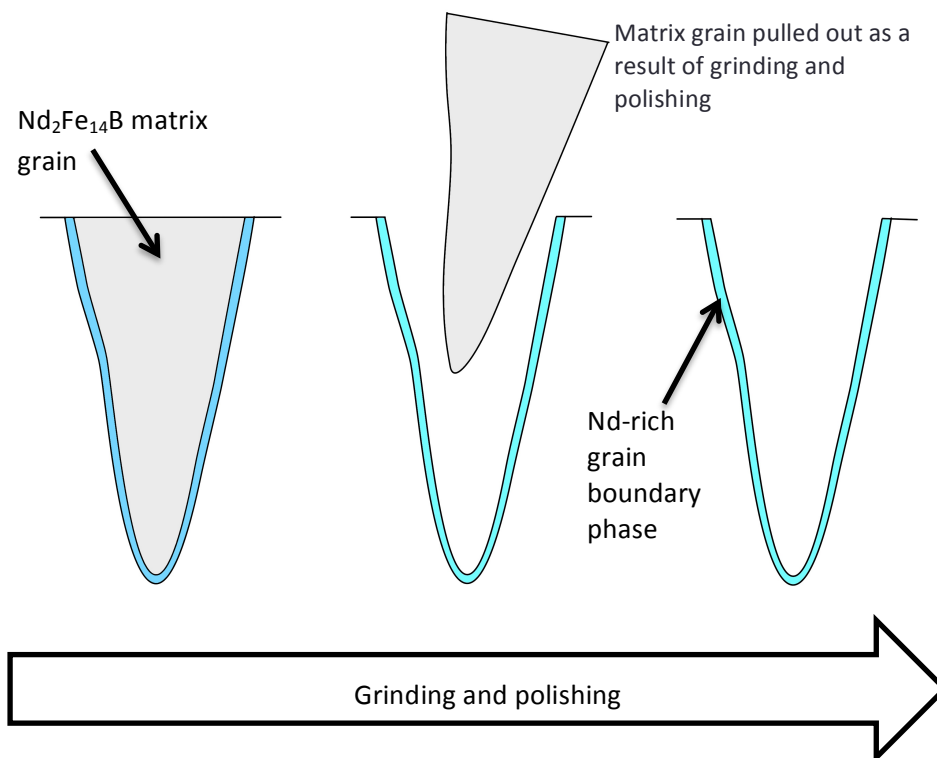
Figure 37 – A schematic showing how grinding and polishing may cause a pit to be formed in the surface of a NdFeB alloy

These pits, as shown in Figure 38 can be observed to 'fill up' during atmospheric exposure over the course of 3 hours. The rate at which these pits fill up appears to be more rapid than the oxide/corrosion growth observed on the surface of flat triple junctions. It is possible that,

when the NdFeB matrix grains are pulled out during grinding, the Nd-rich grain boundary phase is left behind. This would expose a significantly larger surface area of Nd-rich material with a rough (highly reactive) surface compared to the triple junctions on the surface of the material. This large area of Nd-rich, highly reactive material could then oxidise/corrode at an increased rate to fill the pit. It is possible that, as the pit is filled, the rate of oxidation/corrosion would decrease as the exposed surface area decreases in size and becomes more similar in size to that of a surface triple junction. More research is required to determine the exact process that is occurring within these pits.

Figure 38 shows a comparison of the pit measurements for the voice coil material imaged at the start of the experiment and again after 3 hours. When comparing the measurements, it is clear that these pits are being filled by oxidising material. The average change in depth over the 3-hour period, for the voice coil material, is 0.86μm, which is a larger change in height than is observed on the surface triple junctions (0.3-0.7μm).
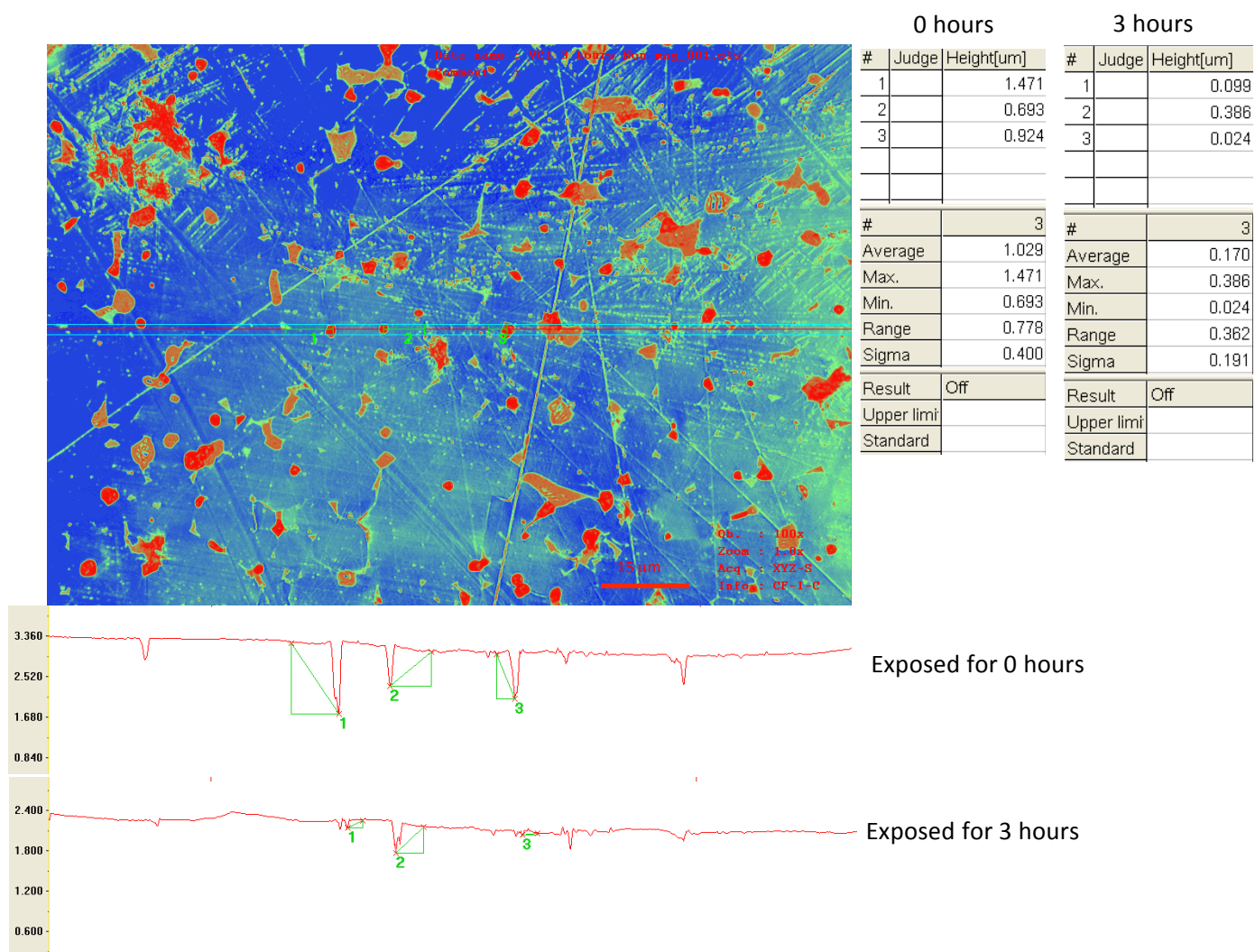
Figure 38 – A comparison of depth measurements of surface pits in the VC material taken from 3-D confocal microscope line scans.

SQ Pit Measurements

No.	Height (μm)	
	0 hours	3 hours
1	0.276	0.155
2	0.579	0.515
3	0.559	0.497
Average	0.471	0.389

Exposed for 0 hours

Exposed for 3 hours
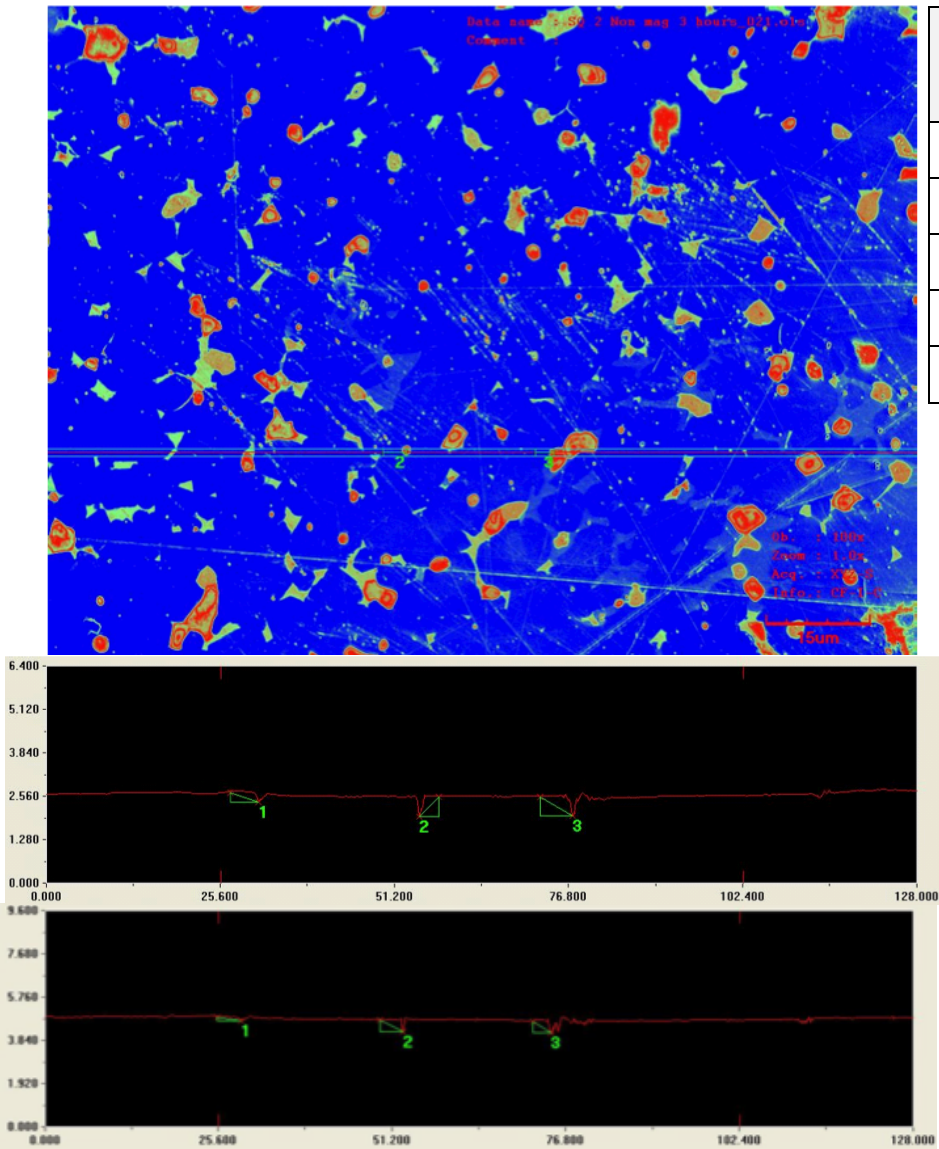
Figure 39 – A comparison of depth measurements of surface pits in the SQ material taken from 3-D confocal microscope line scans.
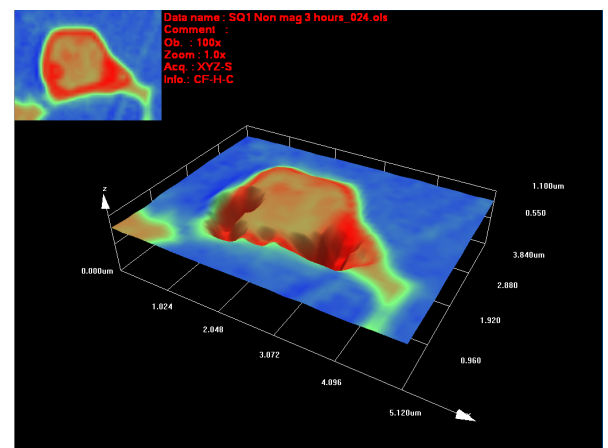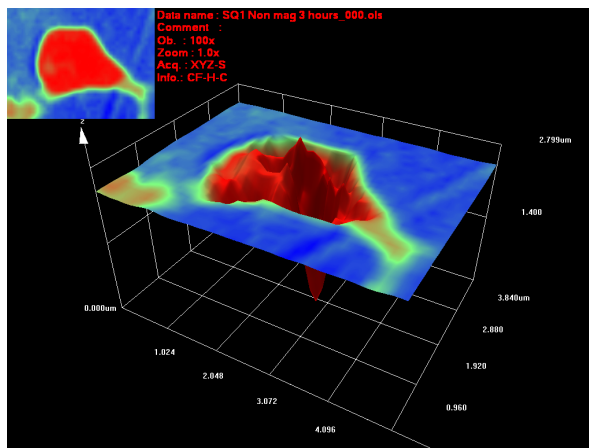
Figure 40 – 3D confocal microscope images of an individual NdFeB triple junction imaged at a higher magnification in order to illustrate the pit filling process (SQ material)

Figure 40 shows 3D images of one of these pits in the square material at the start of the experiment and after 3 hours. It was shown that the pit has almost entirely filled up with oxidised material during the course of the 3-hour oxidation/corrosion experiment.

Figure 39 shows the pit measurement data for the square material. It was observed that the average change in pit depth, at 0.082µm, is significantly lower than that of the voice coil material.

When comparing the oxidation/corrosion behaviour for both the SQ and VC materials, taking into account both surface triple junctions and the surface pits, a clear trend can be observed. The SQ material appears to possess a greater resistance to oxidation/corrosion than the VC material. The SQ material has higher concentrations of both Co and Dy, which has been shown to make the material more stable and less reactive to oxygen at higher temperatures [Skulj, 2008]. Kim (1996) demonstrated that the addition of Co leads to the formation of a Nd_3Co or $Nd(Fe,Co)_2$ grain boundary phase, which is less reactive than the Nd-rich phase, thus further increasing the corrosion resistance of the material. While there is an abundance of literature discussing the effects of Dy additions on magnetic properties, there is very little

relating to its effect on corrosion behaviour. However, it is thought that the addition of Dy will increase the corrosion resistance of NdFeB type magnets [Skulj, 2008] and this is due to Dy being one of the least reactive rare earth elements [Hamric, 2007]. Yan (2003) who investigated the effects of Dy addition on corrosion reported that the presence of Dy in the NdFeB system actually accelerated the rate of corrosion. This accelerated rate was thought to be caused by the increased volume of the Nd-rich phase produced as a result of the Dy addition. With a greater volume of Nd-rich phase, more corrosion would occur. Yan's (2003) study was conducted using hot and humid conditions and may not yield the same results as the dry, room temperature oxidation/corrosion studies conducted in this project.

5.3 Raman Spectroscopy

Although it is clear from the confocal microscopy that the triple junctions react with the atmosphere, it is not clear whether this is an oxidation reaction or due to corrosion as the air will contain water. Therefore, Raman spectroscopy was carried out in order to identify the specific oxide/corrosion products, which may have formed on the triple junctions of each material. Samples were oxidised in air for 3 hours prior to testing. The spectra for the sintered NdFeB magnets was compared to both standard materials (e.g. Nd_2O_3) measured on the same system and to data available in the literature. The Renishaw inVia Raman spectrometer is equipped with a confocal microscope, which allows the triple junctions alone to be imaged and analysed.
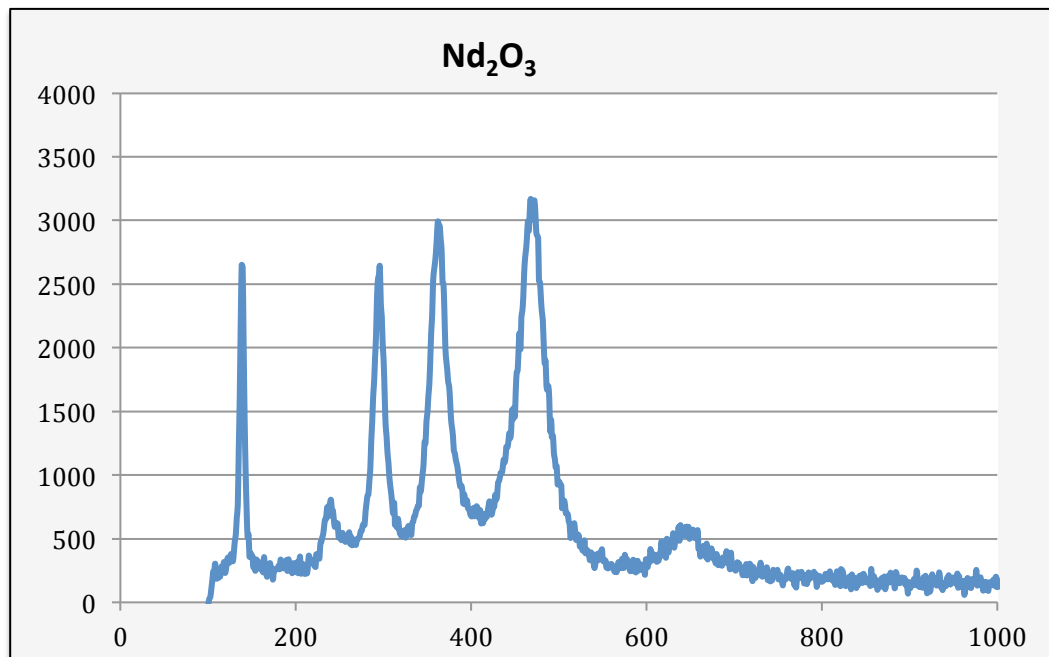
Figure 41 – Raman trace showing the peaks for pure Nd$_2$O$_3$ (supplied by Sigma Chemical Co. (N-1751. Lot 129F0287)). The laser wavelength used was 633nm.
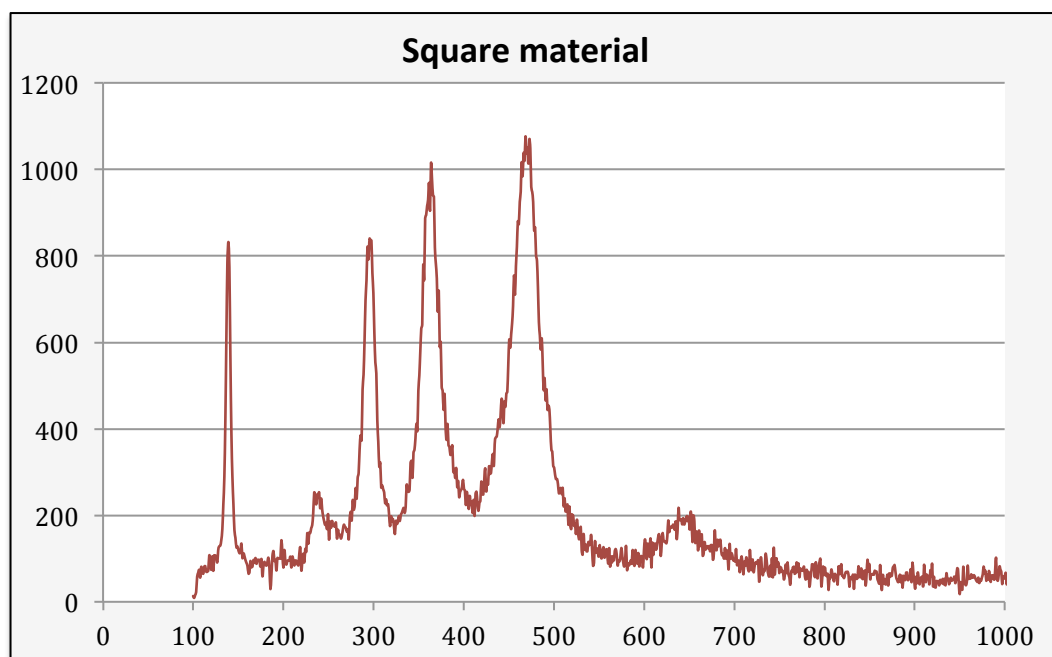
Figure 42 – Raman trace for the SQ material. The laser wavelength used was 633nm.

Figure 41 and Figure 42 show raman traces for pure Nd_2O_3 and Nd_2O_3 detected in the SQ material respectively. By comparing Figure 41 with Figure 42 it can be observed that the peaks observed in the square material match perfectly with those displayed for pure Nd_2O_3. Edgley (1997), who studied the composition of the oxide layer found on sintered NdFeB magnets between 350°C and 600°C found that a planar oxidation front was observed, which contained α-Fe nanocrystals and Nd-oxide particles. It was reported by Edgley (1997) that the $Nd_2Fe_{14}B$ matrix phase broke down during the oxidation process, however, the planar oxidation front is not observed here; rather, under these conditions, oxidation is only observed at the triple junctions.

It is interesting to note that no evidence could be found for any other peaks, including $Nd(OH)_3$. This would suggest that the main mechanism for triple junction growth is oxidation, rather than corrosion caused by moisture. It should be noted, however, that the confocal measurements were performed in an air-conditioned room where moisture levels will be fairly low. It would be interesting to look at dry vs. controlled humid conditions using this technique in the future.
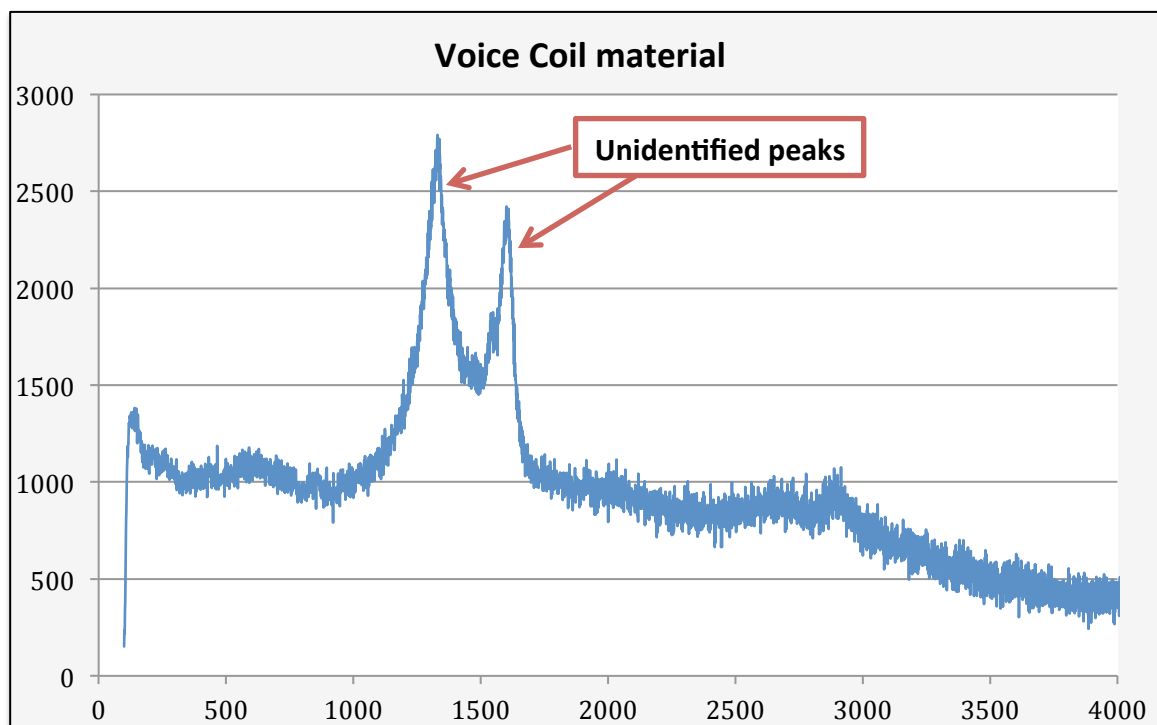
Figure 43 – Raman trace showing unidentified peaks in the voice coil material. The laser wavelength used was 633nm.

Raman spectroscopy of a single triple junction on the surface of the voice coil material showed no trace of neodymium oxide or dysprosium oxide (Figure 43). An unidentified peak was identified in the voice coil material. These peaks were compared with traces for all of the available oxidation/corrosion products, including; Fe oxides, Nd oxides, Dy oxides and Nd hydroxides, from the limited data in the literature. Unfortunately it was not possible to identify the peak shown above. Woodcock *et al.* (2012) reported that the Nd-rich triple junctions contain multiple phases, including crystalline oxides such as $(Nd,Pr,Dy)_2O_3$. It is possible that that a mixed oxide is forming on the surface triple junctions and the limited data in the literature means that it cannot be identified. More research is required in order to determine the composition of the triple junction oxide product found in the voice coil material.

Pure Dy oxide was also analysed and the Raman trace is shown below.
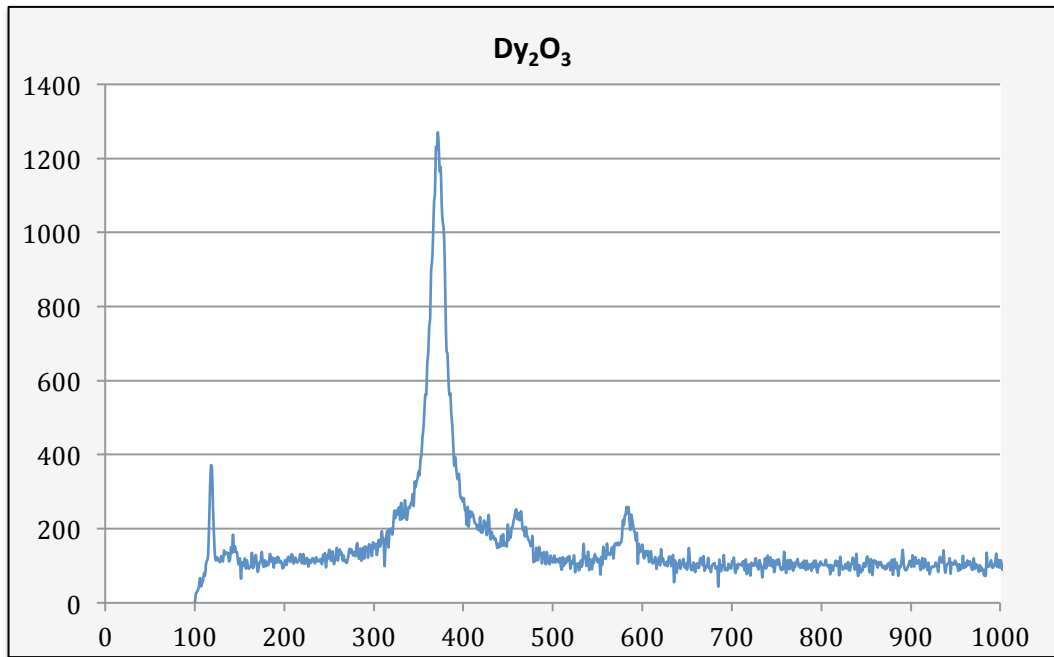
Figure 44 - Raman trace showing the peaks for pure Dy₂O₃ (supplied by Sigma Chemical Co. (D-0381. Lot 123H3508)). The laser wavelength used was 633nm.

These Raman studies did not show any evidence for the presence of dysprosium oxide in either the square or the voice coil material. Dy is one of the least reactive rare earths and it has been shown that Dy additions to the NdFeB system improve the material's corrosion resistance [Skulj, 2008]. Given this fact and the relatively small quantities of Dy in these materials (1.8 at% in SQ material and 0.53 at% in the VC material) this is unsurprising.

5.4 SIMS Analysis

Confocal microscopy and raman spectroscopy have been used to investigate the surface oxidation of NdFeB magnets. It was established that the oxide product grows up above the surface, however it was not known whether it penetrates into the material as well. SIMS analysis was conducted in order to map the oxygen profile and penetration depth for VC samples that had been oxidised for controlled periods of time. SIMS was used in this project, as previous cross sectional SEM studies have proved difficult due to the brittle nature of the material resulting in the surface breaking up during mounting, grinding and polishing. The voice coil material was chosen as it demonstrated the most rapid oxidation during confocal studies. The results from these experiments are presented below.

Oxygen Intensity Profiles

Nd-rich phase

Nd$_2$Fe$_{14}$B matrix phase

3.5 μm

X-Y Slice of:16.00u - O-
MC: 117; TC: 4.201e+006

A

X-Z Slice of:16.00u - O-
MC: 141; TC: 3.872e+006

B

Y-Z Slice of:16.00u - O-
MC: 142; TC: 3.802e+006

C

X-Y Slice of:16.00u - O-
MC: 116; TC: 3.984e+006

D

X-Z Slice of:16.00u - O-
MC: 139; TC: 4.679e+006

E

Y-Z Slice of:16.00u - O-
MC: 137; TC: 5.010e+006

F
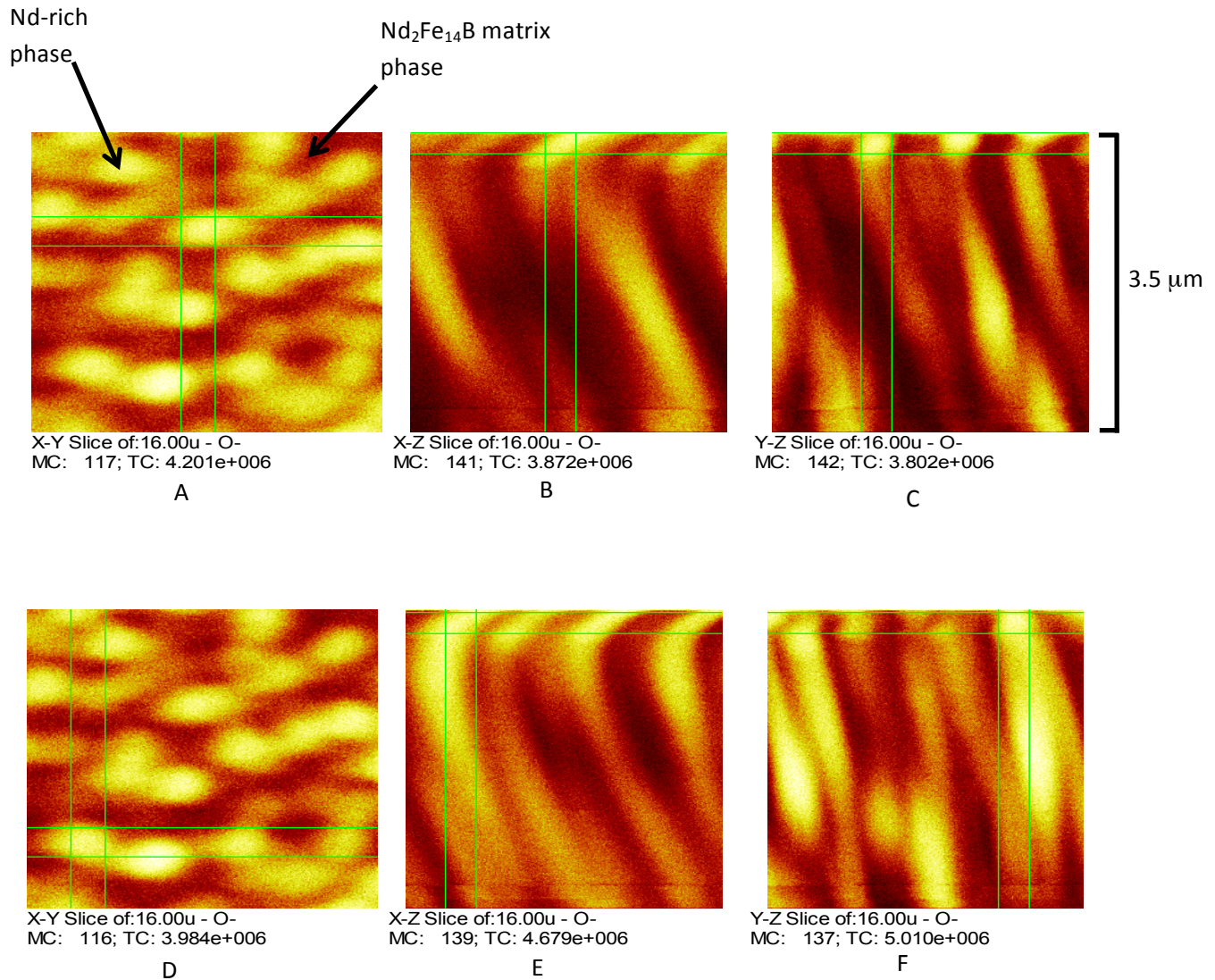
Figure 45 - Oxygen intensity profiles taken from inside the SIMS analysis area. All images show different areas or orientations of the same sample. VC material exposed to air for 6 hours.

Figure 45 A and D show the oxygen profiles from the top view of the voice coil material oxidised for 6 hours. Images B, C, E and F show cross sectional slices in the X-Z and Y-Z directions. B and C correspond with the areas within the green guide lines in image A and images E and F correspond with the guide lines in image D.

It is thought that the bright yellow areas show the oxidised Nd-rich material and the dark red areas show the matrix phase. The top down images (A and D) correspond with the confocal microscope images that show a clear distinction between the triple junctions and the $Nd_2Fe_{14}B$ matrix phase.

The cross sectional profiles (B, C, E and F) show that the oxygen levels appear higher towards the surface and that the oxygen follows the Nd-rich grain boundary phase down into the material. It is difficult to identify whether the trailing off of the bright yellow areas is a reduction in the oxygen concentration, or whether it just shows the shape of those individual triple junctions. Figure 46 shows a simplified version of what is thought to be shown in Figure 45 B, C, E and F. The grain boundary phase, shown in yellow, can be more clearly distinguished from the $Nd_2Fe_{14}B$ matrix phase (dark red) as it descends into the sample.
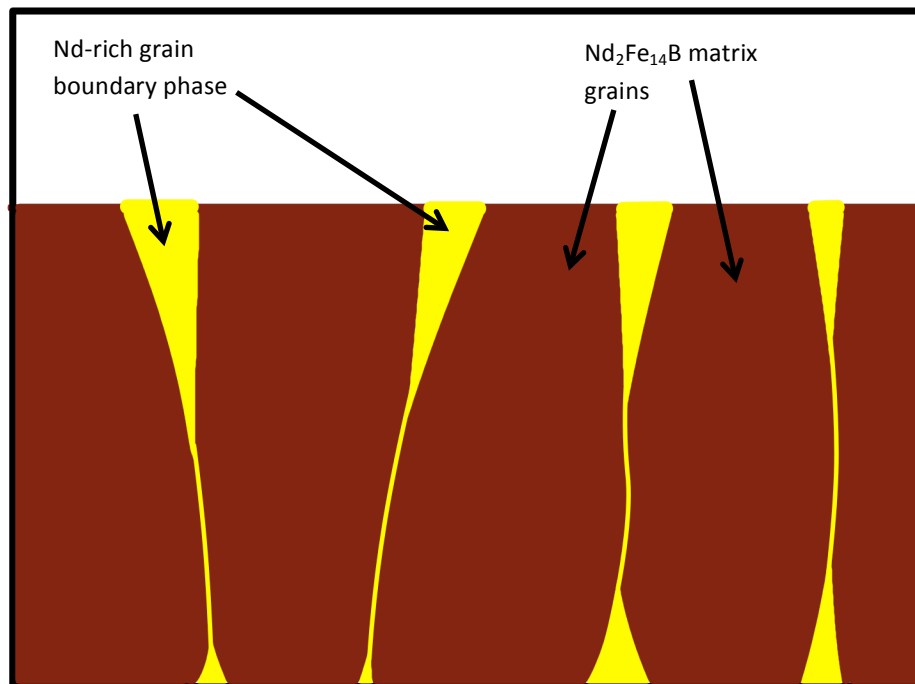
Figure 46 – A schematic showing a cross sectional slice (as seen in Figure 45) of an oxygen intensity profile produced using SIMS analysis.

However, the signal is noisy due to the preferential sputtering of the grain boundary phase so it is difficult to accurately identify the different phases from Figure 45. The curved oxidised regions observed in the images near the surface of the material are formed as a result of 'shift', which is caused by the analytical software used to process the data.

Sputter crater
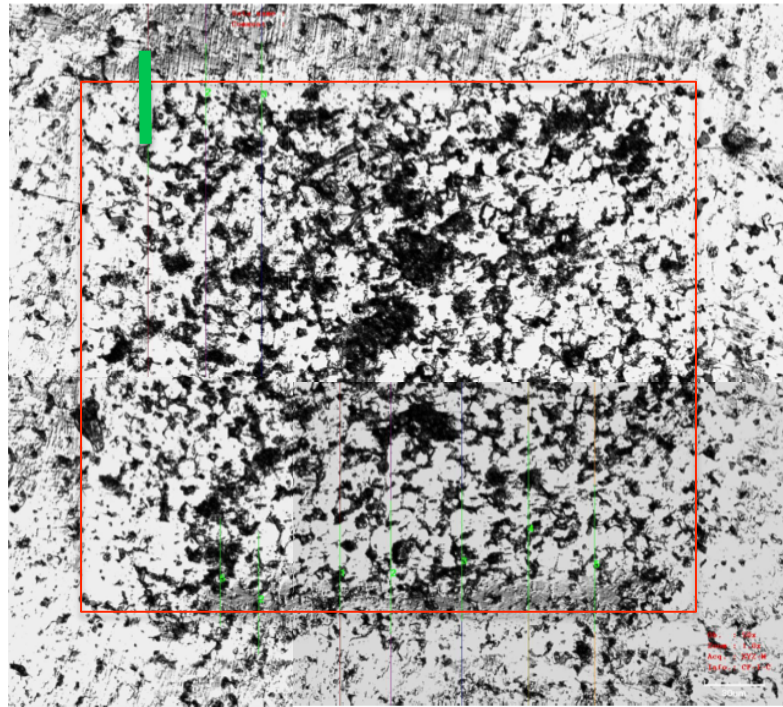
Figure 47 - A composite of 4 confocal images showing the SIMS sputter crater. The red box indicates the edge of the crater and the green bar shows where the line scan below was taken from.
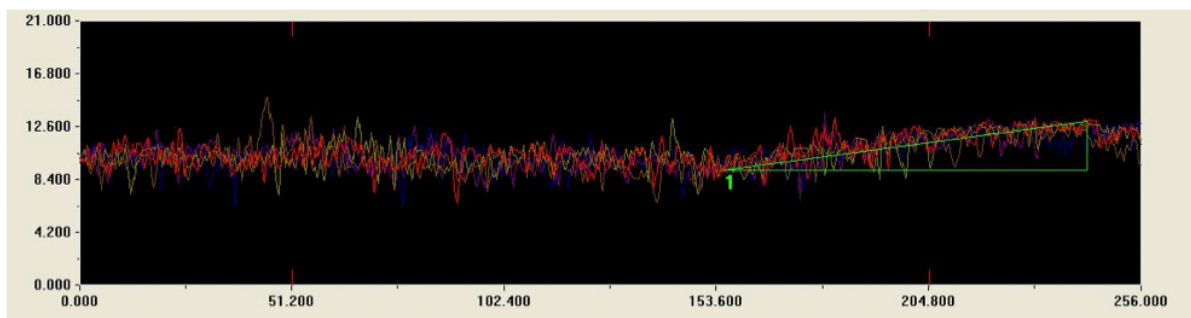
Figure 48 – Confocal microscope line scan of the edge of the SIMS sputter crater including one measurement of its depth.

Confocal microscopy was used to try to identify the sputtering rate of the SIMS equipment used for this study. Figure 48 shows a line scan, from the confocal image, of the edge of the

sputter crater made by the SIMS apparatus. 20 step measurements were taken around the edge of the sputter crater and were averaged in order to work out the crater depth. The average depth of the sputter crater was measured to be 3.54μm. From this depth measurement, the sputter rate for this SIMS system can be calculated to be approximately 1μm per hour. It can be observed from Figure 47 that the surface inside the sputter crater is significantly rougher than the polished outer edges. This is likely to be due to a differential sputtering rate of the different phases in the sintered NdFeB magnet, which has led to grain pull out over time. The increased surface roughness will also produce more noise in the SIMS data and could lead to a distortion in the observed amounts of different phases being identified with sputter time.

Oxygen Trace
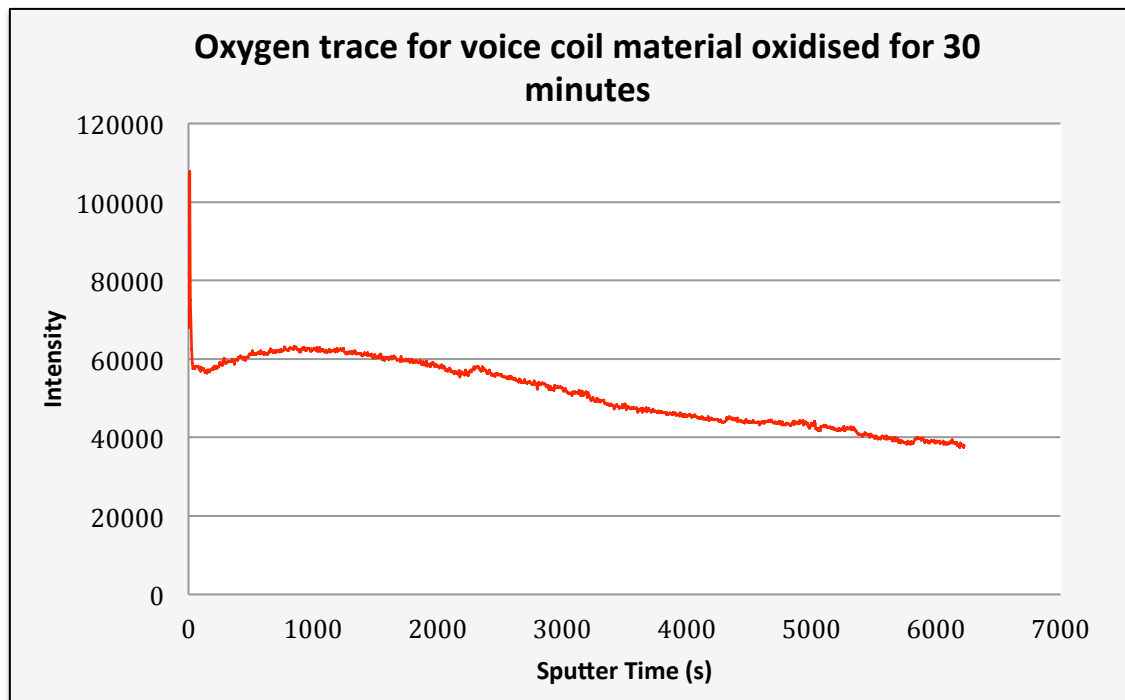
Figure 49 – SIMS oxygen trace for the voice coil material that had been exposed to air for 30 minutes.
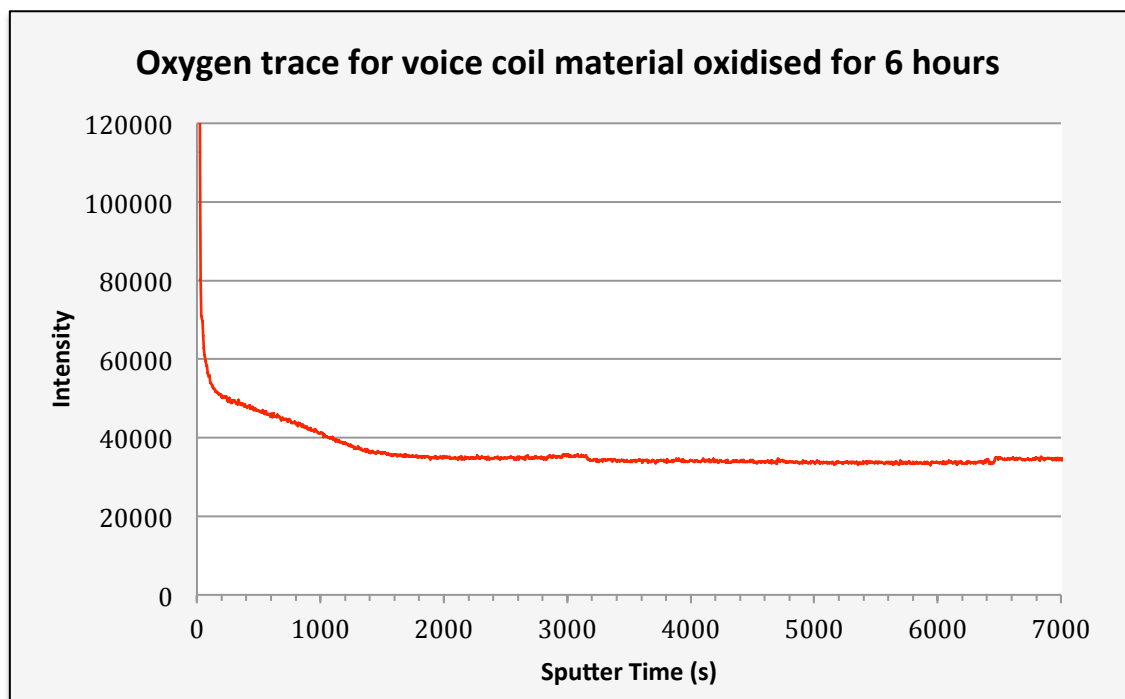
Figure 50 - SIMS oxygen trace for the voice coil material that had been exposed to air for 6 hours.

Figure 49 and Figure 50 show oxygen traces for an area that was 100×100 μm, therefore data for both the Nd-rich phase and the $Nd_2Fe_{14}B$ matrix phase is taken into account. These traces were produced in order to determine whether there was a drop off in oxygen at a certain depth within the material, thus indicating the depth of oxide penetration.

It can be observed that the traces produced from these SIMS experiments have an unusually high start point for all of the samples. This high point quickly drops off within the first few minutes of sputtering, as can be observed in all figures containing SIMS traces. There are two possible explanations for this initial dramatic drop off. Firstly, there is often contaminating substances on the surface of the samples as a result of polishing and loading. The drop off will occur as these substances are 'scrubbed off' to reveal the chemistry of the actual sample. Secondly, some samples require some time to reach an equilibrium sputter state, which can manifest itself as an initial increase or decrease in all data [Dr David, personal communication, Feb. 20, 2013; Ronsheim, 2000].

Figure 49 shows the oxygen trace for the voice coil material that was exposed to air for 30 minutes. Along the x-axis, sputter time corresponds with penetration depth where 0 seconds represents the outer surface of the material and, as time proceeds, data is collected from deeper within the sample. Due to the noisy data it is not possible to use the 'intensity' reading as an accurate measure of the oxygen content; general trends, however, can be observed.

For the sample exposed to air for 30 minutes (Figure 49) the oxygen level appears to continue falling even after 2 hours, which would suggest that the penetration depth is greater than 2μm. This seems unlikely, as the penetration depth in the material exposed to air for 6 hours (Figure 50) appears to be much more shallow, at 0.4μm where the trace levels off. It would be expected that the penetration depth for the oxygen would be significantly deeper for the

sample that was exposed to air for 6 hours. The reason for this difference is unknown and more research is required in order to investigate this.

It is evident that the SIMS technique may not be appropriate for sintered NdFeB samples due to grain pull out and the preferential sputtering of the Nd-rich grain boundary phase. Additionally, the sputtering rates were relatively low (1µm per hour), therefore a system with a faster sputtering rate may be more appropriate.

When scrap NdFeB material is recycled, any entrained oxygen will be mixed into the decrepitated powder and become distributed throughout the entirety of the material. This has been shown to have a detrimental effect on the magnetic properties of the recycled material [Zakotnik, 2009]. The oxygen penetration data together with the average sputter crater depth of 3.54µm confirm that there is penetration of oxygen below the surface of the material, which extends beyond one grains depth. However, the material was not sputtered away to a depth where a dramatic reduction in oxygen content could be observed. If it were possible to use the SIMS technique to identify a depth at which oxygen levels drop off it would be possible to grind off the surface of the material to this depth. This would remove the oxide layer, thus dramatically reducing the amount of oxygen that is entrained in the final recycled magnet.

5.5 Recycling Magnets and Oxygen Analysis

Oxygen analysis was conducted on samples taken from each stage of the magnet recycling process. The processing stages, as mentioned earlier in this work, are as follows:

1. Starting material

2. HD powder

3. Burr milled powder passed through 45μm sieve

4. Green compacts

5. Sintered magnets

The purpose of this study was to track the oxygen content of the material throughout the recycling process in order to identify the stages at which most oxygen is introduced into the material. Powder was also removed after the milling and sieving stage in order to investigate the particle size that had been achieved. The results from these experiments are shown below.

Particle Measurement

 Figure 51 and Figure 52 show optical microscope images of both the square and the voice coil materials that have been hydrogen decrepitated, burr milled and then sieved using a 45μm sieve. Although a 45μm sieve is used, it is clear that the average particle size is significantly smaller than this. It has been shown that the particle size of hydrogen processed sintered NdFeB magnets matches that of the grain size in the starting magnet (~10 μm. The particle size is retained because the HD process breaks the material apart along the grain boundary phase, thus leaving the matrix grains intact.

Square Material
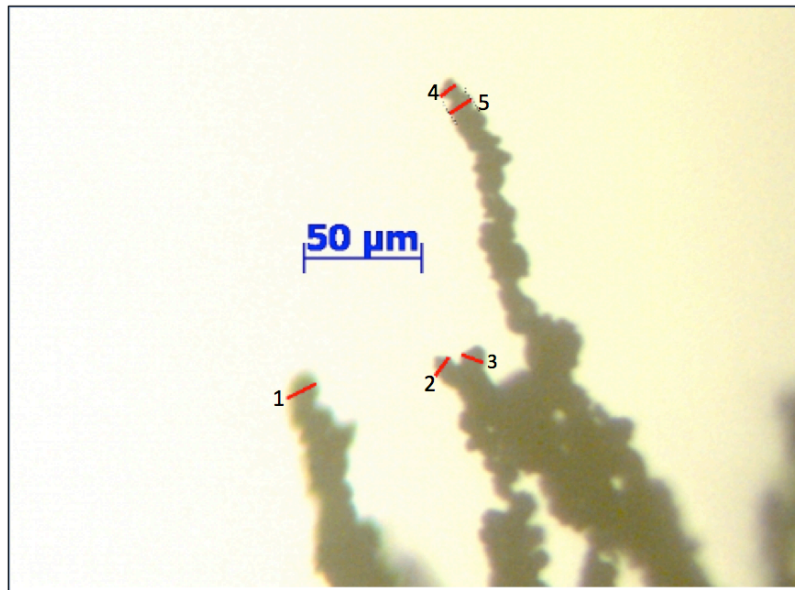
Particle	Particle size (μm)
1	7.59
2	13.46
3	9.37
4	9.26
5	11.04
Average	10.14

Figure 51 – Square material HD powder particle measurements using optical microscopy and image analysis software. Particle sizes shown in image.

Voice Coil Material
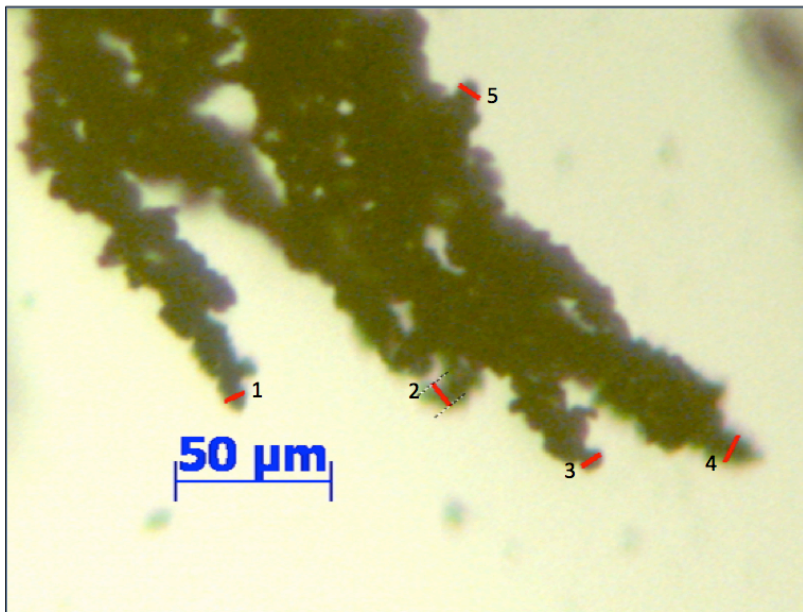
Particle	Particle size (μm)
1	6.63
2	6.68
3	7.32
4	9.32
5	8.89
Average	7.77

Figure 52 – Voice coil material HD powder particle measurements using optical microscopy and image analysis software. Particle sizes shown in image.

Oxygen Analysis
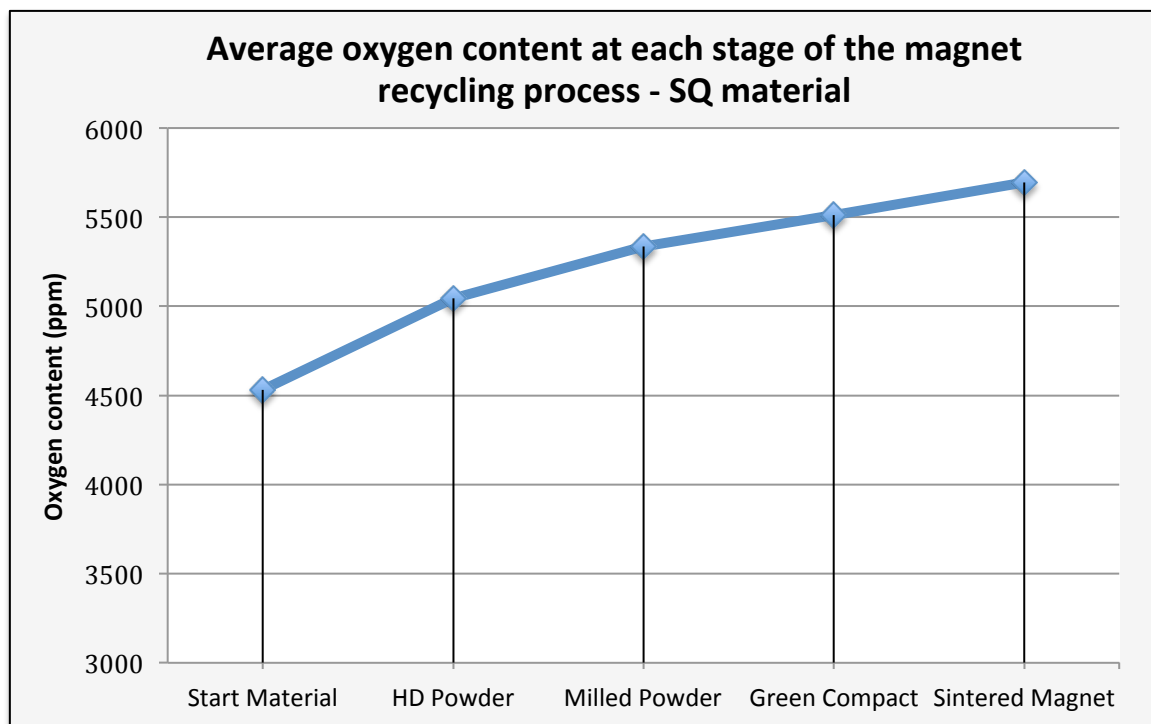
Figure 53 – Average oxygen content at each stage of the magnet recycling process for the SQ scrap material.

The LECO TC 136 oxygen analyser at Less Common Metals is accurate to 1ppm.

Figure 53 shows the average oxygen content at each stage of the magnet recycling process for the square material. It can clearly be observed that the concentration of oxygen within the material increases between each of the processing steps. Although all stages are performed inertly, it is impossible to completely eliminate oxygen contamination. During the hydrogen decrepitation stage of the recycling process, the solid magnet breaks down to a high surface area powder, which increases the oxidation rate. Between each stage the material is transferred outside the glove box and while every effort is made to do this as inertly as possible, it is possible for some oxygen contamination to occur. These transfers were performed using an argon filled isostatic bag, which is sealed with a rubber bung and

electrical tape. While this should form a good seal, the graph above indicates that oxygen can enter and react with the material. Inert environments will, however, always contain some level of oxygen.

The findings of Lian and Wallace (1995), who studied the oxygen content at various stages in the conventional processing of NdFeB magnets (see Figure 12), showed that the majority of the contaminating oxygen is introduced at the milling stage of primary production. The milling stage in this project was performed using burr milling within an argon filled glove box, which caused an increase in oxygen content of 290 ppm. This is a significantly smaller increase than is observed in the milling stage of primary production, where oxygen content can increase up to 1600-4400 ppm during jet milling [Namkung, 2011] and 5000 ppm for dry ball milling [Lian, 1995]. While Lian and Wallace (1995) showed that the largest single increase in oxygen content was in the milling stage of production, Figure 53 shows that the most significant increase in oxygen content in the recycling process occurs between the scrap material and the HD powder, however increases between all the steps are similar in magnitude and the increase is almost linear.

By comparing this data with that of Lian and Wallace (1995) it can be observed that the starting oxygen content in this study is similar in quantity to the final oxygen content in that of Lian and Wallace (~4500ppm). Scrap sintered magnets will always have a much higher oxygen content (2000-5000 ppm) than the primary cast material (300-400 ppm). However, it is interesting to note that the overall increase in oxygen content is significantly lower in this study. The overall increase, shown in Figure 53, was 1165ppm compared to that of Lian and Wallace, which was ~5000ppm for sintered material produced from a cast alloy. This large comparative increase in oxygen content is likely due to the less stringent oxygen controls that are used in the primary production of NdFeB magnets and the fact that the primary hydrogen

decrepitated powder will be more reactive than the, already oxidised, powder produced by decrepitating scrap sintered magnets. The recycling route has more stringent oxygen control in order to minimise oxidation and ensure that the properties of the final recycled magnet are as close as possible to the starting scrap material. It is also possible that, as the material had already oxidised significantly and moves towards saturation, there is not much Nd-rich phase remaining that can oxidise.
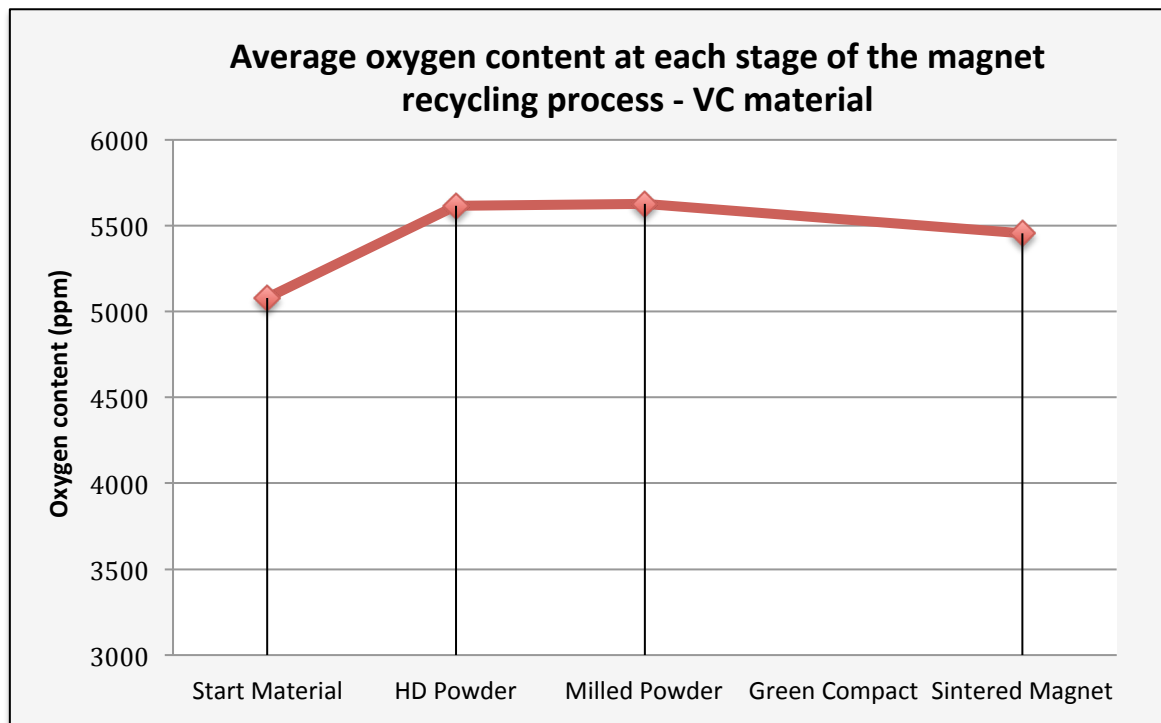
Figure 54 - A graph showing the average oxygen content of the VC scrap material at 3 of the 5 stages in the magnet recycling process.

Figure 54 shows the average oxygen content in the VC material for the starting material, HD powder, milled powder and the final sintered magnet. The results for the green compacts were unfortunately unavailable. When compared to the oxygen analysis for the square material, it can be observed that the starting voice coil material has a higher starting oxygen content

(5080 compared to 4530). This could be due to less stringent manufacturing techniques as these magnets were produced at an earlier date (1980's-1990's) than the square material or because there was contamination during the coating process.

The oxygen content rises from starting material to HD powder, however it then appears to plateau and fall slightly. It is possible that, at this concentration, the material stabilises and does not oxidise further. This levelling off could occur because most of the remaining Nd-rich phase has oxidised. This levelling off appears at a similar oxygen concentration in both the voice coil material and the square material.

After the milling stage, the oxygen content appears to reduce as the recycling process progresses. The variation in oxygen content could be caused by fluctuations in the oxygen levels inside the glove box that was used to prepare the samples. Although all samples were taken from the same batch, they were prepared at different times inside the glove box. While every effort was made to keep the oxygen content in the glove box consistent there were some fluctuations, meaning that some of the samples will have been exposed to more oxygen than others. During sample transfer, both during sample preparation and transferring for oxygen analysis, it is also possible that oxygen will have been introduced into the material.

6.0 Conclusions

The surface oxidation/corrosion of two different commercial sintered NdFeB compositions has been studied and characterised at room temperature. Surface oxidation, at this temperature, appeared to be exclusive to the Nd-rich triple junctions. This confirms that the mode of oxidation/corrosion is grain boundary diffusion and that it occurs at a greatly accelerated rate compared to the matrix phase. Surface triple junctions were observed to grow to a greater extent in the VC material compared to the SQ material. Further study of the surface of sintered NdFeB materials showed that there were relatively large pits present that were formed as a result of grinding and polishing the samples. These surface pits were observed to fill up with oxidised material over time. The pits in the SQ material were observed to fill up to a lesser extent than those in the VC material. The SQ material has higher Dy and Co contents than the VC material and this is thought to be the cause of the improved stability in this material.

Confocal microscopy does not allow for identification of the oxidation/corrosion reaction products. Therefore, raman spectroscopy was performed on the oxidised Nd-rich triple junctions for both materials in order to determine the composition of the reaction product after exposure to air. Nd_2O_3 was identified as the only reaction product in the square material, confirming that oxidation is the predominant reaction mechanism; however there was no indication that it was present in the voice coil magnets. It was interesting to note that although peaks could be identified on the VC material, they could not be identified as Fe oxides, Nd oxides, Dy oxides or Nd hydroxides using reference samples or from traces available in the literature. It is possible that a mixed oxide is formed, as has been reported by Woodcock *et al.* (2012). Very little raman data exists for rare earth oxides/hydroxides; therefore a much wider

study is required in order to identify the reaction products for room temperature air exposure on the VC material.

It would appear that the higher Dy/Co content SQ material is more stable in air. It could therefore be assumed that this material could be stored in air for longer periods of time than VC magnets without significant oxide growth. It has been assumed in previous studies that more rapid oxide growth would lead to a less reactive surface to hydrogen [Meakin, 2013]. However, Meakin *et al.* previously observed that high Dy content magnets would not react in hydrogen after 'fresh' material had been exposed to air for more than 1 hour [Meakin, 2013]. Contrary to this, Yi *et al.* observed that VC magnets could be broken in half and exposed to air for 30 days and then still all react in hydrogen [Yi, 2012]. This effect may be due to the different oxidation/corrosion products that form on the different compositions. For example, the higher Dy content magnets may be forming a very coherent oxide, which is difficult for hydrogen to penetrate. More work is required in order to investigate the composition of the oxidation/corrosion reaction products using a wider range of standard materials. This information is useful when considering the commercialisation of the magnet recycling process as it highlights the importance of the scrap storage conditions required to improve recycling efficiency.

SIMS analysis was conducted to investigate the depth of penetration of oxygen into the surface of the VC material. The SIMS apparatus used for this project is limited in terms of sputter rate; therefore the depth at which oxygen concentration dramatically reduces could not be determined. It was possible to observe sub surface oxygen penetration in the grain boundaries, however it is not clear whether the depth of penetration is limited or whether the oxygen will continue to travel through the material indefinitely. The oxygen intensity profiles support the findings of the confocal microscope studies by showing that oxidation appears to

be almost exclusive to the triple junctions and grain boundaries. If the thickness of this surface oxide could be identified on a system with a higher sputtering rate then it may be possible to grind off the initial oxide layer prior to recycling, thus reducing the overall oxygen content in the re-processed magnet.

Oxygen analysis of samples taken from each stage of the magnet recycling process was conducted to identify the stages at which oxygen contamination occurs. It was shown that, for the square material, the oxygen content increased at each stage of the recycling process. The largest single increase was observed between the start material and the HD powder, during the hydrogen decrepitation stage, however the increase was almost linear across all steps. The voice coil material showed a large initial increase from the starting material to the HD powder, however it then appeared to plateau. It may be the case that the material begins to stabilise at a certain concentration of oxygen as the Nd-rich grain boundaries/triple junctions begin to become saturated with oxygen. The overall increase in oxygen content for the whole recycling process was shown to be 1165 ppm and 535 ppm, for the SQ and VC materials respectively, which is much smaller for the oxygen pick up expected for primary production from a cast NdFeB alloy (typically 2000-5000 ppm) [Lian, 1995; Namkung, 2011].

Oxygen analysis of both the SQ and VC materials showed that there is not a significant increase in oxygen content during burr milling (290 ppm for the SQ material). This is much lower than that observed during jet milling of primary alloys (typical increases in oxygen are between 1600-4400 ppm [Namkung, 2011]). The burr milling technique has the advantage that it can be performed inside an argon filled glove box, unlike jet milling, used in primary production, where the equipment is too large. Burr milling is also a very rapid, with 150 grams of powder being processed in 2 minutes. The burr milling processed has not previously been reported in the literature. The main reason that burr milling can be used to break down

the hydrogen processed sintered magnets is because the material breaks down during both hydrogenation and milling along the grain boundaries of the sintered magnets. As the grains in the sintered material are already very small, then a low energy milling technique such as burr milling can be effectively employed.

7.0 Future Work

There are many areas of this work that require further investigation. For example:

- 3-D confocal microscopy and raman spectroscopy of a wider range of standard alloy compositions to investigate the effect of Dy and Co on the room temperature oxidation of NdFeB alloys.

- Raman spectroscopy of triple junctions that have been exposed to dry and controlled humid conditions.

- Further SIMS studies on a machine with a faster sputtering rate (although this could cause issues with even more grain pull out due to preferential sputtering of the grain boundary phase).

- Investigate the effect of air exposure on the initiation of hydrogen for a wide range of alloy compositions. For example, with increasing Dy and Co content.

- Oxygen analysis could be performed on re-sintered samples that have had the initial oxide layer ground off prior to decrepitation to determine whether it makes a significant difference in the final recycled material when compared with samples where the oxide layer is intact.

- Investigate the oxygen pick up that occurs during recycling on much larger batches of material.

Reference List

Akhtar, S., A. Haider, Z. Ahmad, M. Farooque, **Development of NdFeB Magnet through Hydrogen Decrepitation,** *Key Engineering Materials,* Vol. 442, pp. 263-267, 2010

Arrot, A.S., **Generalized Curie-Weiss Law,** *Phys.Rev.B,* Vol. 31, pp. 2851-2856, 1985

Bai, G., Gao, R., Sun, Y., Han, G., Wang, B., **Study of high-coercivity sintered NdFeB magnets**, *Journal of Magnetism and Magnetic Materials*, Vol. 308, pp. 20-23, 2007

Blank, R. and Adler, E., Proc. 9th Int. **Workshop on Rare Earth Magnets and their Applications**, Badsoden, Germany, p. 537, 1987

Breton, J.M.L, and J. Teillet, *J. Magn. Magn. Mater.* 101, pp**.** 347, 1991

Brown, D., Ma, B.M., Chen, Z., **Developments in the processing and properties of NdFeB-type permanent magnets,** *Journal of Magnetism and Magnetic Materials,* 248, pp. 432-440, 2002

Chandrasekhar, R., Mapps, D.J., O'Grady, K., Cambridge, J., Petford-Long, A., Doole, R., **Studies on the effect of Cobalt and Titanium substitution in NdFeB thin films for magnetic recording media,** *Journal of Magnetism and Magnetic Materials, 196-197,* pp. 104-106

Coey, J.M.D, **Rare-earth magnets**, *Endeavour,* Vol. 19, pp. 146-151, 1995

Cygan, D. F. and McNallan, M. J., **Corrosion of NdFeB permanent magnets in humid environments at temperatures up to 150°C.** *Journal of Magnetism and Magnetic Materials,* Vol 139, pp 131-138, 1995

Drak, M., Dobrzanski, L.A., **Corrosion of Nd-Fe-B permanent magnets,** *Journal of Achievements in Materials and Manufacturing Engineering,* Vol. 20, Issues 1-2, pp. 239-242, 2007

Edgley, D.S., Le Breton, J.M., Lemarchand, D., Harris, I.R., Teillet, J., **Dissociation of Nd$_2$Fe$_{14}$B during high temperature oxidation,** *Journal of Magnetism and Magnetic Materials,* Vol. 128, L1-L7, 1993

Edgley, D.S., Le Breton, J.M., Steyaert, S., Ahmed, F.M., Harris, I.R., Teillet, J., **Characterisation of high temperature oxidation of Nd-Fe-B magnets,** *Journal of Magnetism and Magnetic Materials,* Vol. 173, pp 29-42, 1997

Fidler, J., **On the role of the ND-rich phases in sintered ND-FE-B magnets**, *IEEE Transactions on Magnetics*, Vol. 23, pp. 2106-2108, 1987

Geochemical Instrumentation and Analysis, <http://serc.carleton.edu/18395> [Accessed 23 February 2013]

Givord, D., Li, H., Moreau, J., **Magnetic Properties and Crystal Structure of Nd$_2$Fe$_{14}$B,** *Solid State Communications*, Vol. 50, No. 6, pp. 497-499, 1984

Gutfleisch, O., *J. Appl. Phys. D: Appl. Phys. 33, R157-R172*, 2000

Hamric, D., **Rare-Earth Metal Long Term Air Exposure Test,** <http://www.elementsales.com/re_exp/> [Accessed 1 May 2013]

Harris, I. R., Noble, C. and Bailey, T., *Journal of Less-Common Metals, No. 106,* 1985

Harris, I.R., **The Potential of Hydrogen in Permanent Magnet Production**, *Journal of Less-common Metals, Vol. 131, pp. 245 – 262*, 1987

Hatch, G. P., **Recent Dynamics in the Global Rare-Earths Market,** *Proceedings of the 22nd International Workshop on Rare-Earth Magnets and their Applications,* Nagasaki, Japan, p4-9, 2012

Herbst, J.F., Croat, J.J., Pinkerton, F.E., **Relationships Between Crystal Structure and Magnetic Properties in Nd$_2$Fe$_{14}$B,** *Physical Review B,* Vol. 29, No. 7, 1984

Herbst, J.F., Croat, J.J., Yelon, W.B., **Structural and magnetic properties of Nd2Fe14B**, *Journal of Applied Physics*, Vol. 57, pp. 4086-4090, 1985

Higgins, B.E., Oesterreicher, H., **Properties and Stability of Nd$_2$Fe$_{14}$B Particles,** *IEEE Transactions on Magnetics,* Vol. 23, No. 1, 1987, pp. 92-93, 1987

Huang, Y.K., Wu, C.H., Chuang, Y.C., Fu-Ming Yang, De Boer, F.R., **First-order magnetic transition in (Nd, Pr)$_2$Fe$_{14}$B,** *Journal of the Less Common Metals*, Vol. 132, Issue 2, pp. 317-325, 1987

Jacobson, J., Kim, A., **Oxidation behaviour of NdFeB magnets,** *Journal of Applied Physics,* Vol. 61, pp. 3767-3765, 1987

Kaneko, Y., **Proceedings of the 16th International Workshop on Rare-Earth Magnets and Their Applications**, Sendai, Japan, pp. 83, 2000

Keane, E., **Will Lack of Rare Earths Kill the Green Economy,** <http://www.slideshare.net/EamonKeane/rare-earth-elements-and-the-green-economy-5210467> [Accessed 30 May 2012]

Kim, A., Camp, F., Stadelmaier, H., **Relation of Remanence and Coercivity of Nd,(Dy)-Fe,(Co)-B Sintered Permanent Magnets to Crystallite Orientation,** *Journal of Applied Physics,* Vol 76, pp. 6265-6267, 1994

Kim, A., Camp, F., **Effect of Minor Grain Boundary Additives on the Magnetic Properties of NdFeB Magnets,** *IEEE Transactions on Magnetics*, Vol.31, pp. 3620-3623, 1995a

Kim, A., Camp, F., **High Performance NdFeB Magnets***, Journal of Applied Physics*, Vol. 79, pp. 5035-5040, 1996

Kim, A., Camp, F., **The Role of Oxygen for Improving Magnetic Properties and Thermal Stability of Sintered (Nd,Dy)(Fe,Co)B Magnets,** *IEEE Transactions on Magnetics*, Vol.31, pp. 3656-3658, 1995b

Lemarchand, D., Delamare, J., Viaier, P., *J. Appl. Phys,* Vol. 72, pp. 1996, 1992

Li, H. E. Evans, I. R. Harris and I. P. Jones, **The Oxidation of NdFeB Magnets ,** *Oxidation of Metals,* Vol. 59, Nos. 1/2*,* 2002

Lian F.Z., Wallace W.E., **Proceedings of the 3rd ISPM**, Seoul, 736, 1995

Liu, W.L., Liang, Y.L., Ma, B.M., Bounds, C.O., **Effects of Nb Addition and/or Casting Method on the Amount of Precipitated Fe in NdFeB Alloys,** *IEEE Transactions on Magnetics,* Vol. 28, No. 5, pp. 2154-2156, 1992

Liu, Z.W., Davies, H.A., **The practical limits for enhancing magnetic property combinations for bulk nanocrystalline NdFeB alloys through Pr, Co and Dy substitutions,** *Journal of Magnetism and Magnetic Materials,* Vol. 313, pp. 337-341, 2007

Makita, K., Yamashita, O., **Phase boundary structure in Nd-Fe-B sintered magnets,** *Applied Physics Letters,* Vol. 74, No. 14, pp. 2056-2058, 1999

Man, H.H., Man, H.C., Leung, L.K., **Corrosion protection of NdFeB magnets by surface coatings – Part I: salt spray test,** *Journal of Magnetism and Magnetic Materials,* Vol. 152, pp. 40-46, 1996

McGuiness, P. J., Harris, I. R., Scholz, U. D. and Nagel, H., *Zeitschrift fur Physikalische Chemie Neue Folge,* Vol 163, pp. 687-692, 1989.

Meakin, J., **Targeted hydrogen decrepitation of NdFeB magnets from large commercial assemblies (Masters Thesis),** University of Birmingham, Birmingham, UK, 2013

Namkung, S., Kim, D. H., Jang, T. S., **Effects of particle size distribution on the microstructure and magnetic properties of sintered NdFeB magnets,** *Rev. Adv. Mater. Sci.,* Vol. 28, pp 185-189, 2011

Néel, L., **Propriétés magnétiques des ferrites. Ferrimagnétisme et antiferromagnétisme**. *Ann. Phys*., 3, pp. 137-198, 1948

Ohmori, K., Li, L., Graham, C.D., **Effect of Added Cu on the Nd-Rich Phase in Hot-Deformed NdFeB Magnets,** *IEEE Transactions on Magnetics,* Vol. 28, No. 5, pp. 2139-2141, 1992

Osawa, Z., Higuchi, S., Hinohara, S., *J. Mater. Sci.,* Vol. 27 pp. 5445, 1992

Pandian, S., Chandrasekaran, V., Markandeyulu, G., Iyer, K.J.L., Rama Rao, K.V.S., **Effect of Al, Cu, Ga, and Nb additions on the magnetic properties and microstructural features of sintered NdFeB,** *Journal of Applied Physics,* Vol. 92, Issue 10, pp 6082-6086, 2002

Ribitch R.W., **Proc. 11th Int. R.E. Conf. Mag. & Appl.**, pp 93, 1990

Ronsheim, P.A., Murphy, R. J., **Study of pre-equilibrium sputter rates for ultrashallow depth profiling with secondary ion mass spectrometry,** *Journal of Vacuum Science & Technology B: Microelectronics and Nanometer Structures,* Vol. 18, pp. 501-502, 2000

Sagawa, M., Fujimura, S., Togawa, N., Yamamoto, H., Matsuura, Y., **New material for permanent magnets on a base of Nd and Fe**, *Journal of Applied Physics*, Vol. 55, pp. 2083-2087, 1984

Scott, D.W., Ma, B.M., Liang, Y.L., Bounds, C.O., **The effects of average grain size on the magnetic properties and corrosion resistance of NdFeB sintered magnets,** *Journal of Applied Physics,* Vol. 79, pp. 5501-5503, 1996

Shinba, Y., Konno, T.J., Ishikawa, K. and Hiraga, K., *J. Appl. Phys.* 97, 053504, 2005

Simon, M.D., **Diamagnetic levitation: Flying frogs and floating magnets,** *Journal of Applied Physics,* Vol. 87, Issue 9, pp. 6200-6204, 2000

Skulj, I., Douvalis, A.P., Harris, I.R., **Characterisation of oxidation of modified Nd-Fe-B type magnets,** *Journal of Alloys and Compunds,* Vol. 407, pp. 304-312, 2006

Skulj, I., Evans, H. E., Harris, I. R., **Oxidation of NdFeB-type magnets modified with additions of Co, Dy, Zr and V,** *Journal of Materials Science,* Vol. 43, pp. 1324-1333, 2008

Smart, J.S., **The Néel Theory of Ferrimagnetism,** *American Journal of Physics,* Vol. 23, Issue 6, pp. 356, 1955

Takada, K., Etizen, Y.*,* **Process for the corrosion protection of neodymium-iron-boron group sintered magnets.** *United States Patent Application,* Patent No. 4917778, 1990

Takeshita, T., Nakayama, R., *Proceedings of the 12th International Workshop on Rare Earth Magnets and their Applications*, Canberra, Australia, pp. 670, 1992

Walton, A., **A newly developed zinc coating process for NdFeB magnets. Low Pressure Pack Sublimation (PhD Thesis),** University of Birmingham, Birmingham, UK, 2001

Walton, A., Han Yi, Mann, V.S.J., Bevan, A.I., Speight, J.D., Harris, I.R., Williams, A.J., **The Use of Hydrogen to Separate and Recycle NdFeB Magnets from Electronic Waste,** *Proceedings of the 22nd International Workshop on Rare-Earth Magnets and their Applications*, Nagasaki, Japan, p10-13, 2012

Wang, S.C., Li, Y., **A new structure of $Nd_{1+\varepsilon}Fe_4B_4B$ phase in NdFeB magnet,** *Journal of Materials Science,* Vol. 40, pp. 3853-3855, 2005

Wang, S.C., Li, Y., **In situ TEM study of Nd-rich phase in NdFeB magnet,** *Journal of Magnetism and Magnetic Materials*, Vol. 285, pp. 177–182, 2004

Woodcock, T. G., Hrkac, G., Schrefl, T., Gutfleisch, O., **Multiscale Characterisation and Modelling of Grain Junctions in Nd-Fe-B Sintered Magnets,** *Proceedings of the 22nd International Workshop on Rare-Earth Magnets and their Applications*, Nagasaki, Japan, pp. 61-65, 2012

Yan, G., **An investigation of sintered neodymium iron boron magnets with dysprosium additions (PhD Thesis),** University of Birmingham, Birmingham, UK, 2003

Yan, G., McGuiness, P.J., Farr, J.P.G., Harris, I.R., **Environmental degradation of NdFeB magnets,** *Journal of Alloys and Compounds,* Vol. 478, pp. 188-192, 2008

Yi, H., **The use of hydrogen and mechanical processing to separate NdFeB from electronic waste (Final Year Project),** University of Birmingham, Birmingham, UK, 2012

Yu, L., Liu, R. S., Dong, K. T., Zhang, Y. P., **Key techniques for ultrahigh performance sintered Nd-Fe-B magnets preparation,** ISBN: 978-81-7895-554-4, pp. 1-36, 2012

Yu, L., Wen, Y., Yan, M., **Effects of Dy and Nb on the magnetic properties and corrosion resistance of sintered NdFeB**, *Journal of Magnetism and Magnetic Materials*, Vol 283, pp. 353-356, 2004

Zakotnik, M., I.R. Harris, A.J. Williams, **Multiple recycling of NdFeB-type sintered magnets**, *Journal of Alloys and Compounds,* Vol. 469, pp. 314–321, 2009

Zakotnik, M., I.R. Harris, A.J. Williams, **Possible methods of recycling NdFeB-type sintered magnets using the HD/degassing process**, *Journal of Alloys and Compounds,* Vol. 450, pp. 525–531, 2008